ADDIS ABABA UNIVERSITY

ADDIS ABABA INSTITUTE OF TECHNOLOGY

AFRICAN RAILWAY CENTER OF EXCELLENCE

Effect of Concrete Sleeper Type and Spacing on Lateral Resistance of Curved Track

A Thesis in Civil Infrastructure

By Ayantu Mitiku

Jul, 2019

Addis Ababa

A Thesis

Submitted in Partial Fulfillment of the Requirements for the Degree of Master of Science

The undersigned have examined the thesis entitled '**Effect of Concrete Sleeper Type and Spacing on Lateral Resistance of curved Track**' presented by **Ayantu Mitiku**, a candidate for the degree of **Master of Science** and hereby certify that it is worthy of acceptance.

Dr. Esayas G/youhannes	_____	_____
Advisor	Signature	Date
Dr. Celestin Nkundineza	_____	_____
Co- Advisor	Signature	Date
Dr. Abrham Gebre	_____	_____
Internal Examiner	Signature	Date
Dr. Ing. Adil Zekaria	_____	_____
External Examiner	Signature	Date
_____	_____	_____
Chair person	Signature	Date

UNDERTAKING

I certify that research work titled “Effect of Concrete Sleeper Type and Spacing on Lateral Resistance of Curved Track” is my own work. The work has not been presented elsewhere for assessment. Where material has been used from other sources it has been properly acknowledged / referred.

_____

Ayantu Mitiku

ABSTRACT

Railway tracks should resist heavy loads that come from the axel of a train without causing excessive defects while allowing reasonable speed of the train. Due to the increment of the speed and the axle load, the amplitude of lateral forces exerted on railway track has been increased hence, affects the track lateral stability especially on curved phase.

In this thesis, variations on the finite element models has been made to study the response of the track when different shape of concrete sleepers and spacing are used at curved section of ballasted railway track. Models with four types of concrete sleepers has been developed and used and the result have been validated using field experiments. The results showed that side-winged sleeper, bottom winged sleeper and frictional sleeper improves lateral resistance by 40%, 41% and 42% respectively, when compared to the conventional Type II sleeper. In addition, three values of sleeper spacing have been used on the developed model to investigate the effect on lateral resistance of the track. The result indicates that decreasing of the spacing between sleepers leads to increasing in lateral resistance of the track but decreasing beyond spacing of 600 mm has insignificant difference. The outcome of this study reveals that frictional sleeper had better lateral resistance compere to other types and can potentially be used on curved section.

Key words: Curved track lateral stability, Concrete sleeper, Sleeper spacing, Lateral load, Abaqus

ACKNOWLEDGMENTS

First and foremost, praises and thanks to the God, the Almighty, for His showers of blessings throughout my research work to complete the research successfully.

I would like to thank my principal advisor, Dr. Esayas G/youhannes, for the continued support, patience, and for inspiring my interest in the subject of the study. Thank you for sharing your wealth of knowledge and expertise with me.

I would also like to express my gratitude to Dr. Celestin Nkundineza who is my co advisor, for his continuing guidance and professional mentoring on Abaqus software. I would not be able to build a good model without the guidance from him.

I would like to acknowledge the financial and technical support of this project by the railway center of excellence. The internship opportunity I had at AALRT truly opened my eyes to research in the railway industry.

I am also thankful to all staffs of AALRT maintenance division for providing the whole needed help during my field experiment.

On the last but not the least, I would like to thank my family who, taught me at an early age to value education and to follow my dreams. Without the love and support of my family, I would not be where I am today.

TABLE OF CONTENTS

LIST OF TABLES

LIST OF FIGURES

LIST OF NOMENCLATURES

AALRT	Addis Ababa Light Rail Transit
CWR	Continuously Welded Rail
ERC	Ethiopian Railway Corporation
FE	Finite Element
LVDT	Linear Variable Differential Transducer
PPT	Panel Pullout Test
SNCF	Socié t é Nationale des Chemins de Fer
STPT	Single Tie Pullout Test

CHAPTER 1 INTRODUCTION

1.1 Background

As the demand for railway journeys has been increasing worldwide, an increased volume of rail traffic, heavier axle loads, and higher speed on rail routes has been the result. To support this demand there is a necessity to improve the track system and to understand the behavior of the track with respect to the role of each track components.

The majority of the railway tracks throughout the world consists in principle of the same components as it did over 100 years ago. Rails are laid on the sleepers which are themselves laid across same form of leveled, soil (ballast, sub ballast). What was changed is the quality of materials used, as well as changes including refinements to the rail profile, the introduction of longer rail section which are welded together (continuously welded rails (CWR)), the specification of the foundation and the quality of construction, as well as the greater axle loads and maximum speeds of train using the track.

In general, track resistance can be divided into four different resistant mechanisms: lateral, longitudinal, torsional and vertical. The lateral resistance is defined as the reaction offered by the ballast against lateral movement [1].

Concerning the situations where the lateral resistance is important, on the one hand, the horizontal curves along the railway tracks should be considered. The train passing through curved railway tracks results in centrifugal forces and thus the lateral resistance mechanisms are activated as a response to those forces [2].

The excessive centrifugal force in a railway curve possesses two components including a very short time impact force and a constant quasi-static force. In addition, aggressive acceleration and braking of trains produce large lateral forces.

However, Field investigations have shown that the lateral resistance of the railway track is not adequate for welding the rail joints in the CWT railway tracks. Due to increment of speed and axle load of trains, the amplitude of train lateral forces exerted on railway tracks has been increased and this issue highly affects the track lateral stability.

1.2 Statement of the problem

Railway tracks should resist heavy loads that come from the axel of the train without any excessive defects. Increasing the speed limit of railway tracks is applicable by welding rail joints and employing Continues Welded Rails (CWR).

In curves there results high lateral forces due to high centrifugal effect. Therefore, the design of sleepers should be different at curved section to resist these forces. So far, several studies and field measurements have been conducted to evaluate the lateral shifting of rails in ballasted tracks. For the specific case of this study, the recorded lateral shifting on studied railway curve is attached on Appendix-A. Ballasted track sleepers have the important function of providing sufficient lateral resistance to prevent the lateral movement of rails. If the lateral force induced by the thermal expansion and centrifugal force of steel rails overcomes the lateral resistance of sleepers, rail buckling may occur. More attention has been paid to this problem of lateral stability since the introduction of continuous welded rails. However, there is a high degree of uncertainty in the prediction of the lateral resistance of sleepers.

In response to the above problem, one can improve the track lateral resistance by providing higher lateral resistance component of track. Sleepers are some of these components used to tie the rail in position and also to resist lateral forces that come from the train. Employing winged sleeper, dual block sleepers, sleeper anchoring, frictional sleeper, Xi-track method and large sleeper are some of the methods to increase the lateral resistance of railway track.

In this research several aspects of resistance are considered in order to precisely evaluate the lateral resistance of different design of concrete sleepers on ballasted tracks at curved section. In addition, the paper determines the effect of sleeper spacing on the lateral resistance. The modeling and analysis is done by using simulation of track in ABAQUS software. Then after, field experiment is carried out to validate the finite element results.

1.3 Scope and Limitations

The scope of this paper is focused on the types of concrete sleepers and its influence in terms of ballasted track lateral resistance. The design of sleepers only includes the modification of the shape of sleepers and excluding the reinforcement design. Besides it

includes the effect of sleeper spacing on lateral stability of curved railway lines. The purpose is to develop and design suitable concrete sleepers at curved section on ballasted railway track.

1.4 Objectives

The aim of the research is

- To fully understand the effect of changing sleeper design on ballasted track in a curved section by considering different train speed in terms of loading.
- Characterize the track response due to changing the sleeper spacing on ballasted track at curved section.
- To create full understanding of lateral load distribution on sleepers along the track
- Compare the performance and suggest the effective design of sleeper and their spacing for ballasted track at curved section.

The research is limited to rail infrastructure within the area of lateral stability.

1.5 Research significance

Lots of track lateral stability researches and sleeper lateral resistance problem related works throughout the world have done after the occurrence of the damages and after seeing its consequences. Investigations on the effect of sleepers on lateral satiability of track are done by considering curves, dynamic load and types of sleeper separately. This work has its own significance by giving real image of the actual situation taking all factors under consideration. The outcome of this research contributes to the ongoing researches in this domain area, it can be un input for any organization on railway who wants to improve railway track lateral stability and increase the speed limit of train on curved section. Respective measurement on sleeper types and spacing is proposed.

1.6 Outline of the Thesis

Following the introduction, the thesis is organized into five further chapters, chapter 2 concerns the review of literature and previous works. It has two distinguished parts. The first part, contains the general review of railway track structures, components of ballasted track and loads on the track. The second part assembles the information gathered on the track lateral stability.

Chapter 3 elaborates on the development of the finite element (FE) model for analyzing track response. It discusses the modeled track components and their material properties, contact interaction properties defined for track components, and the loading procedure used for the FE analysis.

Chapter 4 presents the analysis results of model and discusses the observations associated with each parameter. In addition, the reliability of the model is validated by using numerical method and field experiment.

Chapter 5 includes the summary and main conclusions of the study as well as brief recommendations for future work.

CHAPTER 2 LITERATURE REVIEW

2.1 Introduction

2.1.1 Ballasted track

Ballasted track is a traditional type of rail track structure widely used in almost every country. This type of railway track structure consists of rail, supported by sleepers on a ballasted bed. The ballast bed rests on layer called sub ballast or sub grade. The main advantages of ballasted track are its relatively low cost constriction cost, the ease of maintenance of track components and geometry and its good drainage properties. However, ballasted track has some disadvantages, one is the tendency to move both laterally and vertically after a period of time.

A rail vehicle negotiating a horizontal track curve is beside track irregularities and the curve steering to additional lateral influences. The vehicle at quasi-static curving condition, running at speed v through a curve with radius, is subjected to centrifugal acceleration v^2/R and the gravity g [2].

2.1.2 Sleepers

Sleepers are one of the component of ballasted track, to be laid between the rails and ballast to tie the rails at the correct gauge, and distribute the load transmitted through the rails over a larger area of ballast underneath. They are typically formed as rectangular blocks with most lengths between 2500 to 2600 mm for standard gauges [3].

2.1.3 Track forces

To design track structure, a basic understanding of type and, magnitude of forces that the track substructure must support is needed. Types of forces imposed on track structure are classified as mechanical (dynamic or static) and thermal. The track structure needs to restrain repeated vertical, longitudinal, and lateral forces as well as moment loading resulting from traffic, and changing temperature.

Temperature change induces thermal stresses in the rail which cause expansion or contraction of the steel. In a continuous welded rail, thermally induced forces acting in the longitudinal direction may tend to compress the rails potentially leading to buckling in the

vertical or lateral direction, or tend to tension the rail potentially leading to breakage if the resistance is not sufficient.

Lateral forces act perpendicularly to the longitudinal direction of a track. On canted tracks the lateral force may be resolved into vertical and horizontal components. Zakri et al. [4] described two principal sources of lateral forces:1) lateral wheel force and 2) buckling reaction.

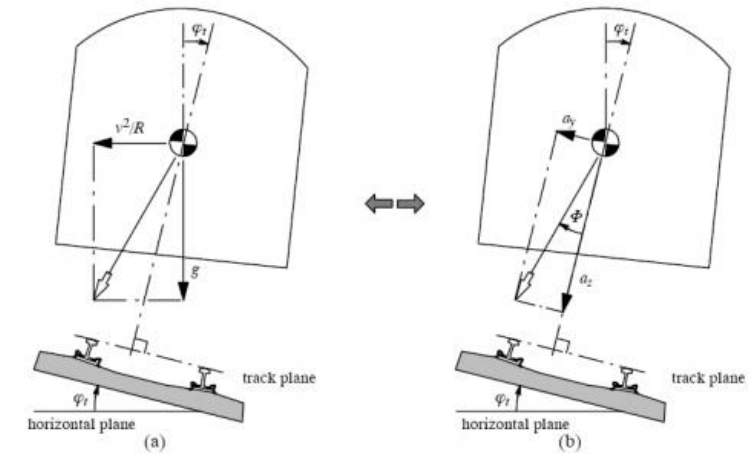

Figure 2-1 Rear view of rail vehicle car body at curving

(a) Lateral acceleration in horizontal plane, (b) Lateral acceleration in track plane [4]

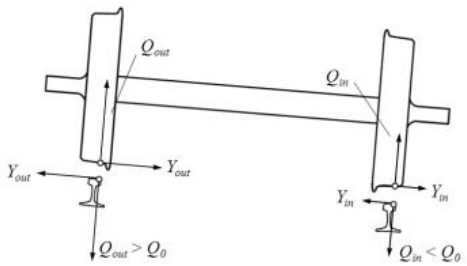

Figure 2-2 wheel rail forces during curve negotiation at cant deficiency [4]

Lateral force Y, vertical force Q, outer and inner wheel/rail. $Q_{in} < Q_0 < Q_{out}$, where Q_0 is the normal vertical wheel load. The outer wheel-rail contact is close to the wheel flange. If the inner wheel-rail contact is lost the vehicle may overturn about the outer rail.

A lot of research works on the determination of lateral resistance of sleeper to maintain railway track stability, have been made in the last decades. Kish A. [1] reviewed fundamental of track lateral resistance, its measurement and its key influencing parameters, provides a test/data summary of US measurement of date, analysis results on influence on track stability, and offers insights on research needs for future research study for track lateral resistance improvement. He included his research and other works on track lateral stability is reviewed in this chapter [1].

2.2 Types of sleeper

Zakir et al. compared the lateral resistance of wooden, steel and concrete sleepers. According to the experimental results, concrete sleeper B-70 has the most lateral resistance among three types of sleepers. According to the experimental results, concrete sleeper B-70 with 2.06 tons has the most lateral resistance among three types of sleepers [5].

The lateral resistance of the railway track increased by 64% by using frictional sleepers [5]. In addition, a field investigation was conducted on an actual track with and without B70-F sleepers in order to extend the results and the conclusion was that the resistance of the railway track to lateral displacement increased by approximately 68% when using B70-F sleeper that means the B70-F resistance to lateral displacement is approximately 1.68 times more than B70 resistance. Approximately the same results observed by researchers [5] in which the comparison of the calculated value of the lateral resistance for a frictional sleeper with that for a conventional B-70 sleeper showed a 63 to 70% 64%-68% and increase in value of the lateral resistance respectively [5, [6].

A research carried out analytically through a comparative assessment of traditional mono, bi block sleepers and new devised and parented sleeper called “HP-BB”, evaluating the lateral resistance of single sleeper though as an independent of other constituents of the track by [7]. In the case of ballast in good condition, a bi- block sleeper provides an average resistance increase by about 23% compared to mono-block sleeper. On the other hand, a HP-bb sleeper provides an average resistance increased by 32% and 63% in comparison with bi-block and mono-block sleepers respectively [7].

The research by Laura et al. [8] showed that the lateral resistance of winged sleepers is better than others. Six types of concrete sleepers were prepared, whose size were 1/5 of the actual part and based on the test results they proposed a new calculation method for

estimating the lateral resistance of sleepers in track panel tests for a wide range in numbers of sleepers. The result revealed the difference between the cross section shapes of winged sleepers had little effect on the lateral resistance, whereas the widths of their wings did deem to have a significant effect [8].

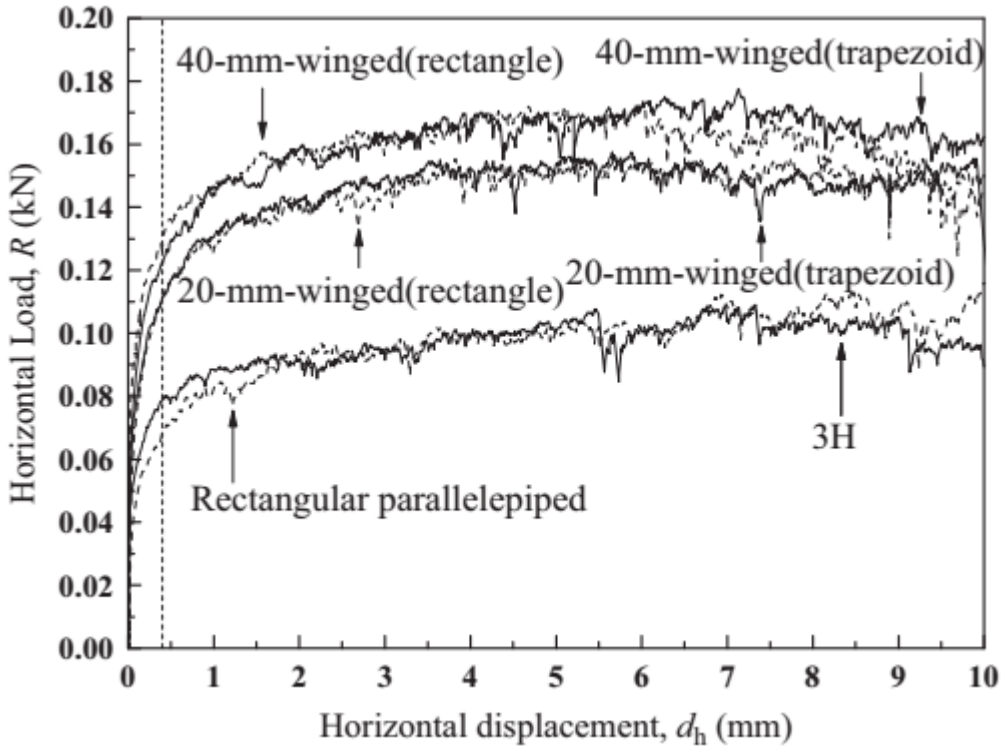

Figure 2-3 Horizontal load versus displacement for different types of sleepers [8]

Study the response of the track for wooden, conventional concrete and winged concrete sleepers through finite element method; by taking tangent, clothoid and circle combination of curved CWR tracks have been done by researchers. [9] They developed a new sleeper design to provide higher lateral resistance for a problematic railway track, which is placed in Cantabria (Spain) by comparing four new winged sleepers. The new sleeper improved the lateral resistance between 39 and 55% with respect to a track with conventional sleepers made of wood or concrete [10].

Zakri et al. conducted a comparative study of track-ballast resistance for railroad tracks built with four different types of sleepers. [4] The first set of sleepers was made of steel, the second one was made of wood, the third one of pre-stressed concrete and the fourth one of two-block concrete. By convention, the maximum longitudinal track-ballast resistance corresponds to a displacement of 15 mm. the pre-stressed concrete sleeper setup

showed the greatest longitudinal track ballast resistance per sleeper, which is around 69 kN, for the displacement of 10 mm [11].

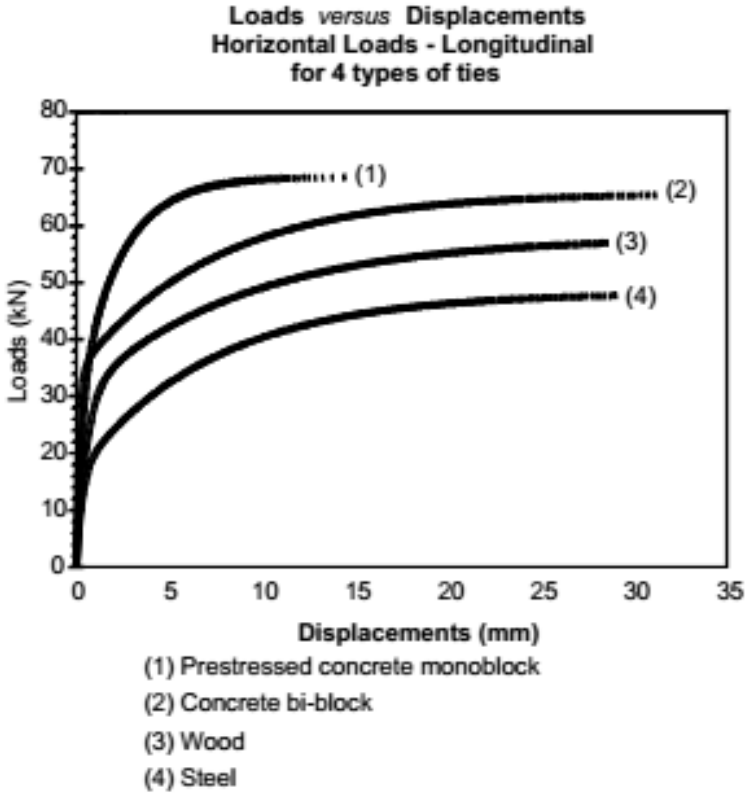

Figure 2-4 Comparison among the curve loads longitudinal displacements for the for types of sleepers [11]

In addition to the design of the sleepers using safety caps is one way to increase the lateral resistance of sleepers. In [12] the result showed that, when the safety cap is placed every three sleepers, the lateral ballast resistance is increased by 22%. Application every 2 sleepers increase the lateral resistance of ballast by 40%, and a safety cap on every sleeper in a 90% increase in lateral resistance of ballast. He also did a parametric study for six different defect configurations (amplitude- wavelength) and the result is as shown below

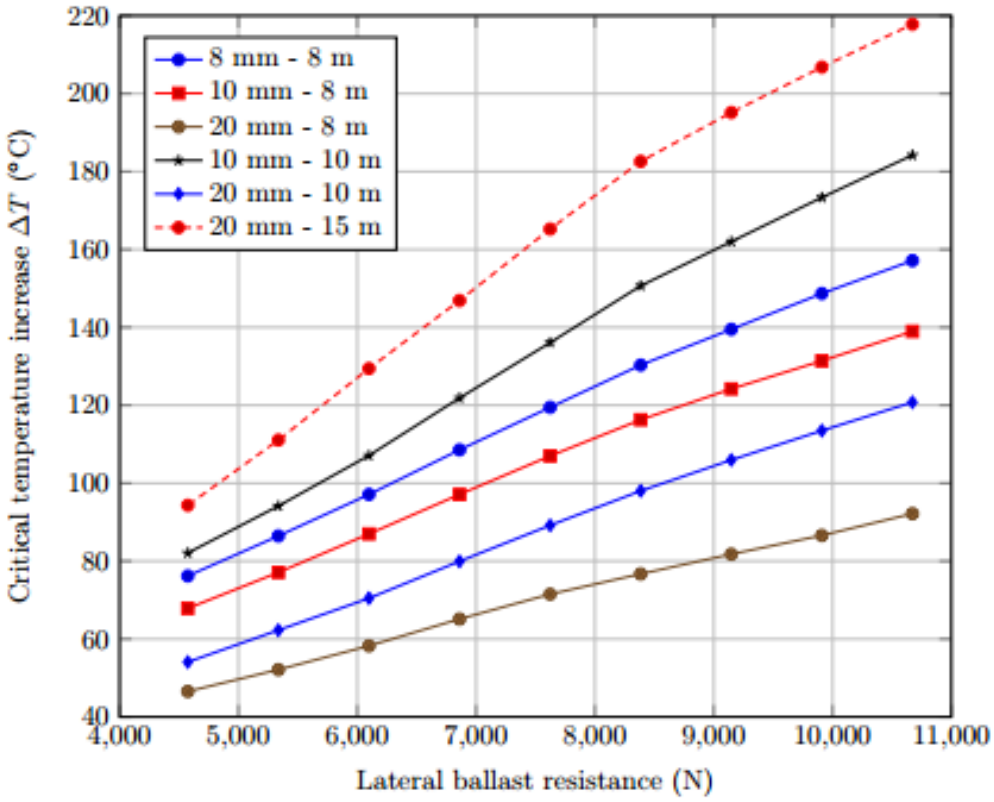

Figure 2-5 Parametric analysis of the ballast resistance **[12]**

2.3 Sleeper spacing

According to research on the lateral resistance per sleeper in track panel pullout tests decreases with an increasing number of sleepers. To avoid high degree of uncertainty when predicting the lateral resistance of single sleeper and the to clear up the effect of sleeper spacing on lateral resistance, Single Tie pullout test (STPT) and track panel pullout tests (TPPT) conducted in order to investigate the effects of the sleeper shape, the sleeper spacing, and the number of sleepers on the lateral resistance. The horizontal load obtained from the single-sleeper pullout tests were larger than those obtained from the track panel pullout test. He proved that, the lateral resistance per sleeper in track panel pullout tests decreases with an increasing number of sleepers [8].

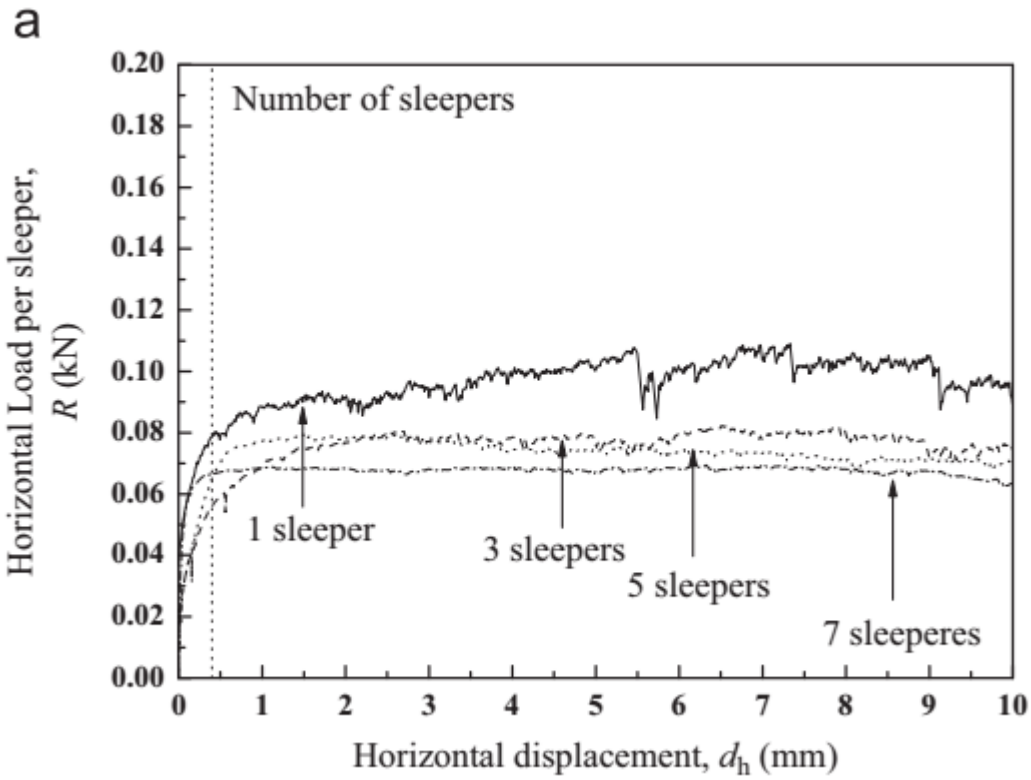

Figure 2-6 Horizontal load per sleeper vs horizontal displacement for different numbers of sleeper test [8]

2.4 Effect of Curve on Track Lateral Stability

Study showed that, curve track radius has a great effect on the stability of the CWR track. The track tends to be more stable with increase in curved track radius. Concerning to this, the influences of the lateral resistance of the ballast, invalid sleepers and curved track radius as well as initial flexural deformations on the stability of continuously welded rail track were investigated by Shigeru M. [13]. In order to understand comprehensively the stability characteristics of the CWR track, they analyzed the track for 4 cases; the influence of lateral resistance of the ballast, influence of invalid sleeper, influence of the curved track radius, and influence of initial flexural deformation.

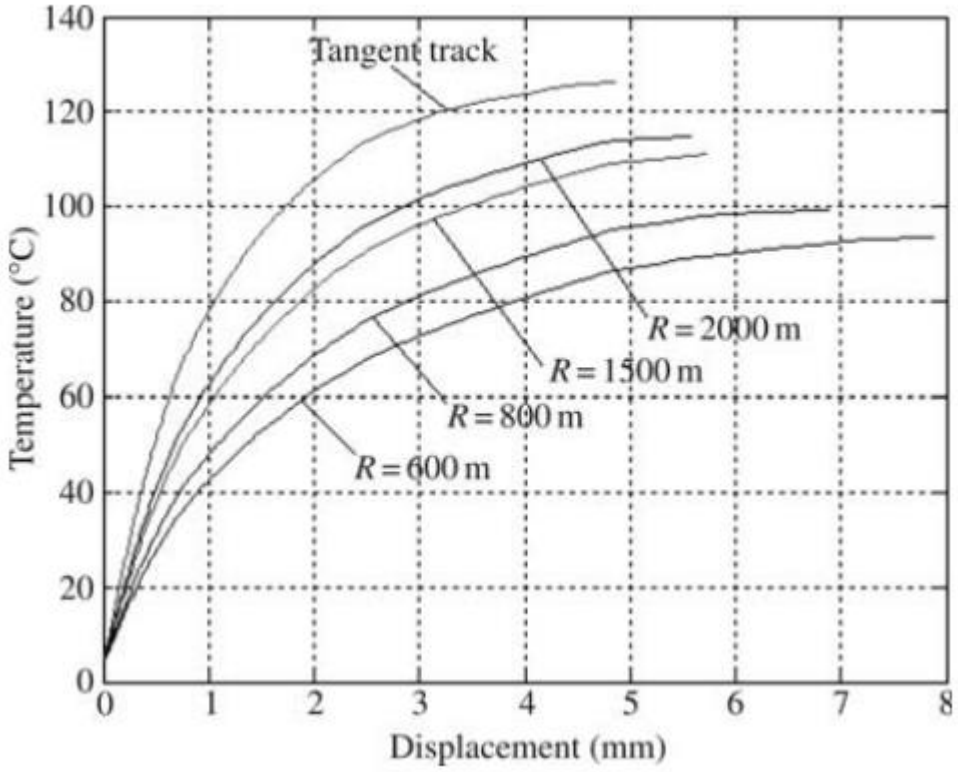

Figure 2-7 Lateral Displacement in the center of CWR track versus critical temperature for different curved track [13]

In order to make clear the relation between the minimum bulking strength and the load that actually induces buckling, on tangent and curved track were carried out [14] in Japan. The load that induced bulking in the tests were found to be distributed in an approximately normalized form where theoretically calculated minimum buckling strength constituted a lower limit volume of railway traffic. Because of wear is high on sharp curve sections; the size of sleepers on the narrow gage lines is so small that the lateral resistance is not sufficiently maintained. Due to this reason CWR use has been limited to curve sections in which the radii of curvature exceed 600m before the study of Miura S. [14].

Conducted test results by [15] on simple and frictional concrete sleepers in actual railway track curve with radius of 250 meters by employing frictional concrete sleeper. And he does recommend using a frictional sleeper on curved section [15].

As shown in Figure 2-8, Kish A. [4] research showed that the curvature in the presence of thermal loads is found to have a significant effect on track shift. For the condition of T =

50° F, a 6° (R=291m) curve will have a deflection of 40 percent greater than that of the tangent track under the same conditions. The rate of increase for all conditions shown is linear with respect to curvature.

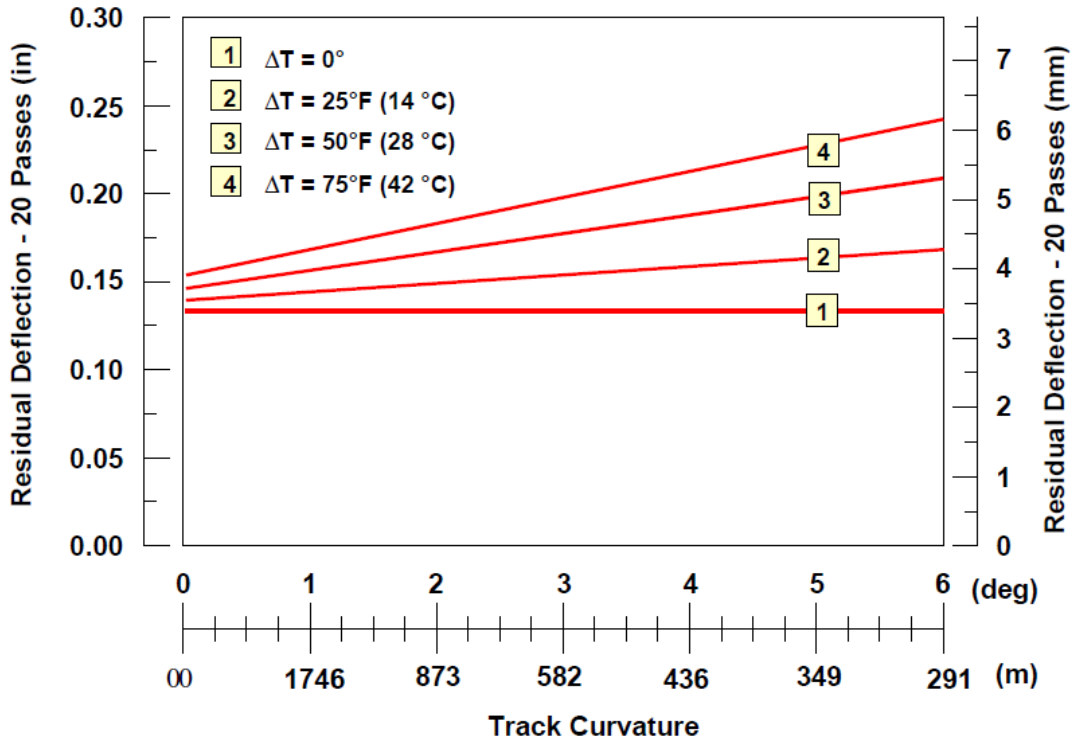

Figure 2-8 Influence of curvature and thermal force on track residual deflection [4]

2.5 Sleeper/Ballast interaction

Several researches were done regarding to the interaction between different surfaces (base, crib, and shoulder) of concrete sleeper and their adjacent ballast layer along with the related parameters under lateral impact loading condition [16]. And an Experimental research is done by Esmaeili et al. [17], on sleeper- ballast resistance along the lateral and longitudinal directions on a single tangent track approximately 200 m. Although identification of the strength contributions offered by base, crib and the shoulder to global resistance of the track in horizontal plane is done [18, 17].

As shown in Figure 2-9 the results of the aforementioned research indicated that the strength percent contribution from the crib, the sleeper base, and the shoulder are,

respectively, equal to about 50%, 25%, and 25% in the lateral direction [17], which is slightly different from the result obtained in [16].

The test scenarios used to determine lateral resistance are [17]:

a. For lateral pull test: four sleeper surrounded by ballast up to the upper surface level (namely with crib and shoulders- BBB)
b. Four sleepers and ballast removed from the crib (BCB); four sleepers and shoulder swept down to the sleeper base (BBU) and
c. Four sleepers and ballast removed from the side (BCU)

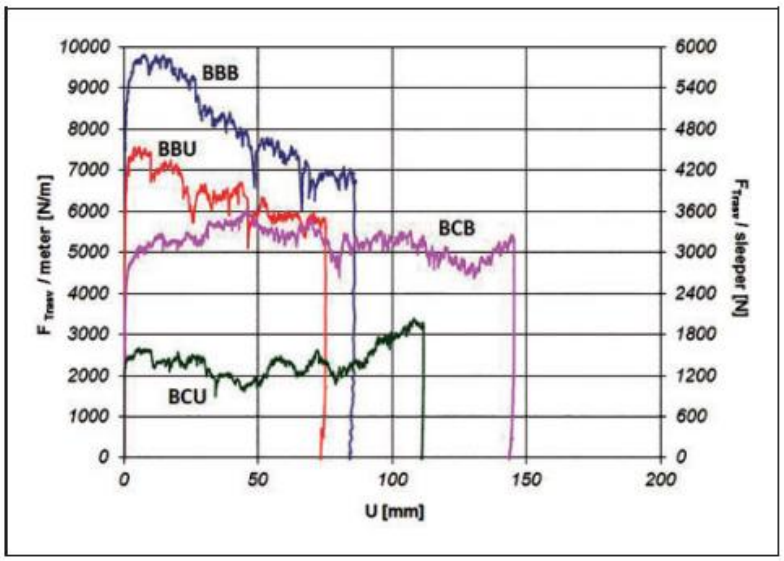

Figure 2-9 Lateral pull test: load-displacement curve [17]

On their research the resistance at 2 mm, the mean from 2 to 20 mm and the mean from 20 to 90 mm were found to be important way to characterize sleeper resistance. It has been found experimentally that the sleeper/ballast interface mobilized friction angle is about 24º at 2 mm of deflection, this is less than the internal angle of friction of the ballast and therefore there is a potential to increase the lateral failure resistance of sleeper ballast interface by roughing of the sleeper base [2].

Other result indicated that increasing the ballast shoulder from 25 to 40 cm resulted in about a 16-22% increase in lateral resistance. On the other hand, on decreasing the ballast layer thickness from 30 to 20 cm, the lateral resistance increased by about 12-17% [5].

In this regard, a series of lateral impact test performed on an instrumented concrete sleeper, considering full, semi-full, and incomplete sections of ballast zone. On the bases of the experiment results, the average contribution of base, crib, and shoulder zones in total dynamic lateral resistance of the sleeper was calculated as 48%, 23%, and 29% respectively. [16] This indicated eliminating the shoulder zone has no less influence on the time required for mitigation of wave compared to the crib zones of the sleeper. And linear relationships can be observed between the induced maximum lateral accelerations a_{max} of sleeper and lateral impact force F_{im} as

$$a_{\max.} = 2.5F_{\mathrm{im}\ .}\ , \qquad R^2 = 0.86$$

Also They concluded that, the removal of crib zones will increase sleeper lateral velocity noticeably. Moreover, they found a static friction coefficient of 0.82 at the lateral impact force of zero. In lateral impact domain of 13-28 kN, this coefficient is in the range 0.8 – 1.5 for the base zone.

The contributory effects of bottom resistance, side resistance, and end resistance on the total resistance for each sleeper type, using developed analytical equation. (Figure 2-10). [8].

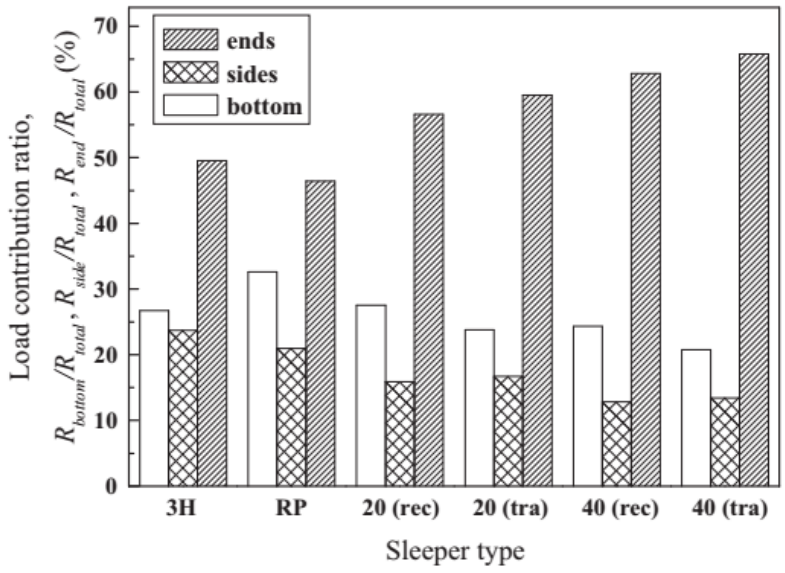

Figure 2-10 Contribution of bottom resistance, side resistance, and end resistance to total resistance [8]

Interface

The tests reported by Abadi T. [3] have quantified and demonstrated the potential for different ballast/sleeper combinations to improve the number and area of contacts at the sleeper to ballast interface and some exert to modify these parameters at ballast to subgrade interface. The changed in contact area imply large change in real contact stresses. More significantly showed that under normal conditions the sleeper to ballast contact area is less than 1% of the sleeper footprint and the contact stress that this implies are orders of magnitude greater than those calculated from the simplistic pressure distributions commonly used. Thus the contact behavior couldn't be understood without considering the discrete nature of the contacts at interface. Larger numbers of contacts and larger contact areas imply lower stresses and greater homogeneity of load transfer from sleeper to ballast. Twin block sleeper showed the smaller contact area while the concrete mono block sleeper on the finest ballast gradation showed the highest contact area.

2.6 Friction coefficient between concrete sleepers and ballast

Frictional coefficient has not a very significant role on the threshold release of phenomenon of shifting but has an influence on the amplitude of displacement following the shifting [18].

Using track panel displacement method, the frictional coefficient is estimated to be 0.86 between the frictional concrete sleeper and the ballast, and 0.45 between the concrete sleeper and ballast, in the presence of a static vertical load [19].

Hosseini A. and Esmaeili M. [15] considered a frictional coefficient between concrete, wooden, and steel sleepers, and the ballast layer as 0.8, 0.6 and 0.45, respectively. In [5] revised this result and improve that, increase in lateral resistance whereas increasing the frictional coefficient from 0.1 to 0.8 led to bout a 22-28% increase in the lateral resistance. In order to analyze the sensitivity of the system to the frictional coefficient (tangential contact), 0.1 was considered to be the value between the ballast and sleeper [15].

A linear relationship between vertical and frictional forces (Coulomb friction) has been assigned. Friction coefficients of 0.1, 0.3, 0.5, and 0.8 have been studied [20].

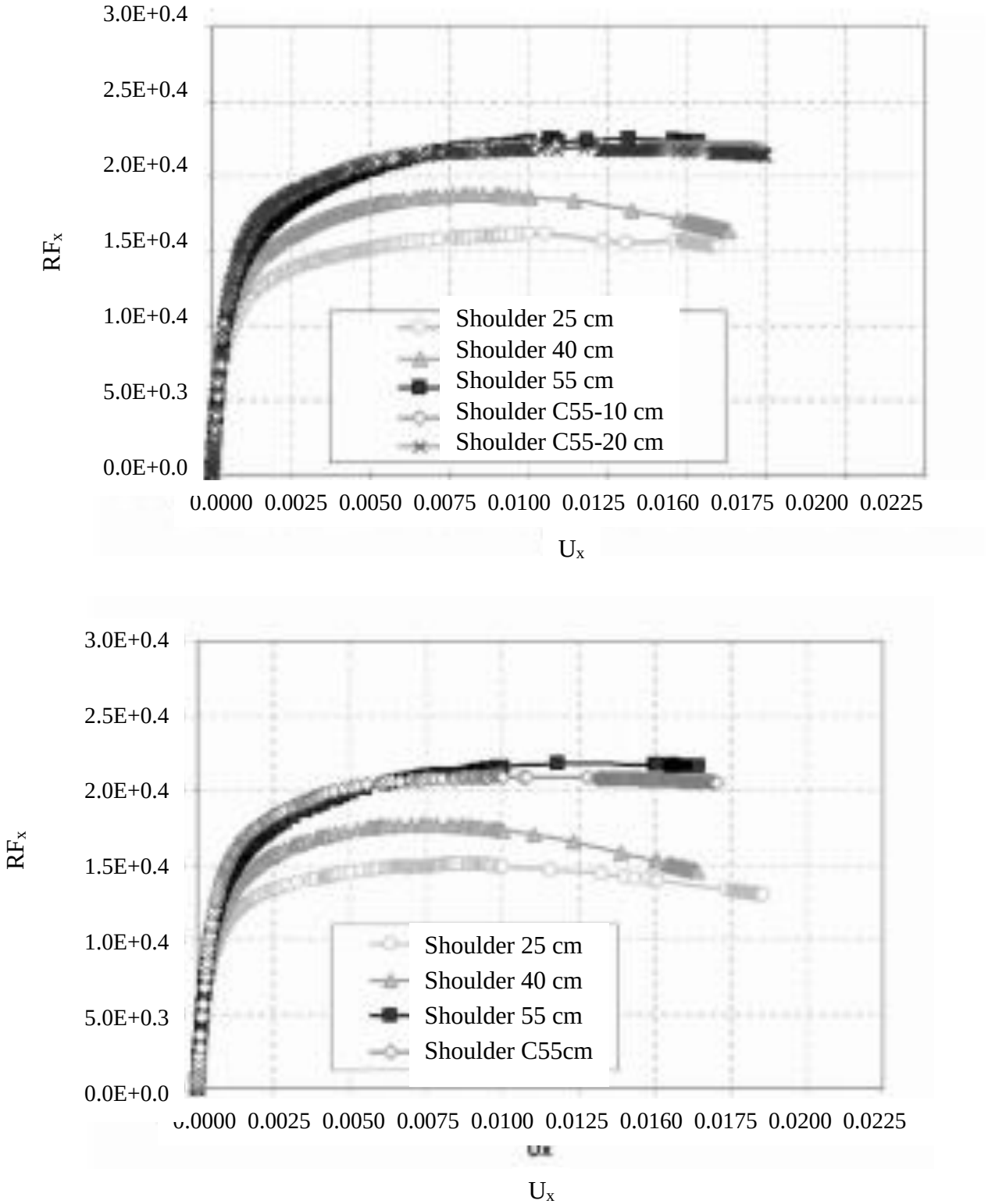

Figure 2-11 Influence of ballast geometry on reaction (N) as a function of lateral displacement (M) combined with a vertical load fy. Coefficient of friction between ballast and sleeper is v. C denotes elevated ballast shoulder used on sharp curves: Fy = -15, v=0.1; b) Fy = 1kN, v= 0.1; c) Fy = -15kN, v= 0.8; d)Fy= 1 kN, v= 0.8 [20]

The researcher in [21] studied the influence of friction coefficient between ballast particle and between ballast and sleeper using discrete element method [21]. He concluded that with larger friction coefficients, the lateral resistance increases and it is important only at the beginning, when the sleeper has been moved 3 millimeters, then, the lateral force is dominated by the resistance of ballast shoulder, and not by friction between sleeper bottom part and ballast stones [18].

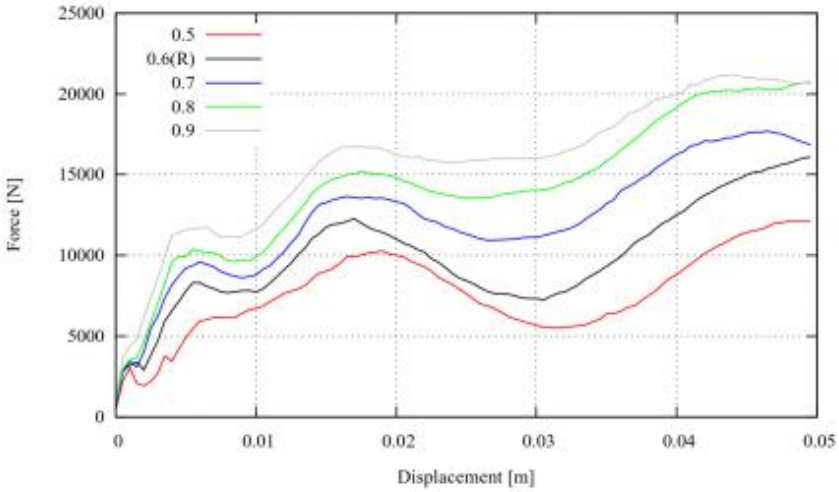

Figure 2-12 Obtained results varying friction coefficient between ballast stones

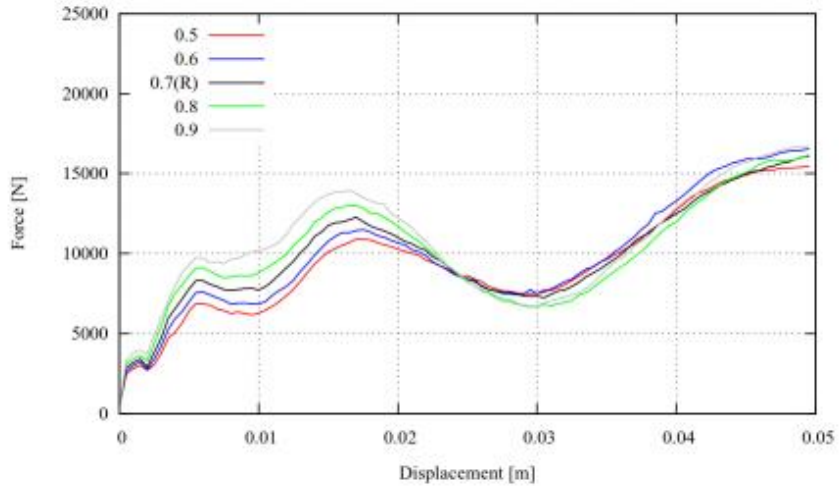

Figure 2-13 Obtained results varying friction coefficient between ballast and sleeper [18]

2.7 Loads

There are two types of loads, that can be applied on track; the load due to braking/accelerating of the train and the thermal loads, but for the analysis of lateral

behavior of the curved track only thermal load can be applied. [22] However, Lim N. et al. [23] considered axel load coming from the rail but not the temperature change.

Research findings in [24] agreed findings in [22] and showed that, in case the buckling temperature (Tmax) is used as allowable temperature of CWR, one has to manage the lateral ballast resistance (lateral tie resisting force, elastic limit displacement) and the maximum amplitude of the track irregularity (alignment defect, gauge irregularity) in priority at the installation and maintenance procedure. Also, in case the safe temperature (Tmin) is used as an allowable temperature of CWR, one has to manage the lateral ballast resistance and the longitudinal ballast resistance (longitudinal tie resisting force, elastic limit displacement in longitudinal direction) in priority at the installation and maintenance procedure of CWR.

Definition of the reason of neutral temperature variation on the curve. Calculations showed that for normal concrete sleepers (lateral resistance 67 kN/m) by changing in rail temperature by 45 degrees Celsius, the natural temperature rises about 10 degrees Celsius. This value decreases to 5.5 °C for frictional sleeper [25].

The research carried out by André Prud'homme at SNCF during the 1950s and 1960s1 concluded that if the lateral force exerted repeatedly by an axle on the track does not exceed a certain value H, the residual deflections do not add up indefinitely and the final deflection stabilizes within acceptable limits. Lateral loads kept constant at all passes provided a relationship between residual deflections and a large number of passes. Results from this were used to define “critical” loads and conditions. Based on the tests, Prud'homme developed the first empirical equation for the lateral strength of a wood sleeper track under vertical axle loads. Over the years, this equation has served as a guideline for acceptable vehicle loads on track, sometimes interpreted also a panel shift limit. This Prud'homme limit, L_P is given by:

$$\mathbf{Lp = 10 + V/3,} \qquad \mathbf{(2.1)}$$

where V is the vertical axle load in kN. This empirical criterion originally defined the limiting track panel strength of a wood tie track with tamped ballast required to prevent lateral shift under repeated loads. This formula did not account for the curvature and the rail thermal load effects. Prud'homme later recommended a multiplying factor of 0.85 to L_P for these effects. This is known as 85 percent of the Prud'homme limit.

The results of tests conducted in the 1990s by SNCF with concrete sleeper track, welded rails and ballast compacted by a dynamic track stabilizer on the Paris - Lyon high speed line did not require any significant changes to be made to the Prud'homme formula, as reflected in current SNCF practice. H is defined as the maximum repeated lateral force which is permitted to be exerted on the track by the vehicle.

According to SNCF, the Prud'homme limit was not exceeded during several subsequent measurements made to evaluate the maximum lateral forces exerted on the track during tests at 408 and 482 km/h. This provided further validation for the use of the Prud'homme limit by designers and manufacturers of 1435 mm gauge rolling stock, and it provides the basis for the allowable maintenance tolerances for vehicles.

Concrete-sleepered track must be designed such that the static lateral panel resistance is not less than

H= 0·85 (10 + 0·33P) maximum lateral force exerted by an axle,

H = (24 + 0·41P) minimum track panel resistance in tamped condition,

H = (38 + 0·63P) minimum track panel resistance after use of stabilizer,

where P is axel load of the train.

In order to determine the lateral loads in the track, the Office of Research and Experiments (ORE) performed test programs for train speeds up to 200 km/h. These studies indicated that the lateral load is influenced only by the radius of the curve, and the following empirical equation was suggested to use:

$$\boldsymbol{P_{Lc} = 35 + \frac{7400}{R_c}} \quad , \qquad \textbf{(2.2)}$$

where, P_{LC} is the lateral force at curved tracks on the outer rail (kN), and Rc is the radius of curve (m).

Accurate assessment of the exerted lateral force transmitted from the outer rail to a single sleeper is very difficult because this portion is function of various parameters such as configuration of bogie axles, type of fasteners, sleeper spacing, ballast and track conditions

and etc. however, according to AREMA. The distribution of the total later force between railway sleepers can be assumed as same as the vertical distribution between them.

A simple analytical representation indicated, lateral resistance as spring load-deflection response characteristic representing sleeper-ballast interaction. Kish Initial linear stiffness, peak (break-away) value, and a decreasing (dropping) portion to a constant "limit" value for strong, average, and weak behavior of concrete sleepers are describe as shown in Figure 2-14.

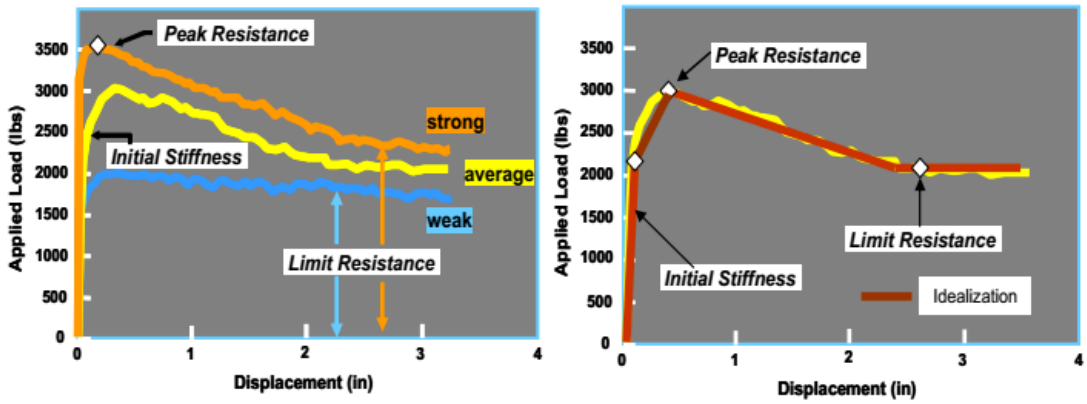

Figure 2-14 Lateral resistance load deflation characteristics [1]

As per the work in [1] the particular requirement is a high lateral resistance elastic limit, which can be achieved through a high peak resistance value. The impact of such high elastic and peak values is an allowance for higher net axle L/v and higher speed [1].

The lateral resistance of track reduced at the mid-section of the bogies (track uplift) and increase in the position under the vertical load.

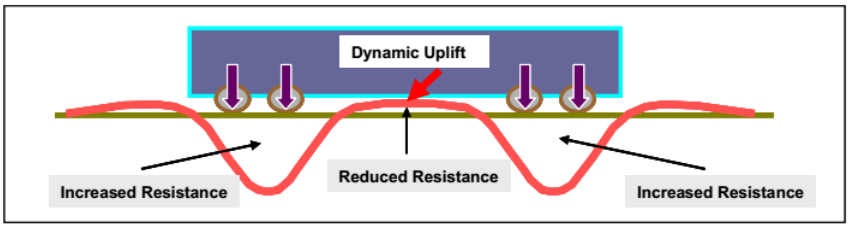

Figure 2-15 Dynamic load resistance concept

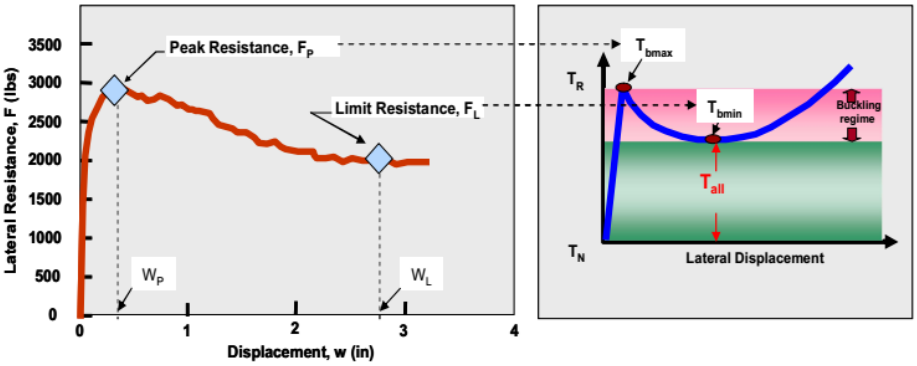

Figure 2-16 Peak and limit resistance impacts on bulking temperature [1]

Numerical simulations of ballast deformation in track carried out by [20], to study the resistance of track under vertical and lateral loading. Sleeper displacements are studied under different conditions in order to find out which lateral resistance the ballast will provide and how this resistance depends on various parameters. He didn't consider material softening property, but he tries to include the effect of vertical loading in three levels, -15, -5, and 1 kN. He assessed the results in terms of force-displacement relationships, sleeper displacements, and localization of highly stressed band.

There is a question that always arise when thinking of CWR tracks and accidents; whether the lateral bulking of track is due to vertical load at time of passing of the train or does it happen while the track is not loaded. To answer such question the researcher in [19], included the effect of vertical load on lateral resistance and stability of a railway track using frictional sleepers in comparison with conventional sleepers.

Based on the theory, with increasing vertical load the curve's inclination also increases this research evidently interpret ballast's nonlinear behavior and prove the rise in ballast's lateral stiffness due to the increase in the applied vertical load. A comparison of values implied that the friction coefficient for the track with the frictional sleeper, when loaded, is approximately 91% higher than the case of a conventional sleeper. As a result of the study, with increasing vertical load, the track's lateral resistance increased in the track with on both concrete sleepers. The result indicated that sleeper resistance increased when the loading rate and lateral movement increased and reached the maximum at a displacement of 2 mm [19].

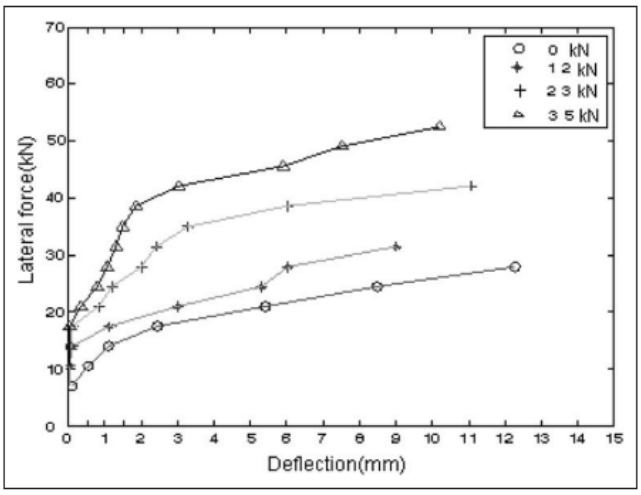

Figure 2-17 The lateral load- lateral displacement curve for the frictional sleeper at four different vertical loading states [19]

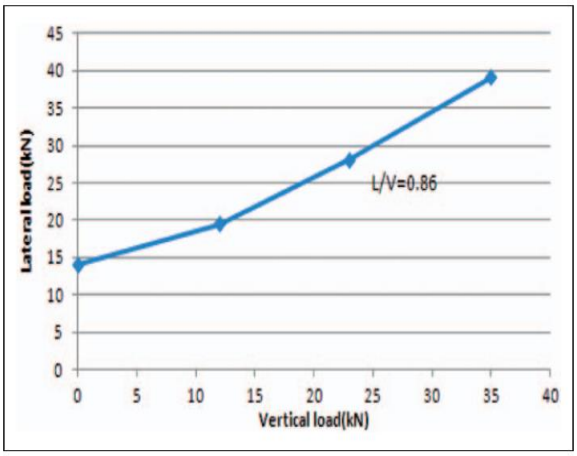

Figure 2-18 The lateral force-vertical force diagram for a 2mm track displacement of track with a frictional sleeper [19]

Surfacing and tamping can reduce track resistance (TLR) by 40-70%, depending on ballast type, ballast section, concrete type, design and condition, etc. [1]. But the investigation has proved that the effect of axial forces on the value of work necessary track displacement under condition of stabilized ballast bed is considerably smaller in comparison with the effect of interaction between the sleepers and the ballast bed. However, the authors do not suggest drawing and univocal conclusions at this stage of the research which has not been completed and requires continuation. On the result, effect of axial force on the value of energy needed to deform the track laterally for s= 10 mm shown on bar chart.

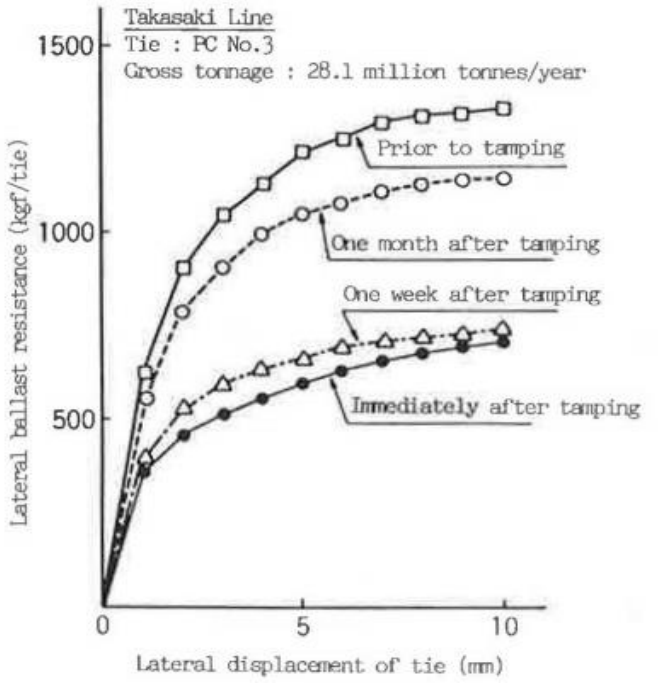

Figure 2-19 Characteristics of lateral ballast resistance [1]

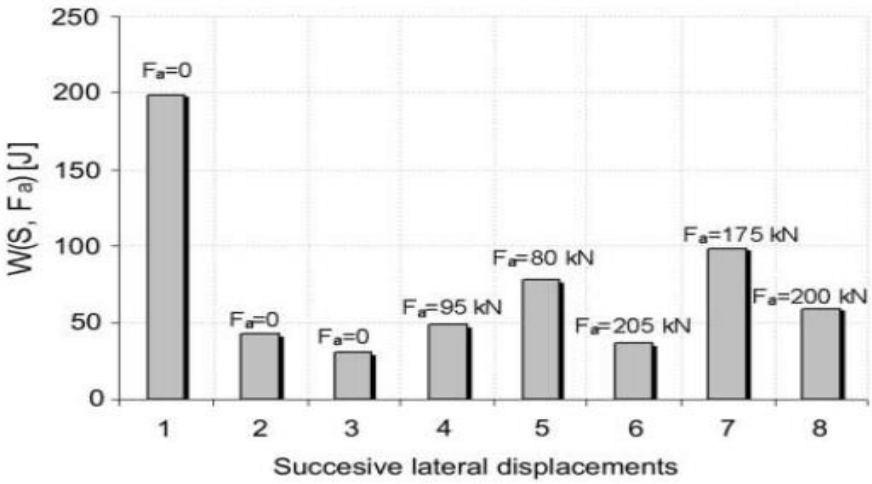

Figure 2-20 Values of energy W(S,Fa) as a function of axial force Fa in the rail with lateral force Ft applied to the same point for displacement S=10 mm [1]

Louis P. [2], quantified likely magnitudes of pendolino train loading for normal and extreme conditions by summing the effects of curving forces, wind load and static axel load on low radius curves. The potential for lateral resistance is largely governed by vertical stiffness of the track. It showed that loading at the wheel/rail interface can be

transferred to individual sleeper loading a BOEF analogy adapted to both vertical and lateral representations of the track.

Over the length of the train the maximum lateral curving force generated can be found using the relation [2]:

$$F= mv^2/R. \quad \textbf{(2.3)}$$

The DAF can be calculated by employing simple empirical equations.

Table 2-1 Summary of equation suggested for calculating the DAF

Researcher	Suggested DAF equation
Talbot(1918)	DAF= 1+ 0.0062(V-8)
Clarke (1957)	$DAF = 1 + \frac{19.65}{D_w\sqrt{k}}$
Sirinivasan (1969)	$DAF = 1 + \frac{0.017V}{\sqrt{k}}$
AREA (1984)	$DAF = 1 + \frac{5.2V}{D_w}$

Impact load

Formerly the main focus area becomes exerted impact load on the rail therefore Koc W. [26] and Iorio A. [16] introduced the related fulfilled works on the track lateral resistance and lateral forces generated in ballasted railway track then, comparison is done between dynamic lateral resistance (DLR) of B70 sleeper and the relevant laboratory works. After two years [26], investigate and compare the dynamic resistance (DLR) of various types of sleepers (concrete, wooden and steel sleepers) under lateral impact loading conditions.

The research in [22] the laboratory test result indicates DLR of concrete, wooden and steel sleepers were calculated as 12.2, 5.1 and 2.35 KN, which were considerably higher than their static lateral resistance(SLR) of 6.2, 3.1 and 1.75 KN, respectively. So they stated the ratio between DLR and SLR of concrete, wooden and steel sleepers as, 1.98, 1.65 and 1.34 repetitively. To know the magnitude of ballast – sleeper interaction they subtract the sleeper inertia force, which is multiplication of hammer mass and impact load on the sleeper lateral face, from the impact load. In addition, the value of track lateral displacement corresponding to maximum lateral force is varied from 2 to 50 mm. The impact load induced on the concrete sleeper lateral face is too much higher value. So they

concluded that the concrete sleeper is more vulnerable to impact loading in comparison with wooden and steel sleeper. They set value of 1.6 can be considered as an impact coefficient for the lateral force [22].

The impact of dynamic uplift is that a percentage of the sleeper bottom component can be lost whereas under load the resistance is increased [1].

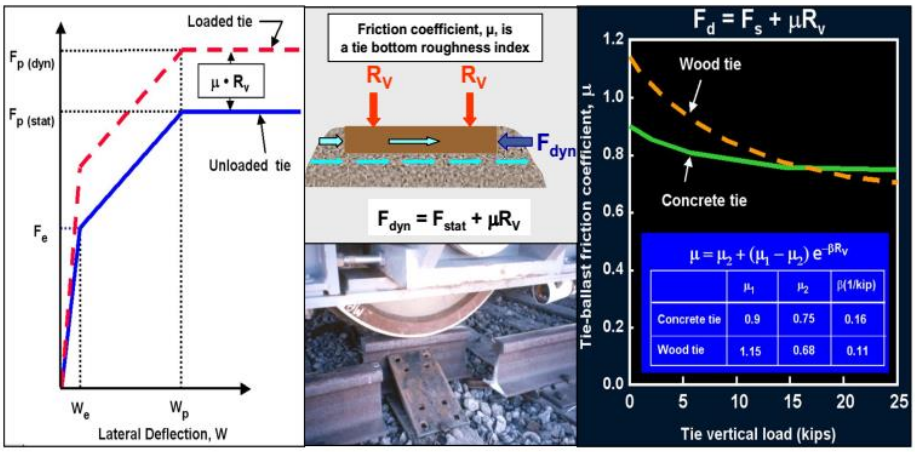

Figure 2-21 Dynamic resistance friction coefficient behavior [1]

Loads likely to reach on the sleeper

It is possible to reach extremes levels which place the trains at risk of overturning provided the track remains structurally sound, attention is now turned to evaluating the proportion of load that are likely to be transferred to the sleeper. By calculating appropriate ranges of sleeper loading it will then be possible to test the sleeper/ballast interface using the laboratory apparatus.

Both vertical loads and lateral loads on single sleeper is made using BOEF analogy. For the lateral loads to decrease the complexity the following modifications is assumed

- The lateral supports are elastic and of constant stiffness,
- The pandol fast clip fixings between the rails and sleepers provide additional torsional stiffness about a vertical axis.

$$F = mv^2/\mathrm{R}\,. \qquad (2.4)$$

The load required to cause failure at the sleeper/ballast base contact area is expected to be proportional to the applied vertical load. The lower the vertical load the lower the portion

of vertical load reaching a sleeper immediately beneath on axel and hence the lower the lateral track modulus the greater the lateral resistance at failure. The greater the lateral track modulus the greater the proportion of the load reaching a sleeper immediately below an axle. Therefore, failure is most likely when low vertical track modulus and high lateral track modulus are present [2].

2.8 Methodologies to determine lateral resistance

In early 20's utilizing tamping machine to investigate lateral resistance of geometrical railway track and they present an analytical approach to the evaluation of lateral resistances based on a continuous registration of the displacement and the force used by tamping machine for displacement of track on a horizontal plane (track shifting) [27].

To avoid high degree of uncertainty when predicting the lateral resistance of single sleeper and to clear up the effect of sleeper spacing on lateral resistance, Single Tie pullout test (STPT) and track panel pullout tests (TPPT) were conducted by [22].

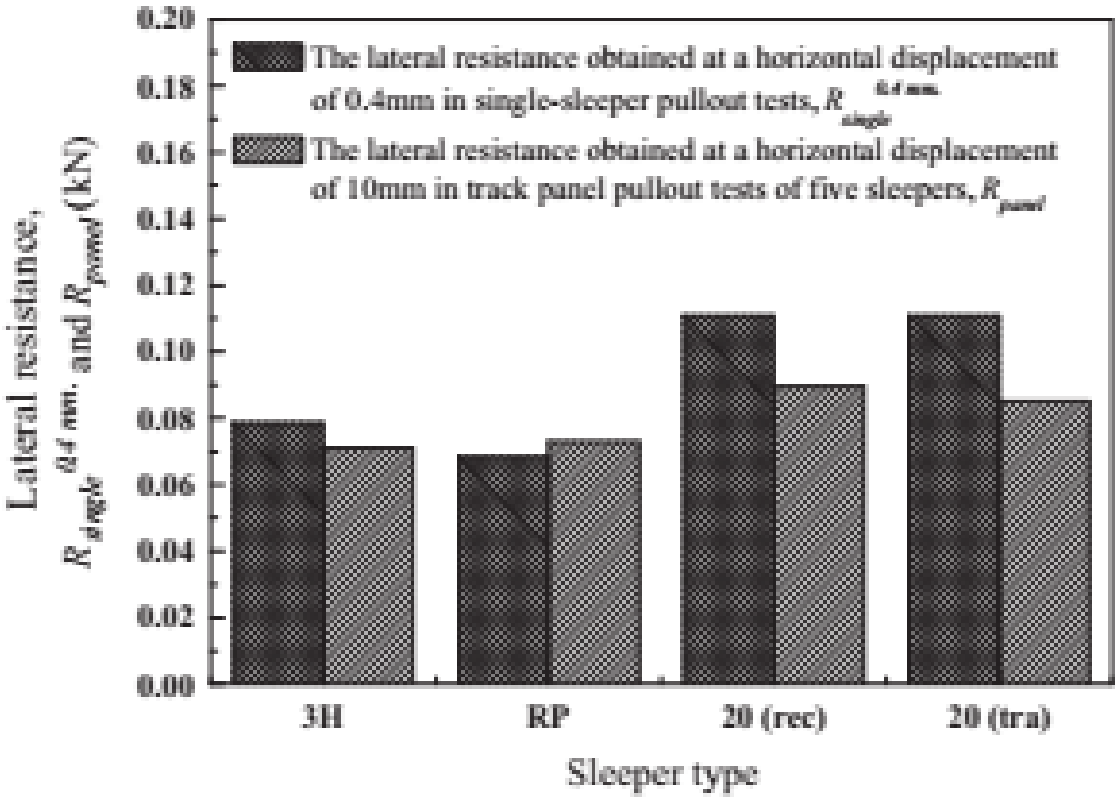

Figure 2-22 Lateral resistance per sleeper obtained from track PPT and STPT [22]

An experiment, both field and laboratory was conducted on a tack with and without frictional sleeper [6].

With the intention of avoiding the need of special test vehicle (derailment wagon) to measure dynamic resistance of ballasted railway track, In Iran university of science and technology [22] develop new experiment method an innovative pendulum loading test device (PLTD) for based on pendulum theory on basis of the process of creating numerical model and manufacturing the PLTD explained using a lumped mass dynamic system. Then [16] utilized the device, for a number of lateral impact tests.

For simple presentation of railway track much of the studies are done by using FEM. For instance, numerical simulations carried out by [20], to study the resistance under vertical and lateral loading using ABAQUS. The ballast modeled as a three dimensional elasto-plastic constitutive continuum model of a granular material that accounts for nonlinear hardening using finite element simulation with deformation in a track (focus on lateral resistance) and the sleeper modeled as an elastic body with material properties of concrete [20].

In 2014 H. Laura et al used elastic linear material for sleepers, rails, and rail pads in their model on stress study. But they confirm that this simplification cannot be adopted for granular materials (share the nodes at the contact surface) like ballast which have elastic response under very low levels of stress and plastic behavior under higher stress. To consider a special treatment to the contact between the sleeper and ballast interface they use bounded degrees of freedom, which is adopted by ORE committee D-117. This required the introduction of different nodes for each material at the contact plane and the nodes con move at different values in the direction parallel to the contact plane. They assumed Druncker-Prager elasto-plastic behavior for the ballast, which is based on hydrostatic stress and implies that the reloading occurs in the same manner as unloading [9].

Researcher in [15] agreed with researcher in [10] model, the materials of sleeper and ballast layer are considered elastic and elasto-plastic, respectively. Because of the reason, for more lateral displacement more than 2mm, the track's behavior is considered to be that of an elasto-plastic state [28].

Researcher in [5] conducted a numerical analysis on frictional sleeper on its lateral resistance for the first time. In this regard, a hardening elasto-plastic behavior model was developed for the ballast layer and ABAQUS software was used to numerically analyze the lateral resistance of frictional concrete sleeper. In ABAQUS two contact properties on interaction module was conducted in modeling studies: first, normal contact and second, tangential contact [5].

Zakri et al. [25] model whole and half-track finite element in which the rails and sleepers are represented with their nominal 3D geometry using solid elements. For the concrete sleeper, they assumed non-prestressed homogenous elastic material behavior and as Simplification of the nominal field condition, they laterally restrict by fixing the nodes of the sleeper connected to the ballast in the lateral direction [29].

Analysis of track lateral behavior of curved track under thermal loading is possible by using a numerical model LONGIN, which is developed for the analysis of creep behavior of CWR by Krakow University of Technology. In the software, rail is considered as prismatic and perfectly elastic beam element (Euler beam), sleeper is modeled as spring element connecting to the rail and providing longitudinal and lateral resistance of track, and the ballast is modeled by horizontal and vertical spring elements which provide the longitudinal and lateral stiffness of track structure [23].

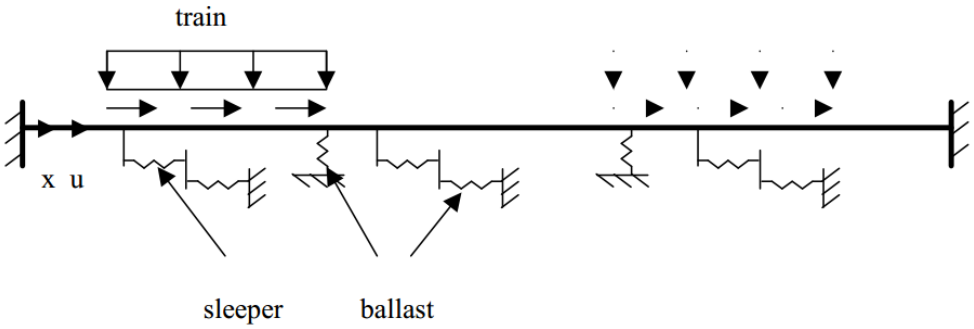

Figure 2-23 Model of track under moving train loading [23]

Gonzales S. [12] created a finite element model of turnout by restraining; all rotational degrees of freedom, two translational degrees of freedom, longitudinal translation, and vertical movement for the rail section; restrained two rotational degrees of freedom and vertical movement along the entire length of the model for the sleepers.

Landuyt B. [21] novel his work by developing the discrete and finite element model able to calculate railway ballast interaction, where other discrete element model representing granular material as sphere aggregates (sphere clusters).

Using elasto-perfect plastic finite element model Yonug- Jong Kang investigated the influence of the lateral and longitudinal ballast resistance. The rail is modeled by a thin-walled mono-symmetric open section beam element with typical 6-degree of freedom and an additional torsional-warping degree of freedom per node. The solid beam on elastic foundation element having 6 degree of freedom per node is used to simulate a cross tie including a vertical and longitudinal ballast resistance. To reduce the number of nodes and elements in the model infinite boundary element (IBE) was used [24].

Using finite element package LS-Dyna to analyze the dynamic response of single span ballasted track in 2018. On the simulation the sleeper and rails are modelled by solid element with eight nodes with three degree of freedom(translation) and truss element is used to model the pre stressing wires by assuming perfect bond between pre stressing wires and concrete (by neglecting the bending moment and shear force on the element). But they did not consider the lateral resistance of sleeper. However, due to the random placement of various size of ballast, sleeper was not completely flatly placed on the ballast bed.[30]

Zakri A. [15] demonstrated that the ratios of numerical to experimental results for concrete, steel, and wooden sleepers ware 1.02, 1.03, and 1.05, respectively.

Miura S. [14] based on the result of CWR, the radii of curvature exceed 600m, developed empirical formula for ballast resistance per sleeper;

$$F = aW + brGe + crGs,$$

where W= track mass on a sleeper,

R = bulk density of ballast,

Ge= statically moment of area around top chord of a sleeper end,

Gs = statically moment of area around top chord of sleeper side face, and

a, b, c, r = coefficients depend on sleeper type and ballast.

CHAPTER 3 MATERIALS, METHODS AND PROCEDURES

3.1 Studied Railway Track

The aim of this study is to compare the performance of different concrete sleeper designs against conventional sleepers in terms of lateral resistance. The analysis for the several railway track settings regarding the sleepers must be carried out under the same conditions in order to allow they are comparable between each other.

In order to create a common ground for all models that is built, one track is selected from AALRT rail way section.

With the definition of the various assumptions, a framework is obtained in which the model can be designed, and compared to other existing models. This framework should also be considered when validating the model, because different assumptions can lead to discrepancies between models. Most of the assumptions relating to the mechanical properties are already clear from the literature review, as there are often conventions in research how certain parameters should be modelled. The boundary conditions of the model however, are not so rigidly defined in existing literature. Therefore, the `real' conditions should be replicated as closely as possible, while also taking the models which will be used for validation into account.

3.1.1 Geometry

A radius of sharpest curve railway track, which is placed in Addis Ababa light rail transit (AALRT), is analyzed. Then, the proposal of a solution to increase the speed of the train though out the curve is made by simulating different track sleeper designs and spacing. the track geometry of AALRT has two phases; North South(NS) line and East West (EW) line. From those two lines the NS line has many sharp curves as indicated in the figure below, the sharpest three curves are on slab track and the rest are on ballasted track. The curve for simulation of a tack is taken from the sharpest curved section on the ballast.

The geometry and subgrade profile of the track 3D FE model developed to simulate the problem is indicated in Figure 3-27, which is composed of layers of rail, sleeper and ballast. The longitudinal dimension of the track model is characterized by small segment of the horizontal curve.

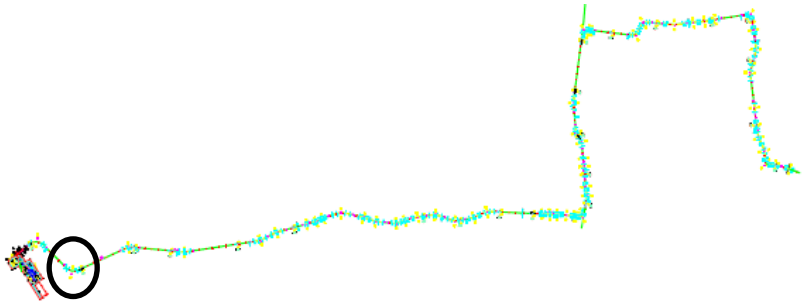

Figure 3-1 AALRT railway track horizontal geometry NS line

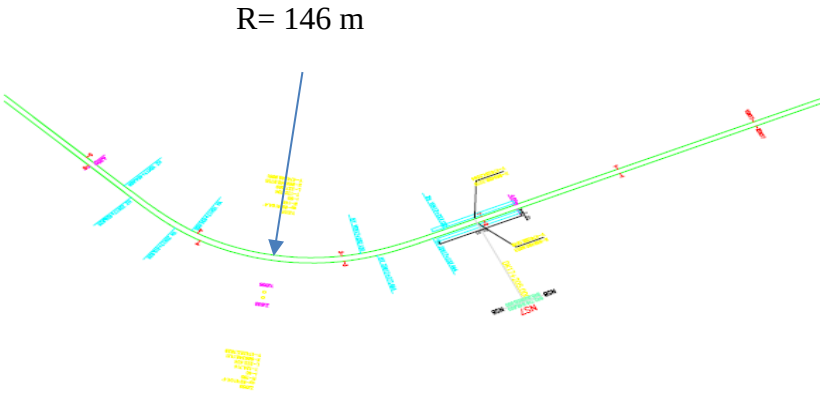

Figure 3-2 Studied track curved top view

Figure 3-3 Studied track on google earth

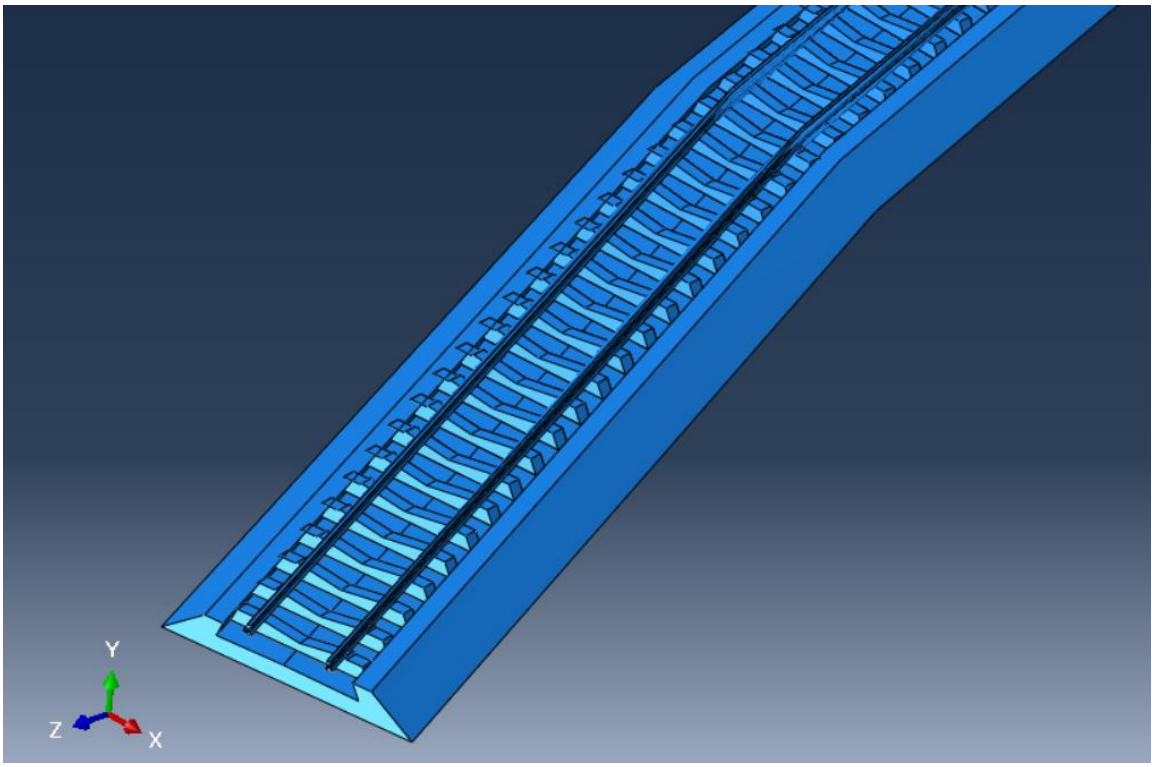

Figure 3-4 Section of simulated curves track

3.1.2 Speed of the train

Even if the track is designed for the design maximum speed of 80 km/h, from a data taken from AALRT indicates that the train speed is limited at curved section up to 12 km/h which made the average speed of a train to 20 km/h. [31] though the lateral strength of track has to be increase the speed limit. The lateral strength could be improved by means of improve design of sleeper that enhances the frictional behavior of the sleeper-ballast contact.

For the current study the design speed applied to the model is 20 km/h, 40 km/h, 80 km/h, and 120 km/h.

3.2 Design of sleepers

A key parameter having a large influence on buckling strength is the sleeper-ballast lateral resistance. This resistance has three contributing components, as shown in Figure 3-5 Lateral resistance components, and indicated by [1]: bottom friction (F_b), side friction (F_s), and end or shoulder resistance(F_e).

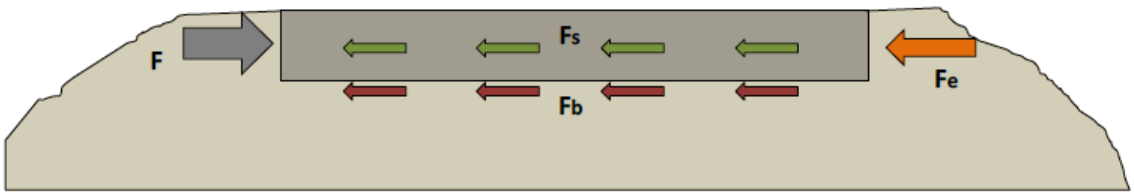

Figure 3-5 Lateral resistance components [1]

$$F_l = F_b + F_s + F_e \text{ ,} \quad \textbf{(3.1)}$$

$$F_b = \mu f Q \text{ ,} \quad \textbf{(3.2)}$$

For uplift

$$F_{pdynamic} = F_b - \mu_f Q \text{ ,} \quad \textbf{(3.3)}$$

For other case

$$F_{pdynamic} = F_p - \mu_f R_v(x) \text{ ,} \quad \textbf{(3.4)}$$

where F_l is the lateral resistance (N), F_b is the base lateral resistance (N), F_s is the side lateral resistance (N), F_e is the end shoulder's lateral resistance (N), μ_f is the roughness coefficent F_p is the peak lateral resistance (N), R_v represents the distributed vertical forces between the sleeper and the ballast (N) and Q is the weight of the sleeper (N).

By increasing any of the components form F_b, F_s and F_e, one can improve the resistance of sleeper against lateral movement. This research focus on increasing track lateral stability by maximizing friction between sleeper and ballast and increasing the mass of the ballast that support the sleeper.

The first modeled sleeper is Chinese Type II sleeper. The detailed drawing and dimensions are shown in Figure 3-6. In order to increase the contact area and friction between the sleeper and ballast, different shapes of sleepers were proposed to be studied. The design was based on the addition of prominent wings and modifying the base surface of the sleeper in order to increase some of the contributing components of the lateral resistance. The four types of sleeper shapes are shown in Figure 3-8. To confirm the dimensions referred drawing from literature [32], the actual sleepers dimension is measured directly from stock as shown on the Figure 3-7.

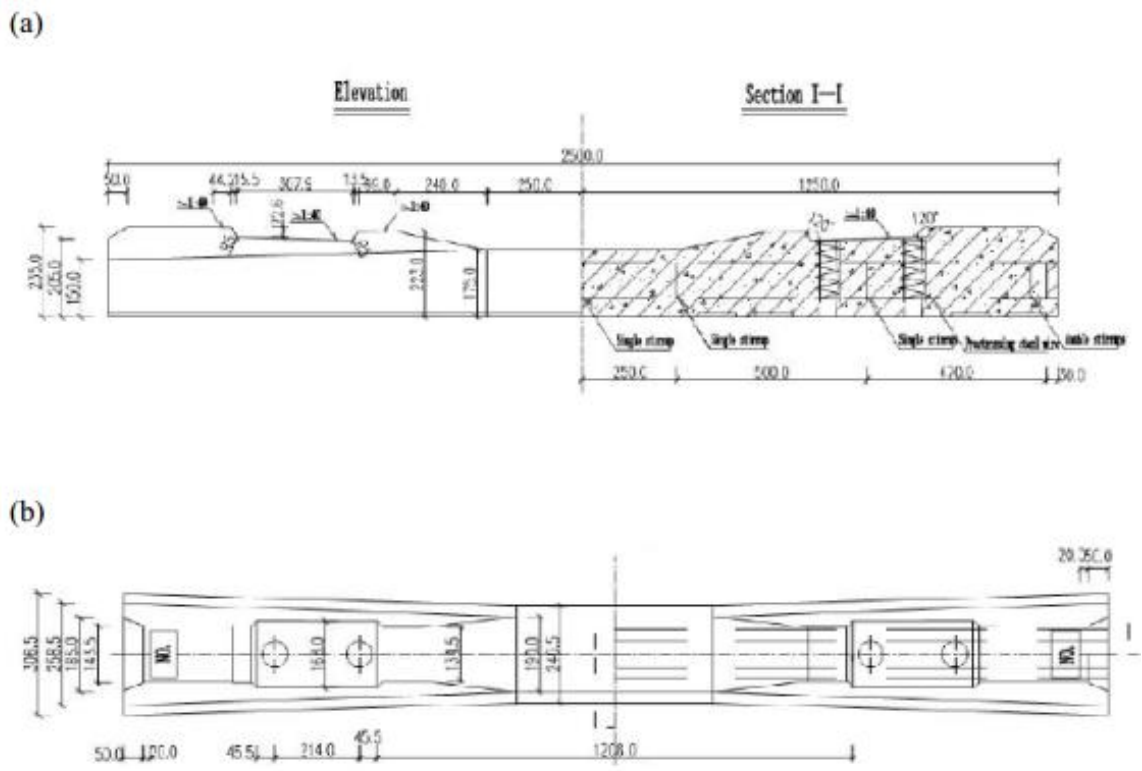

Figure 3-6 Type II sleeper drawing (a) elevation (b) plan

Figure 3-7 Measuring Type II- sleeper from stock

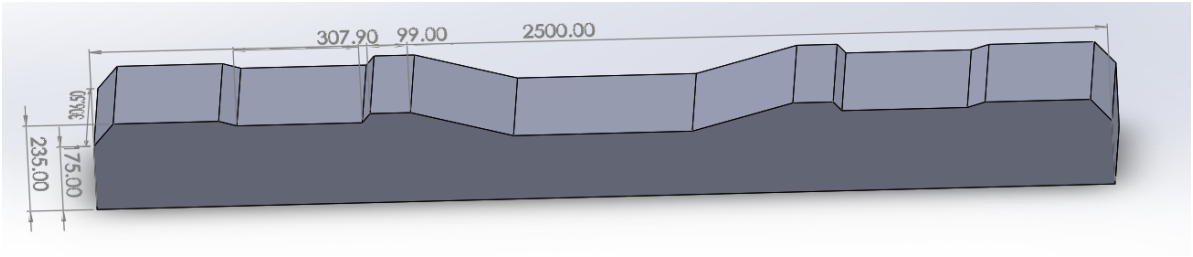
307.90
99.00
2500.00
306.50
235.00
175.00

(a)

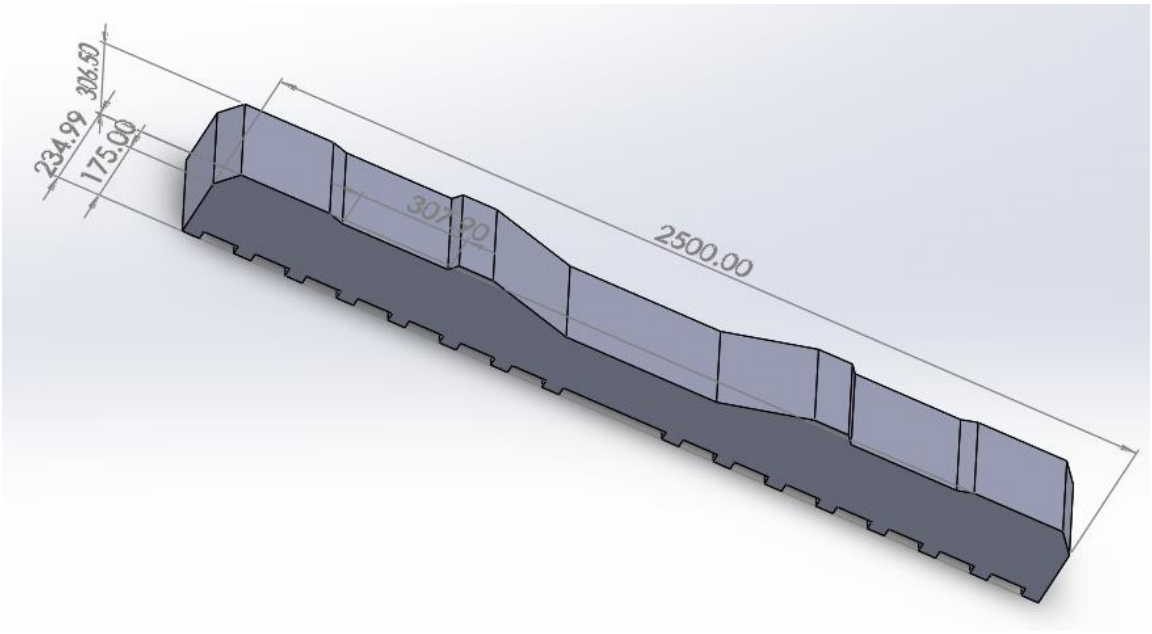
306.50
234.99
175.00
307.90
2500.00

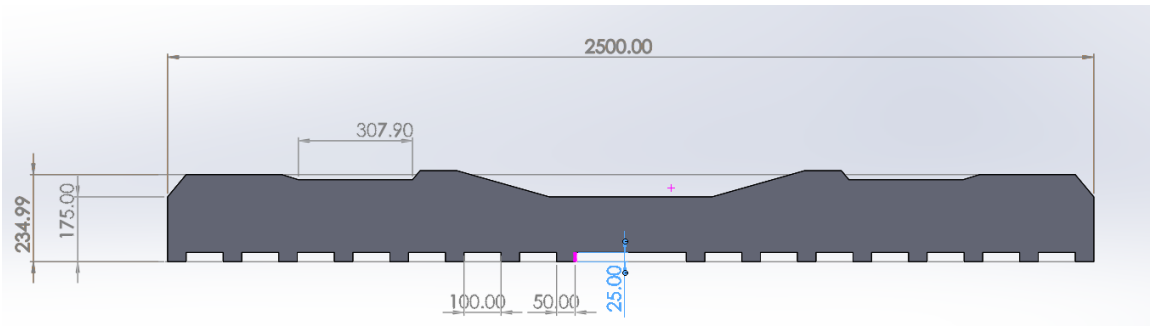
2500.00
307.90
234.99
175.00
100.00
50.00
25.00

(b)

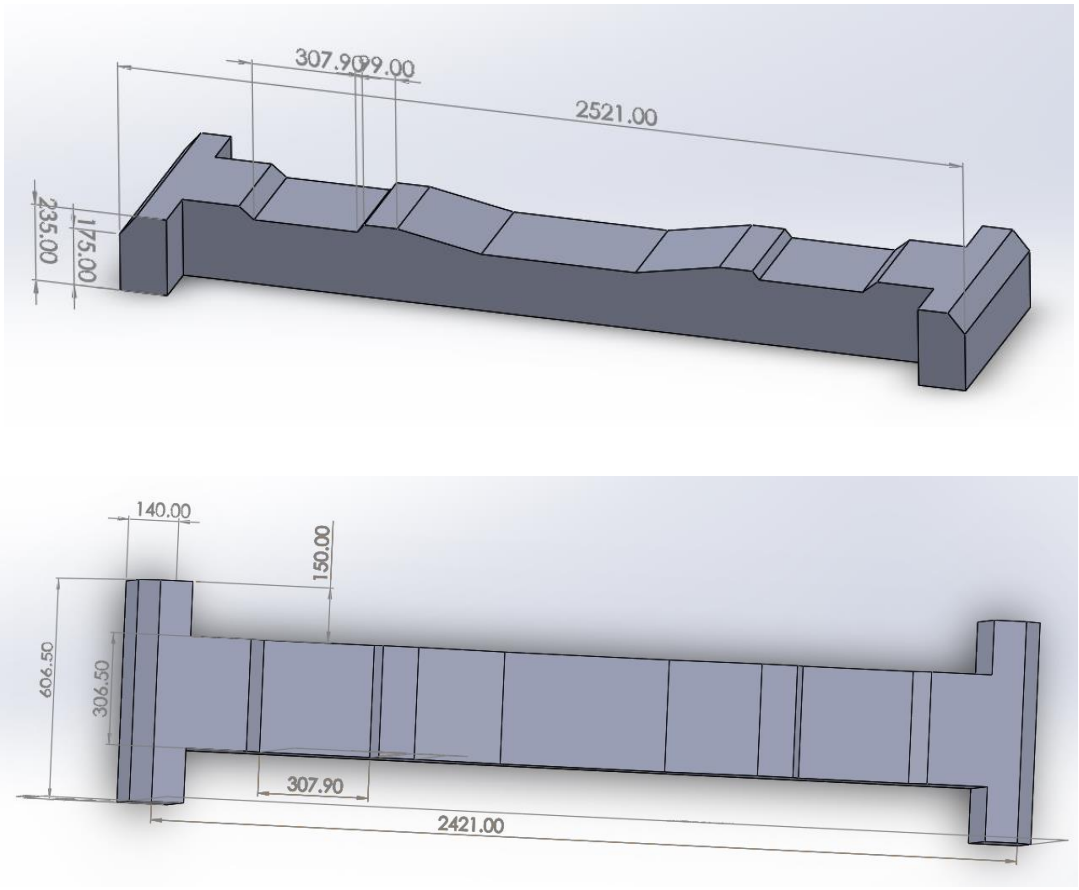

(c)

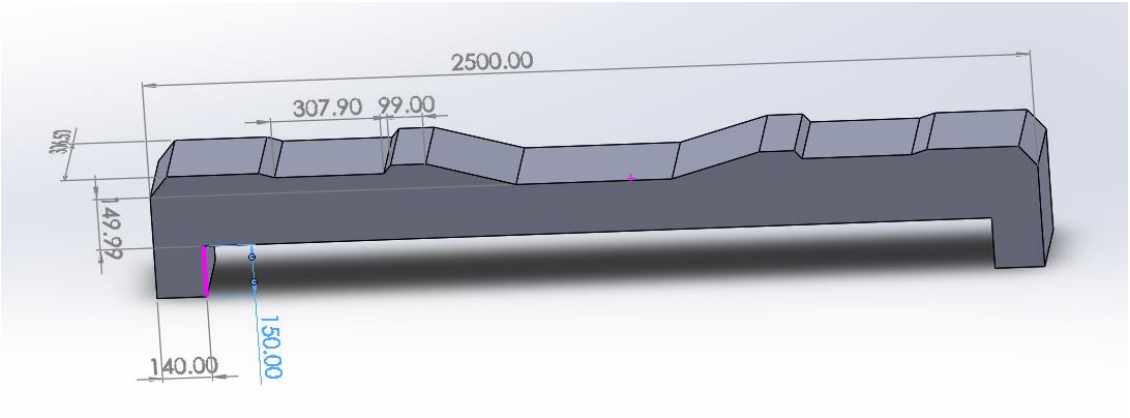

(d)

Figure 3-8 Types of sleeper (a) Chinses type II sleeper (b) frictional sleeper (C) side winged sleeper (d) bottom winged sleeper

The wings at the bottom and side of the sleeper were found to be the more efficient ones to constrain the lateral movement on the literatures. Besides the contribution of ballast bed is higher in lateral resistance. Therefore, making the bottom surface rough have great resistance against lateral movement.

Regarding the size of the wings, it was decided to design a winged equal to 140 mm. The influence of vertical length was investigated concluding that the larger the wing, the higher the lateral resistance, although for just a small difference. However, high wing's length could cause high stress concentration at wing-sleeper joint. Thus, a vertical length of 150 mm was set compromise solution [9].

Sketch and parts of the sleepers is done by solid work 2019 software for simulation purpose. Parameters refer to constraints whose values determine the shape or geometry of the model or assembly.

3.3 Finite element model

The analysis for the different railway track settings regarding the sleepers must be carried out under the same conditions in order to compare each other. Therefore, this research takes the same track condition for all type of sleepers.

The commercial finite element method software, Abaqus is utilized in this study. The software provides both pre-processing and post-processing capabilities. Abaqus 6.11 Abaqus/ CAE user's manual have been followed to develop the finite element model.

In order to choose the numbers of sleeper to be modeled, several trial sections with varying sleeper numbers has been conducted. The models have been analyzed by taking 15, 10, 9, 7 sleepers on one section. From the analysis result it is observed that the lateral load distribution has significant effect up to 9^{th} sleeper and for sleeper beyond 5^{th} sleeper the effect is less than 10%.

The track cross section divided in to two sections; first the section contains rail and sleeper as shown on Figure 3-9 is introduced to determine the distribution of load on sleepers and decide the length of the track that will be affected by the load. Since the section is symmetrical, half of the track cross section is used for the first simulation. Then, the second

section which contains the sleeper and ballast is simulated for different design of concrete sleepers based on the data from the first simulation. (Figure 3-10)

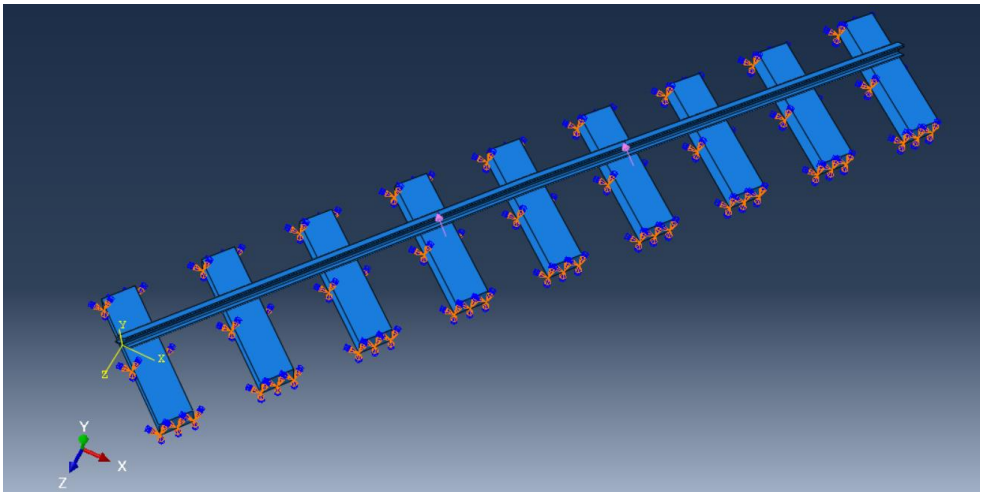

Figure 3-9 Rail-sleeper model

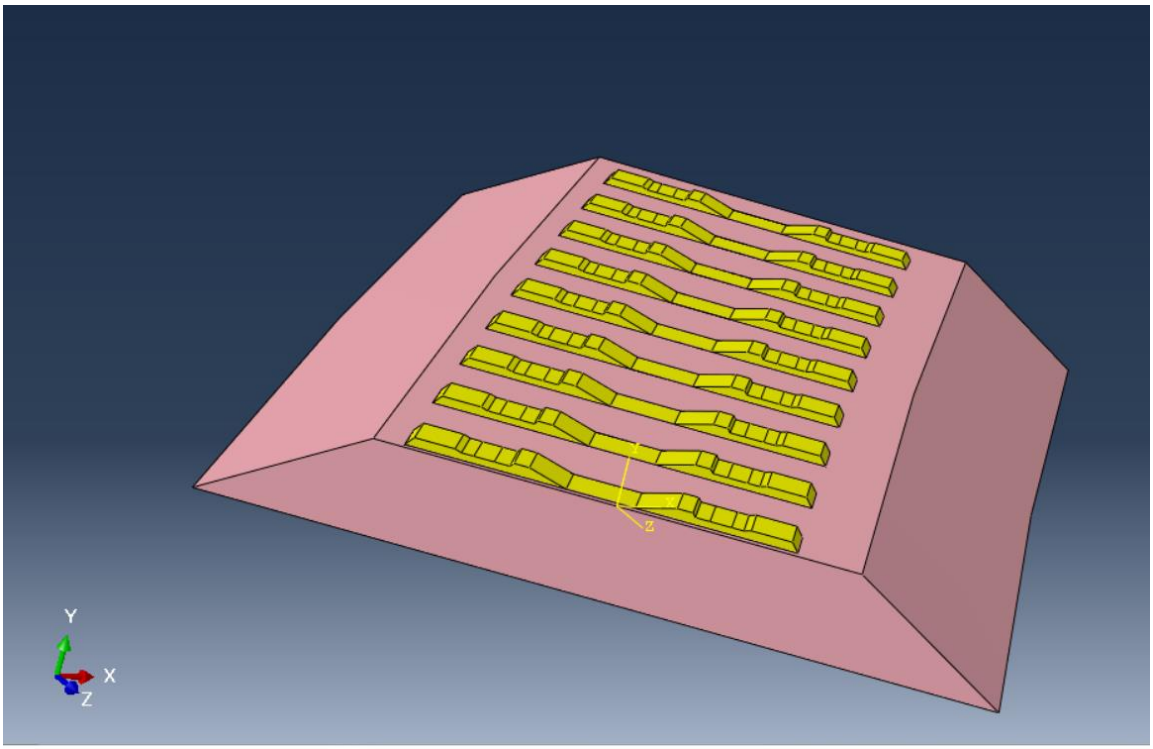

Figure 3-10 Model of track (sleeper-ballast) complete view

A homogenous solid section is assigned for the sections of all components. The interaction property between ballast and sleeper defined as tangential behavior (friction) and normal behavior (hard contact) [33].

A three dimensional model is built by means of free meshing with quadratic tetrahedral elements applied to three-dimensional region; in fact, which very complex models can be meshed using this technique without the help of partitioning [33]. The materials are considered isotropic and linear, except the ballast, which is modeled as a Drucker-Prager material.

The lateral displacement of the sleeper are the needed results to carry out this study. As stress and strains are not requiring output, it is desirable not to use a fine mesh at rail in order to reduce the number of elements in the model, and thus reduce the computation time.

3.3.1 Mesh sensitivity analysis

Before element types and sizes were determined, a mesh sensitivity analysis was performed. Because the mesh density at the contact interface between the sleeper and ballast has a significantly effect on the accuracy of lateral contact force between the two contact bodies during simulation, a mesh sensitivity analysis was performed to determine the optimal mesh density on the sleeper-ballast contact interface. Mesh refinement was only implemented on the perimeter of sleeper and the top of ballast to minimize the number of elements and resulting computational time. Convergence was achieved for lateral displacement of the sleeper under a static wheel load. Four trials were conducted with four mesh sizes: 20, 10, 5 and 3 cm. It was found that decreasing the mesh size by 50%, from 20 cm to 10 cm, led to an 9.37% reduction in the horizontal displacement of sleeper. Further decrease the mesh size by 40%, from 5 cm to 3 cm, only result in a 1% reduction in the horizontal displacement of sleeper. The results indicated a convergence in the last trial.

Based on the results of mesh sensitivity analysis, extremely refined mesh was required to achieve an accurate numerical solution. However, as large number of elements from using dense mesh posed considerably higher computational costs, it was only implemented in the contact area of sleeper and ballast. Coarse mesh was implemented on the other segments of track as they were not directly subjected to the wheel load. 50 mm mesh size is used at the contact and loaded section of the sleeper.

Figure 3-12 shows the final mesh.

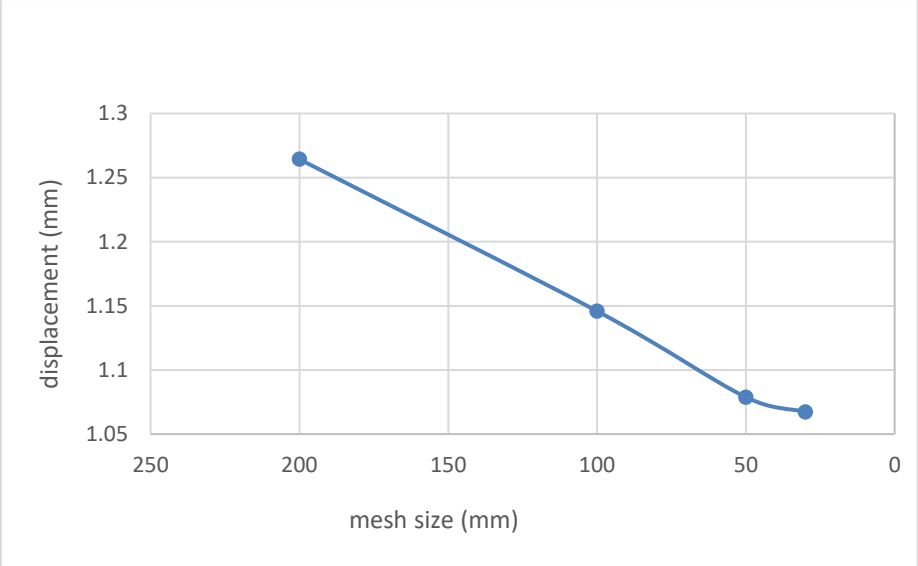

Figure 3-11 Mesh Sensitivity Analysis for sleeper-ballast Contact Interface

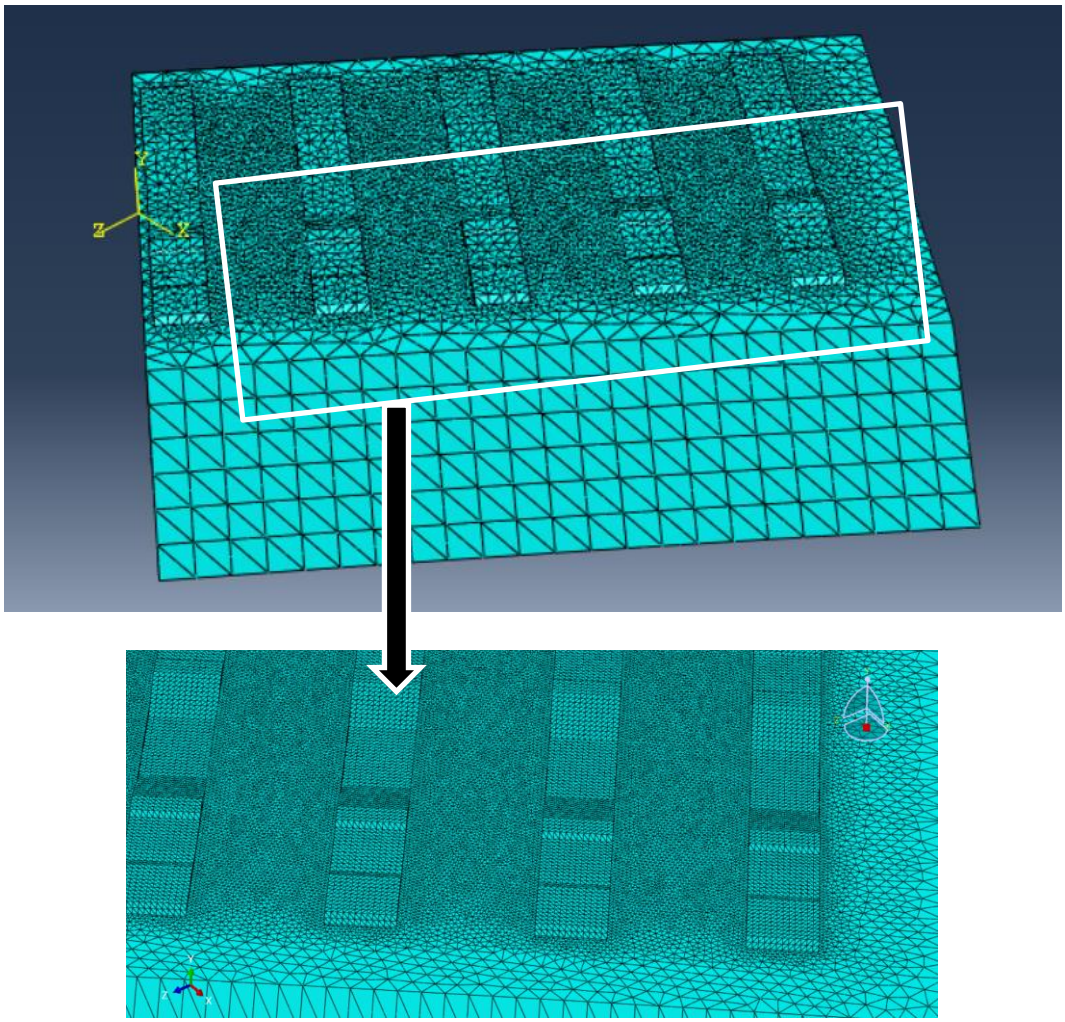

Figure 3-12 Final mesh

3.3.2 Rail Modeling

The rail dimension modeled as shown in the Figure 3-13, which is referred from AALRT. The rail is tied towards the sleepers in order to not allow any movement along all direction relative to the sleeper to avoid the lateral displacement of rail relative to the sleeper. The rail model in the Figure 3-13 is for the existing track with 50 kg/m.

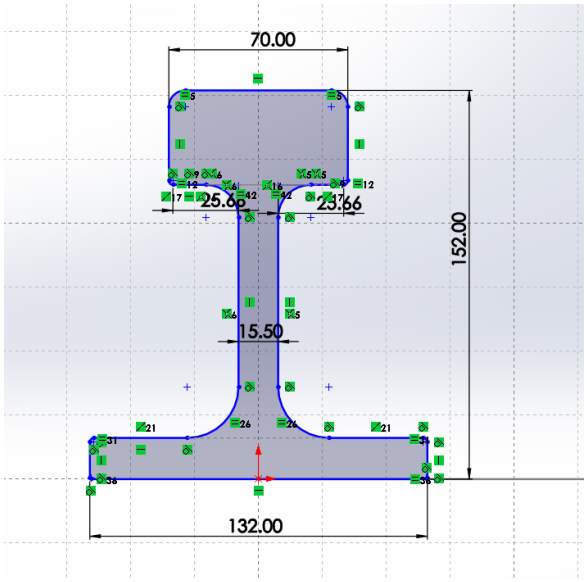

Figure 3-13 Modeled rail section (dimension in mm)

3.3.3 Sleeper modeling

Four different designs of concrete sleeper are considered. One conventional concrete sleeper (Type II sleeper), two winged sleepers, and one frictional sleeper. The conventional concrete sleeper is designed as Chinese type II sleeper. This component modeled to behave like a linear-elastic material, being the modulus of elasticity equal to 36000 MPa and Poisson's ratio of 0.2.

The winged sleeper is sized as the conventional concrete sleepers, and they have wings at bottom and side. The wings have a width of 140 mm and height of 150 mm. The material is considered equal to the conventional concrete sleeper previously mentioned.

The size of frictional sleepers is equal to the concrete conventional one in order to use the same longitudinal setting model. The dimension of the frictional sleeper is showed on Figure 3-8.

For model geometry, accordance to section 4.2, 5 sleepers are placed along the rail at 600 mm spacing to identify the sleeper design with better lateral resistance. The sleeper spacing equal to 600 mm in most ballasted tracks, by taking this value as initial the upper and lower values (500mm and 700 mm) are taken to see the effect of spacing in curved track ballasted railway sleepers.

3.3.4 Ballast Modeling

The elasto-plastic constitutive law based on the Druker-prager yield criterion is commonly used to model the substructure layer in railway track. The extended Drucker-Prager model is available to model frictional materials, which are typically granular-like soils and rock, and exhibit stress-dependent yield (i.e. the material becomes stronger as the stress increases). Furthermore, and also applicable to model materials in which the tensile and compressive yield strengths are significantly different. Thus, the ballast is modeled as elasto-plastic material obeying the Drucker-Prager criterion. The model established the modulus of elasticity: Poission's ratio, the internal angel of friction and cohesion. Used parameters for the track is shown in Table 3-1.

The yield function of Drucker Prager model with linear form is given by,

$$\boldsymbol{F_s = q + \alpha p' - \sigma_Y(\varepsilon_{pl}) = 0} \ , \tag{3.5}$$

where α= material parameter refered to pressure sensitibe parameter,

$$\boldsymbol{q = \left[\frac{3}{2\{s\}^T[M]\{s\}}\right]^{0.5}, \{s\} = deviatoric\ stress\ vector} \ , \tag{3.6}$$

$$\sigma_Y(\varepsilon_{pl}) = yield\ stress\ of\ materal,$$

$$\text{P' = meam effective stress} = \frac{1}{3} * (\boldsymbol{\sigma_x + \sigma_y + \sigma_z}). \tag{3.7}$$

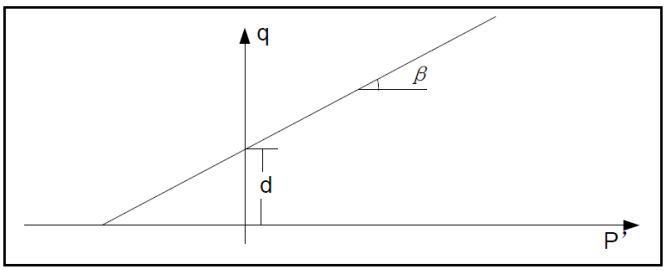

Figure 3-14 Linear Drucker-Prager yield surface in the meridional plane

The non-associated flow rule is utilized in the extended Drucker-Prager material model Isotropic hardening is utilised in the extended Drucker-Prager model.

One of the required parameter for Druker-prager constitutive model is angle of dilation. The angle of dilation controls an amount of plastic volumetric strain developed during plastic shearing and is assumed constant during plastic yielding.

$$\boldsymbol{\Psi = d\varepsilon_v / d\varepsilon_a.} \quad \textbf{(3.8)}$$

For non-cohesive soils (sand, gravel) with the angle of internal friction φ > 30° the value of dilation angle can be estimated as

$$\psi = \varphi - 30°. \quad \textbf{(3.9)}$$

Flow Stress Ratio - The ratio of the flow stress in triaxial tension to the flow stress in triaxial compression, K.

$$0.778 \leq K \leq 1.0. \quad \textbf{(3.10)}$$

The value of equation 3.10 is used to the linear Drucker-Prager model since this is the only model in this class that allows for different yield values in triaxial compression and tension.

By comparing the Mohr-Coulomb model with linear Drucker-Prager model,

$$\boldsymbol{tan\beta = \frac{6sin\Phi}{3-sin\Phi}}. \quad \textbf{(3.11)}$$

Table 3-1 Material properties for the simulation

Track component	Material property	Value
Rail	Modulus of elasticity, E(MPa)	210000
	Poisson's ratio, v	0.3
	Density (kg/m^3)	7829
Ballast	Modulus of elasticity, E(MPa)	180
	Poisson's ratio, v	0.27
	Density (kg/m^3)	1900
	Angle of friction	50
	Cohesion	0
Sleeper	Modulus of elasticity, E(MPa)	36000
	Poisson's ratio, v	0.2
	Density (kg/m^3)	2400

3.3.5 Link and boundary conditions

The boundary conditions of the model are set to constrain the perpendicular movement to the edge surface of the nodes that belong to that surface, movements constrained in the vertical direction of lower surface. Since the aim of this research is to determine the lateral response of the track, pre-stressing of concrete sleepers is neglected.

The ballast and sleeper are placed on a rigid plate, the bottom layer of which does not have any relative displacement to this rigid plate. It must be mentioned that the rigid plate is modeled completely restrained that it results in increasing lateral stiffness and lateral resistance. Loading as lateral displacement was lateral load (preserved throughout the simulation), applied in the center of rail seat and applied statically.

In many researches simulations presented, the lateral displacements are controlled. In practice, the phenomenon is more force controlled. Thus, in this research the simulation is lateral load controlled.

The rails are considered as rigid body. It's bending and shear stiffness's remain, justifying a restraint of all rotational degrees of freedom, and two translational (lateral and vertical) degrees of freedom. No vertical effects are taken into consideration in this study, so the degree of freedom can be fixed. Therefore, the induced track buckling will occur perfectly in-plane.

3.4 Design lateral loads

Lateral forces act perpendicular to the longitudinal direction (centerline) of track. On canted tracks the lateral forces may be resolved into vertical and horizontal components. Research findings in [4] specified that there are two primary causes of lateral loads applied to rails: (a) lateral wheel load; and (b) buckling reaction load. Lateral wheel loads are originated by both the lateral force component of the friction between the rail and wheel and the lateral force imposed by the wheel flange on the rail. The buckling reaction loads in the lateral direction are exerted by the high compressive stresses accompanied with high temperatures in rail.

Lateral loads in tracks are far more complex than vertical loads and are less understood. [23] Similar to vertical force below, lateral force exerted by the wheel on outer rail is also equal to the sum of the quasi-static and dynamic loads, thus,

$$Y_{tot} = (Y_{flange} + Y_{centr} + Y_{wind} + Y_{dyn}),$$

where Y_{flange} : Lateral force in curved track made by flanging against the outer rail,

Y_{centr} : lateral force in curved track made by centrifugal force,

Y_{wind} : lateral force due to the cross wind,

Y_{dyn}: dynamic lateral force part; these are manly hunting phenomenon on a straight track.

If an assumption is made that the centrifugal and wind lateral forces act entirely on the outer rail, then the lateral equilibrium equation obtained will be as follows:

$$\boldsymbol{Y_{max} = G * \frac{h_d}{s} + H_w} \ , \qquad \textbf{(3.12)}$$

$$\text{Or} \quad \boldsymbol{Y_{max} = G/b_t * (\frac{b_t c^2}{g R_c} - h_{s)+} H_w} \ , \qquad \textbf{(3.13)}$$

Where Y_{max} is maximum quasi-static lateral force,

G is static axle load,

S is track gauge width,

h_d is cant deficiency,

h_s is super elevation,

b_t is track width,

H_w is crosswind force,

R_c is radius of track curvature, and

c is cohesion.

For dynamic component of lateral force, the static component of the force can be multiplied by the dynamic amplification factor (DAF), thus,

$$\boldsymbol{Y_{max} = DAF(G * \frac{h_d}{s} + H_w)} . \quad \textbf{(3.14)}$$

The DAF can be calculated by employing simple empirical equations. Eisenman's equation was cited by Kennedy J. [4]

If V< 60 km/h

$$\boldsymbol{DAF = 1 + t\varphi}, \quad \textbf{(3.15)}$$

If 60 < V < 200 Km/h

$$\boldsymbol{DAF = 1 + t\varphi(1 + \frac{V-60}{140})}, \quad \textbf{(3.16)}$$

where *t* is a multiplication factor depending on the confidence interval, φ is an empirical factor depending on the track quality, and *V* is the train speed in km/h. The values used for these factors are presented in Table 3-3 and it can be seen that the DAF increases with an increase in train speed and with a decrease in track quality.

Table 3-2 Parameters used for the determination of the DAF (Esveld,2001)

Probability (%)	**t**	**Application**	**Track condition**	**φ**
68.3	1	Contact stress, subgrade	Very good	0.1
95.4	2	Lateral load, ballast bed	Good	0.2
99.7	3	Rail stress, fastening, supports	Bad	0.3

The distribution of vertical loads to ties indicates that the tie directly under the load will receive from 45% [20 inches (510 mm) centers] to 60% [30 inches (760 mm) centers] of the imposed vertical load while adjacent sleepers will each receive approximately one-half of the balance. This distribution of loading is a function of the rigidity of the track structure, which is greatest about the horizontal axis [34].

Louis P. [2] evaluated the percentage of the exerted lateral force by the wheel which is transferred to a single sleeper in four kinds of tracks with different lateral stiffness using

a beam on elastic foundation (BOEF) model. As the proposed method in the current research represents.

- The typical vertical load reaching a single sleeper immediately beneath an axle is likely to be in the range 33% to 55% of the weight of the axle.
- The lateral load reaching a sleeper immediately adjacent to an axle may be in the range 34% to 60%.

For this study the distribution of lateral load has studied and presented on section 4.2. then based on the results the applied load percentage has been determined. Applied load to the model is considered, first 2 mm compaction is applied to the ballast due to the train passing load then axle load is applied gradually as shown in the Figure 3-15.

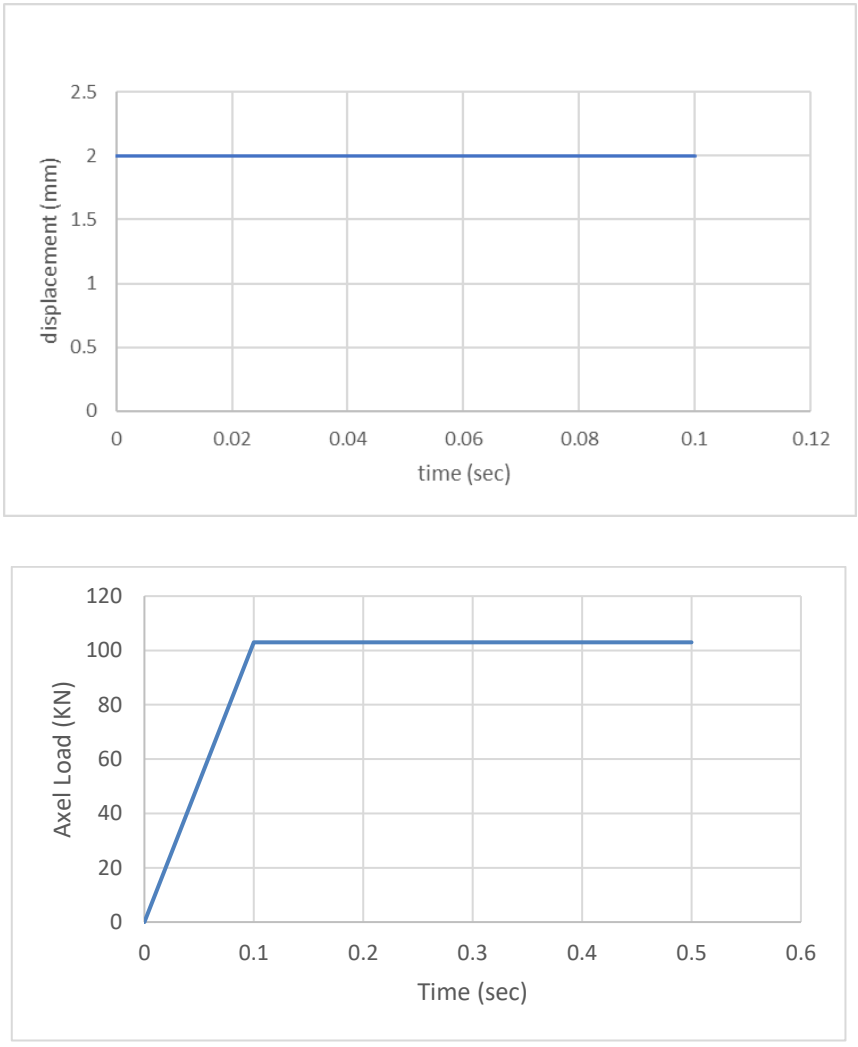

Figure 3-15 Load-Amplitude graph

It should be mentioned that vertical loading was considered low, because the critical status (minimum lateral resistance) is important [19].

According to Kerr (2003), the distribution of rail seat pressure for concrete crosstie track extended less than 7 feet to both sides of wheel load application, which was less than the axle spacing of the passenger coach in the field test.

In order to get the force applied on the sleeper this study develops two steps. In the first step, the total lateral force on the rail is calculated using empirical equation that is developed by Prud'homme.

The simulation contains continuously supported rail by sleeper which is fixed at the bottom. To get accurate result the modulus of elasticity is reduced of the actual one. the force is exerted on the simulated track as a lateral surface traction.

Then for the sake of simplicity and faster analysis the lateral force exerted by the rail on the sleeper is determined by using curve sectioned track simulation. From the analysis result the lateral load distribution on sleeper exactly under the load and adjacent sleepers are determined and compared with literatures and standards.

On the second step track lateral forces due to different speed of the train is determined using Esveld in 2001, the lateral force due to non-compensated centrifugal force which is a function of train axle load and speed, radius and cant of a curved track, gravity acceleration, and track.

$$\boldsymbol{y_{tot} = P\left(\frac{v^2}{12.96R} - \frac{gh}{s}\right)}, \qquad \textbf{(3.17)}$$

where: P= axel load(ton),

V = train speed (km/h),

g = gravity acceleration, 9.81 m/s^2

h = curve cant (m),

R = curve radius (m),

Qo = vertical axel load,

S = track gauge.

This force is applied on the sleeper as a traction force as per the percentage get on step one.

Table 3-3 Parameters used to calculate lateral load on the track

P(ton)	v(km/h)	R(m)	h(m)	Qo(kN)	s(m)	t	φ	DAF
10.5	20	146	0.1	52.5	1.435	2	0.2	1.4
10.5	40	146	0.1	52.5	1.435	2	0.2	1.4
10.5	80	146	0.1	52.5	1.435	2	0.2	1.46
10.5	120	146	0.1	52.5	1.435	2	0.2	1.57
22.5	80	146	0.1	112.5	1.435	2	0.2	1.46

3.5 Interaction

As railway track is a sophisticated system comprising multiple components with a large number of contacting interfaces, the realistic behavior of modeling contact interactions contributes significantly to validity of numerical solutions. Abaqus provides comparative capabilities in modeling contact interactions, including the ability to model interactions between deformable bodies, rigid bodies, and self-contact. Additionally, Abaqus allows for automatic detection of contact between different bodies, which intensely reduces the time required to define contact in complex assemblies such as the railway track system considered in this study.

Contact interactions between track components were formulated using surface-to-surface contact discretization, and a master and a slave surface were defined for each contact pair. This contact formulation method prevents large and undetected penetrations of nodes on master surface into slave surface, providing more accurate stress and strain results compared to other methods. The Basic Coulomb friction model with the penalty friction formulation was used to simulate the frictional force response at the contact.

$$\mathbf{F_f} \leq \mu \mathbf{F_n} \tag{3.18}$$

Contact interaction between the legs of a shoulder and concrete sleepers involves contacts of relatively more complex geometries and was difficult to simulate using conventional contact formulation methods. [35]

3.6 Procedures used for field test

To validate the model used for FE, field test was conducted on the specific section targeted track. The following procedures are used to measure sleeper lateral displacement on the field.

- Prepare a steel rod 1.5 m long and connect it to the transducer by using bolt, as shown in Figure 3-16. (from platform edge to center line 1420 mm),
- Prepare 3 LVDT and 1 strain gauge,
- Connect the LVDT and the strain gauge to a data logger,
- Measure the lateral displacement using LVDT and load position using strain gauge by changing the position of the transducers as indicated from Figure 3-16 to Figure 3-20.

The specification of the train for AALRT is refer to Technical Specifications of Vehicles Addis Ababa E-W & N-S（ Phase I） Light Rail Transit Project. The detail used to simulate the load magnitude is described in Table 3-3. Hence the target section for this study is located around Kality with is the last station, the vehicle weight is laid between the rated passenger and empty vehicle.

Table 3-4 Rated passenger capacity of vehicles [31]

乘客数量（人） Number of passengers (persons)	坐席 Seated	站席 Standing	合计 Total
座　席（AW_1） Seats (AW_1)	65	0	65
定员载客（AW_2）（站席 6 人/m^2） Rated passenger capacity (AW_2) (standing: 6 persons/m^2)	65	189	254
超员载客（AW_3）（站席 8 人/m^2） Overload capacity (AW_3)(standing: 8 persons/m^2)	65	252	317

And the vehicle weight is given in the following table,

Table 3-5 vehicle weight [31]

载　　荷 Loads	车体重量 Carbody weight	乘客重量 Passenger weight	总重 Total weight
空　车（t） Empty vehicle (t)	44	0	44
定　员（t） Rated passenger capacity (t)	44	15.24	59.24
超　员（t） Overload capacity (t)	44	19.02	63.02
轴重（t） Axle load	≤11（1+3%）t		

The test is conducted in five stages to measure the lateral displacement of sleepers when they are subjected to train load. The first set up is done by place the three transducers in parallel to get the lateral movement on the correspondent sleepers. Then to measure the lateral displacement of the fourth sleeper it is required to use another setup which is the second set up. On the second set up, the third transducer removed from the third sleeper and placed on the fourth sleeper. By applying the same procedure, changing the third transducer position, for the remaining sleepers and conducted the lateral movement of sleepers up to the seventh sleeper using five set ups.

Number of tests conducted and configuration

1st Setup: three of the transducers placed in sequence one after the other at curved section with radius of 146 m. the strain gauge is placed on the rail exactly above the first transducer.

Figure 3-16 1st field setup

2nd Setup: two of the transducers located in sequence one after the other but the third one jumped one sleeper and installed on the fourth sleeper.

Figure 3-17 2nd field setup

3rd set-up: two of the transducers located in sequence one after the other but the third one jumped two sleepers and installed on the fifth sleeper.

Figure 3-18 3rd Field setup

4th set up: two of the transducers located in sequence one to the other but the third one jumped three sleepers and installed on the sixth sleeper.

Figure 3-19 4th field setup

5th set-up: two of the transducers located in sequence one after the other but the third one jumped four sleepers and installed on the seventh sleeper.

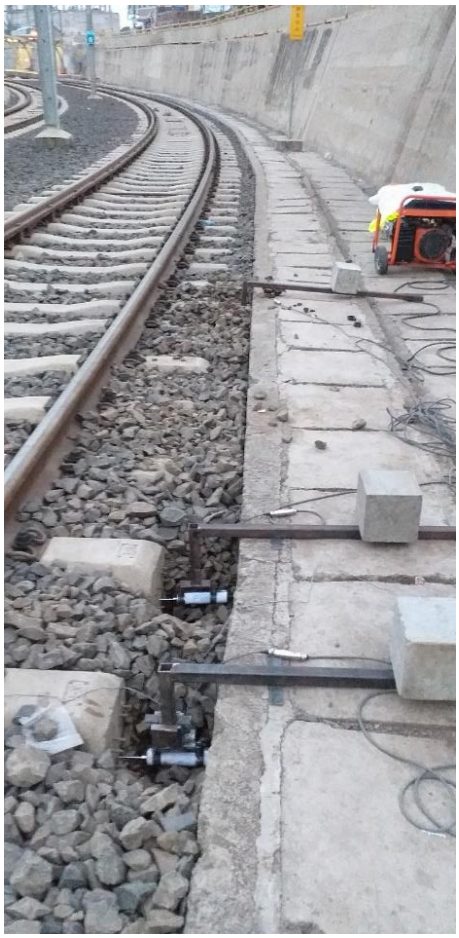

Figure 3-20 5th field setup

CHAPTER 4 ANALYSIS RESULTS AND DISCUSSIONS

This section is divided in three subsections. The aim of subsections 4.2 is to validate the model and try to understand better the governing mechanisms of the phenomenon, section 4.3 describes the track lateral force distribution result and 4.4 and section 4.4 presents the results obtained to date on sleeper's resistance. The geometry, material property, elements used, etc which are parameters used in the modelling are mentioned in the preceding chapter.

4.1 Validation

4.1.1 Numerical Validation of Finite Element Model

In order to test and verify the aforementioned design result, the finite element analysis (i.e. the numerical test) of the ballast and sleeper was performed and presented in this section. The FE model was first validated with popular papers on the domain and then validated using field experiment.

A necessary step in model development is used to validate the result accuracy. Zakri et al [28] model validated against the results in the article of Kabo [20], where STPT experimental and 3D finite element method is used to analyze the effect of sleeper type on track lateral resistance. The work by Zakri et al. [28] use the same setup as in the work by Kabo, thus performed simulations cover a range of different loading conditions. A ballast layer with the shoulder extent 400 mm, shoulder slope of 1:1.5, and sleeper spacing of 600 mm is used and coefficient friction of concrete sleeper with ballast layer is considered 0.1.

On this work of Zakir et al. laboratory experiment and numerical model result is used for finite element model validation. According to Zakri et al., their output result is in good agreement with Kabo's result that makes the paper had appropriate accuracy. Therefore, Zakri et al. is considered as the reference and valid source. [28]

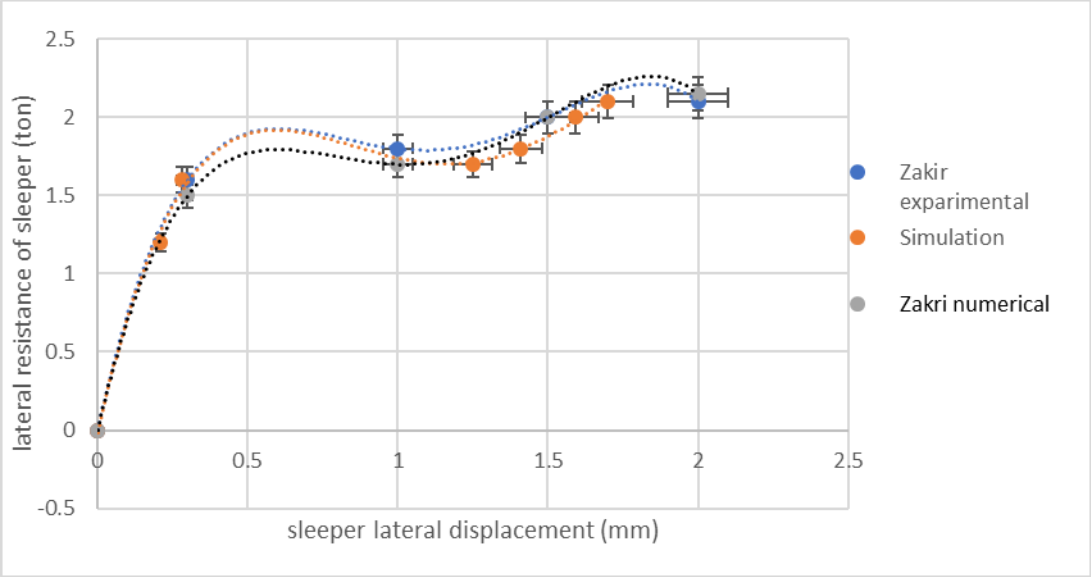

Figure 4-1 Validation of modeling

Figure 4-1 presents the comparison between STPT experiment result and numerical model result with the current used model for validation data sets. Comparing the output from the current finite element model with Zakir et al numerical and experiment, the shape of the three corves exhibited good agreement, which proves the result of the current paper has appropriate accuracy.

4.1.2 Field Validation of Finite Element Model

The second method which is used to validate the model is field experiment. The field experiment is conducted on the NS line of AALRT railway on the simulated curved section. The detail of the studied railway track is described on section 3.1.

The results from the testing on a curved track section were used for model validation. Three transducers were installed on various railway sleepers to record the sleeper movement and strain gauges were installed on the rail to record the dynamic wheel load and rail behavior. The experimental Setup and Program is presented on section 3.6.

a) 

b)

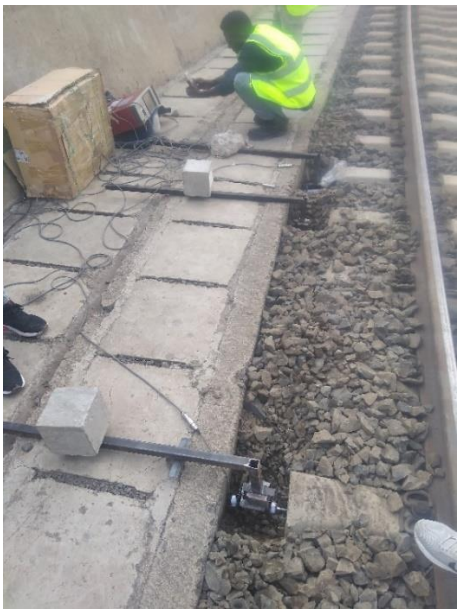

c) 

(d)

Figure 4-2 The Instrumented Track Segment at AALRT

To estimate the effect of lateral loads, the first value after the first wheel passed measured from the three transducers was used to compare with the modeling results. To know the actual position of vertical wheel loads entering the rail head, strain gauges were installed on the rail above the first transducer. As shown in Figure 4-2 (d)

The field condition is modeled in the finite element by using actual parameters that was holed at the time of the experiment. The speed of the trains was ranging from 15 Km/h, the ballast at the shoulder was removed.

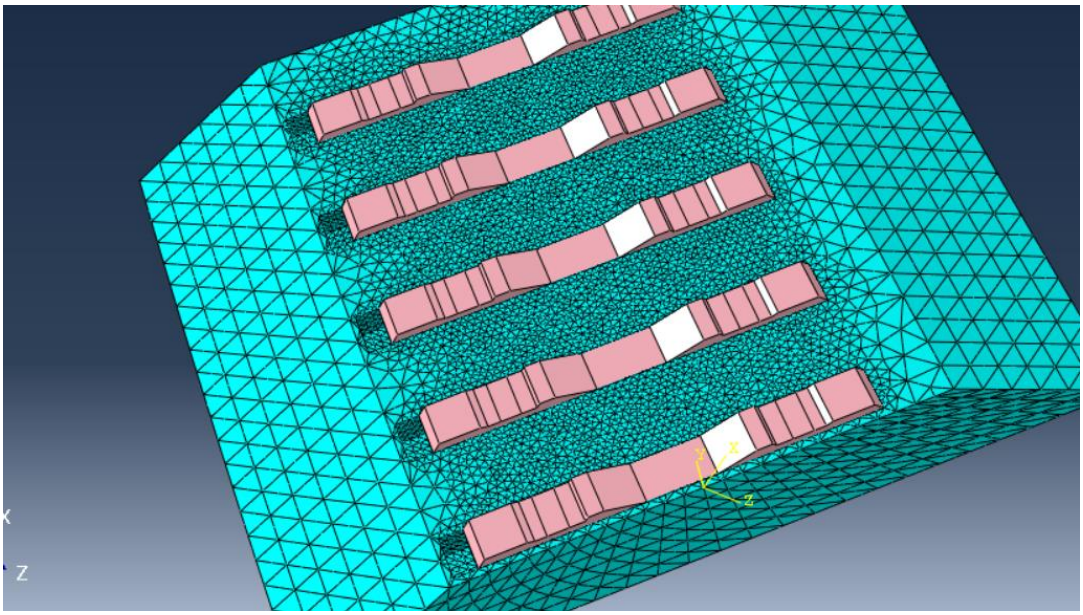

Figure 4-3 modeled track with the end resistance is removed

The validation based on the lateral displacement on the was physically making sense. Figure 4-4 presents the comparisons between the field and numerical results. A section of signal containing peaks is shown, in which the first two peaks are caused by the first two axles of a car. Due to the rail roughness, and other geometry imperfections, slight fluctuation was observed in the field data. Because of the limitation of the length of the track in the finite element model, short during of signal was recorded. To make an appropriate comparison, the peak of finite element output is aligned to the first peak of the field.

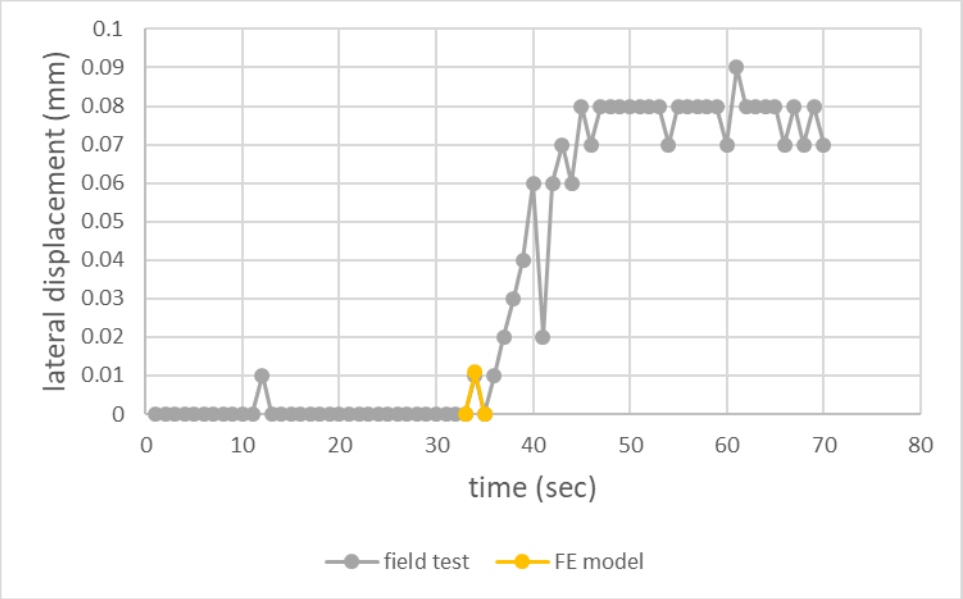

Figure 4-4 Lateral displacement of field test and FE model
(without end resistance and low speed of 20 Km/h)

The FE model gave a maximum displacement value of 0.0108 mm which was 8% higher than the 0.01 mm displacement measured in the field. This difference likely happened due to the speed on the field was not exactly the same on the simulation, due to non-homogeneity of materials the gauge spacer which anchors the track from movement is not modeled and the accuracy of machine. Although the value of displacement for the sleeper from field test results larger displacement, it could be explained by the fact that only one axle pass was modeled in the finite element analysis, which neglected the effect of the following axels. Therefore, a good agreement between field and numerical results for lateral displacement in sleeper was achieved.

4.2 Track lateral force distribution

Primarily, the influence of force distribution to the sleepers has been assessed, in order to evaluate the percentage of load distribution on track panel. By using the concept that, every action has reaction, the load distribution is determined by applying two wheel loads from one bogie (the distance between the bogies is 1.8 m) and define all the reactions on the individual sleepers. To know, up to what extent the load influence continues, the track has been modeled with 5, 7 and 9 sleepers. Figure 4-5 shows the modeled 9 sleepered track

section for the analysis and observed results. Stress along the horizontal axis for the given sleepers are indicated on Figure 4-5.

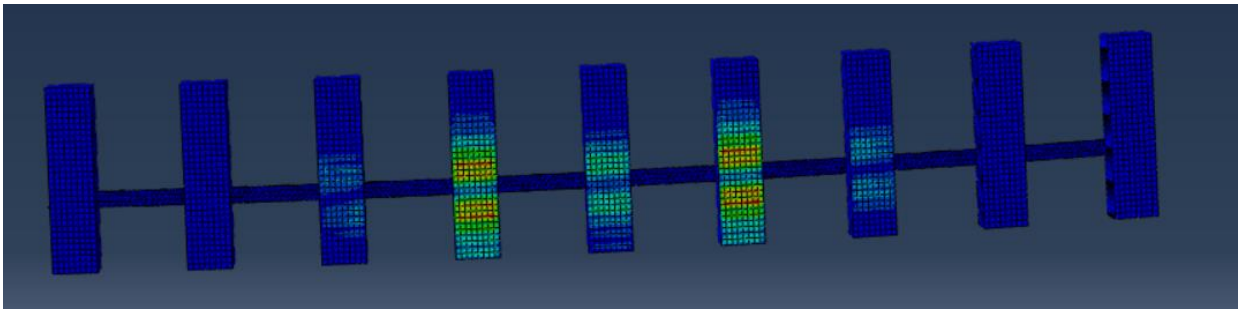

a)

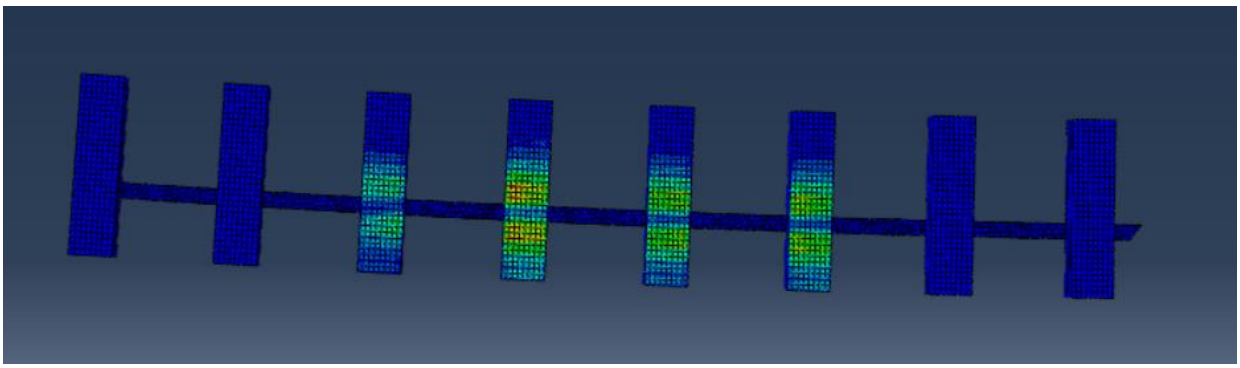

b)

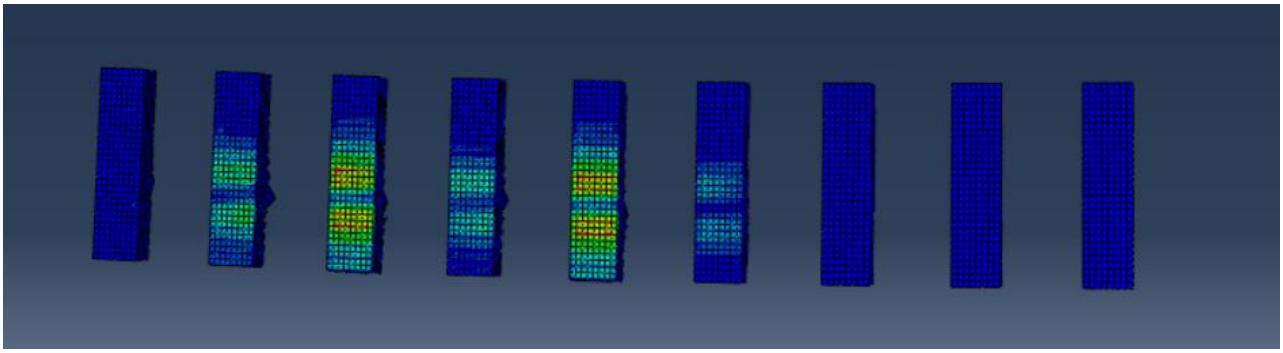

c)

Figure 4-5 Normal stress distribution on sleeper surface a) sleeper spacing 600 mm, b)700 mm c) 500 mm

The load magnitude reduces as distance of the sleeper from the load increases. As indicated on the graph the lateral load exerted on sleeper exactly under the wheel is varying from 57% to 47% when the sleeper spacing decreases from 700 mm to 500 mm. once the sleeper

spacing increases the load distribution drops down fast. Sleepers located exactly under the axels carry more percentage of the loads and they carry higher percentage for the larger spacing. When the spacing of the sleepers goes down the load will have distributed to the adjacent sleeper largely. If the rail is considered as abeam on elastic foundation, the maximum lateral force acting on the sleeper immediately under the vertical load will be 60% of the total lateral force [19].

It can be seen from literature [2] that the lateral load and vertical load are not equally distributed. The vertical load is distributed along a greater length of the track then the lateral one. G44 mono-block sleeper under the load carries around 61% and the adjacent sleeper carries around 25% of the total lateral load. By seeing the result we can conclude that the load distribution is closely agree with the result in [2].

The aim of this simulations is to understand the phenomenon, how does load applied on each sleeper, so the percentage of lateral force applied on the sleepers can be used in section 4.3 and 4.4. Since the distribution of the load beyond the third sleeper is insignificant, the second model neglect sleepers afar the third sleeper from the middle sleeper (sleeper located between the loaded sleepers).

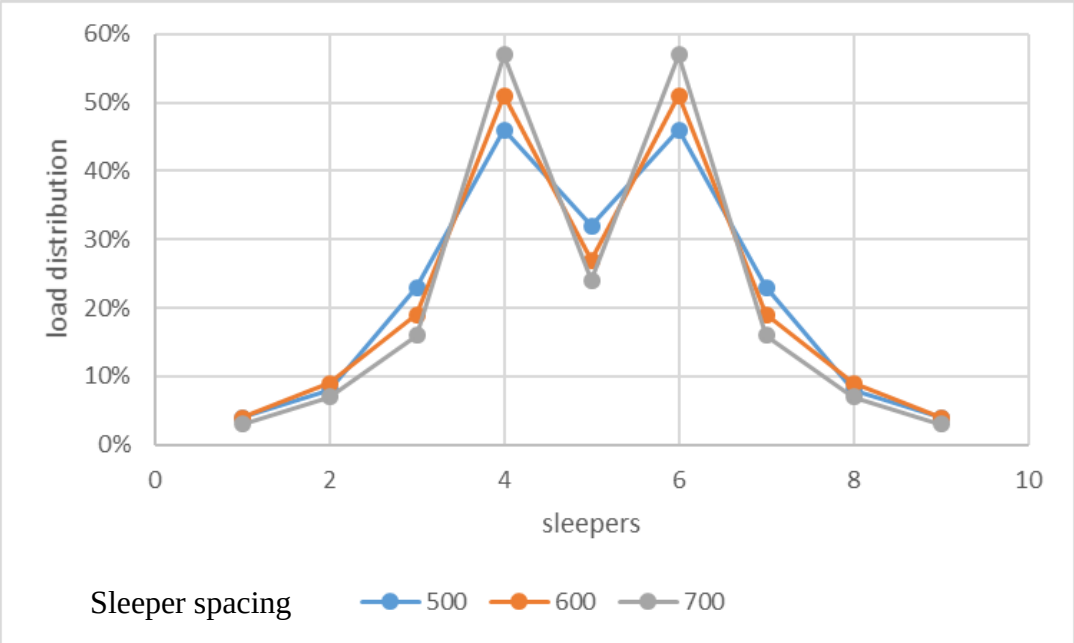

Figure 4-6 Shear force distribution versus sleeper arrangement a) sleeper spacing 600 mm, b)500 mm c)700 mm

For sleeper spacing of 500 mm, 600 mm and 700 mm, the distributions of lateral force were similar (Figure 4-6). Small increase was observed at the loaded and adjacent while the followed sleepers underwent small decrease in percent distribution. Nevertheless, a significant increase, 6 percent points, only took place at the loaded sleepers as the spacing increased from 600 mm to 700 mm whereas the distributions at other sleepers remained smaller. The sole increase at the loaded sleeper deems to be related to the increase in lateral loads experienced by the rail-seats in the vicinity of the wheel due to larger sleeper spacing. Therefore, considering the three sleeper spacing simulated in the FE model, the 600 mm spacing ensured the most uniform distribution of lateral force without requiring too small of a spacing.

Conversely, the influence of the sleeper surrounding resistance, which is formed between ballast and sleeper was also studied. The side frictional resistance, the end resistance, and the bottom resistance significantly affect the total lateral resistance of the sleepers. Therefore, the contribution of side, end and bottom of the four types of sleepers are compared in Figure 4-8. Type II sleeper have 65% end resistance, 20% bottom resistance and 15% side resistance contribution. It can be noticed that the best performance in terms of lateral resistance is obtained at the track composed by the frictional sleepers, which achieves 31% resistance on the bottom, 15 % resistance on the side and 54% on the end. Although the side and bottom winged sleeper shows high resistance on the end section.

a) 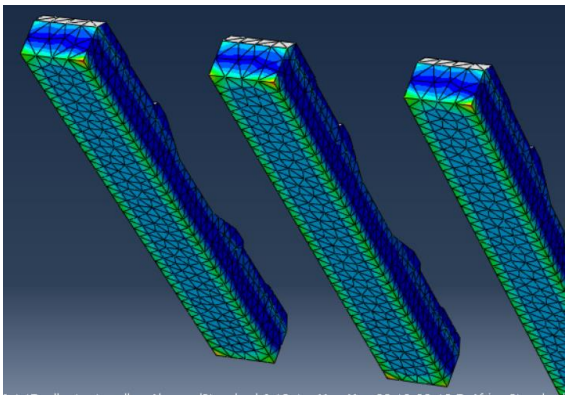 b) 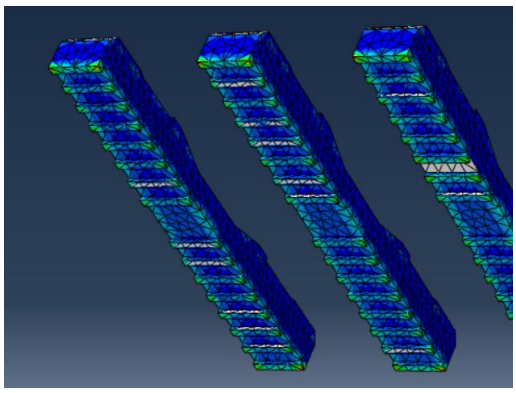

c) 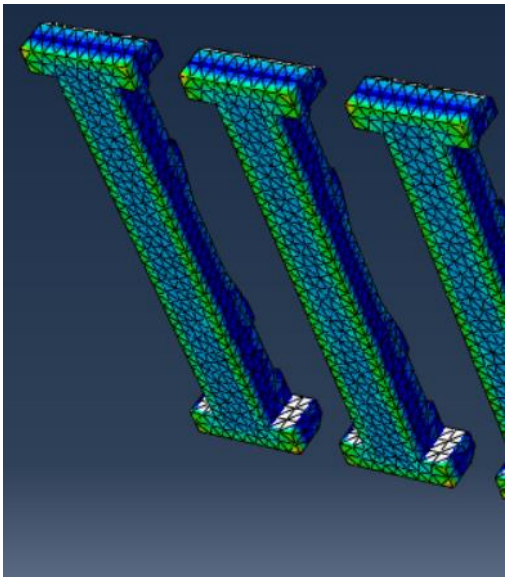 d) 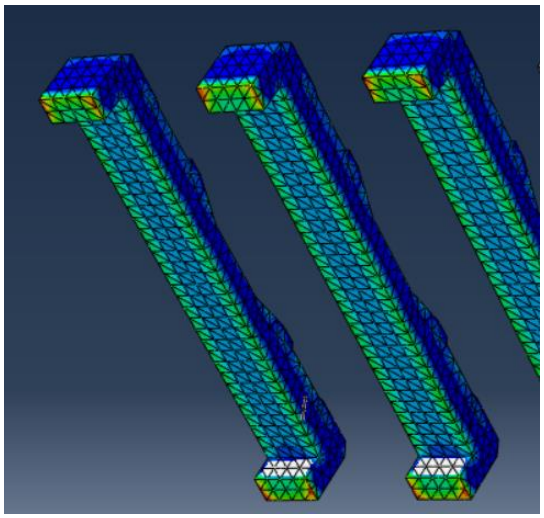

Figure 4-7 Sleeper contact pressure on the surrounding a)Type II b) frictional c) side-winged d) bottom winged sleepers

Table 4-1 sleepers side, end and bottom resistance contribution

	TypeII	side-winged	bottom wing	Frictional
Bottom	20%	21%	15%	31%
Side	15%	12%	10%	15%
End	65%	68%	74%	54%

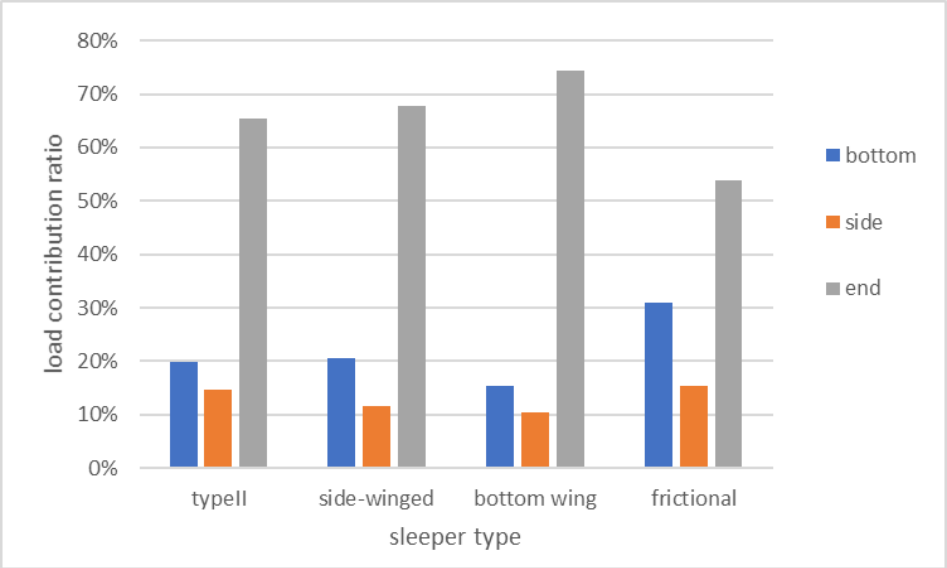

Figure 4-8 Load contribution of the sleeper surrounding

Figure 4-8 illustrates contributory effects of bottom resistance, side resistance, and end resistance on the total resistance for each sleeper type, as estimated by simulation. It can be seen that the contributory effect of the end resistance of the Type II sleeper and that of the side-winged sleeper were both about 65%, whereas those of the frictional sleepers were about 55% and those of the bottom-winged sleepers were about 75%. However, the contributory effects of the side resistance of the bottom-winged sleepers were smaller than those of the frictional and Type II sleepers. Similarly, the effects of the bottom resistance of the bottom-winged sleepers were relatively small.

Overall the lateral force of the track exerted on the sleeper is largely resisted by at the end of the sleeper, nevertheless the frictional sleeper most likely improves the bottom resistance and distribute end resistance to the bottom to some extent.

4.3 Effect of Sleeper Design

Clearly, horizontal displacements are related to the lateral resistance of the track: the higher the horizontal displacements the lower the lateral resistance. Thus, the horizontal displacements of the sleepers in the models with different designed shape are compared.

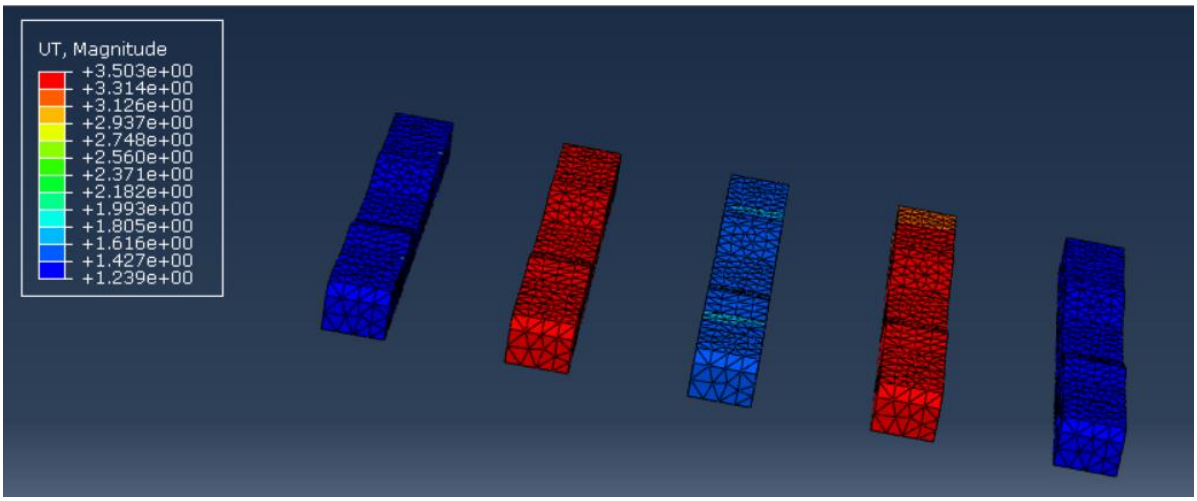

a)

b)

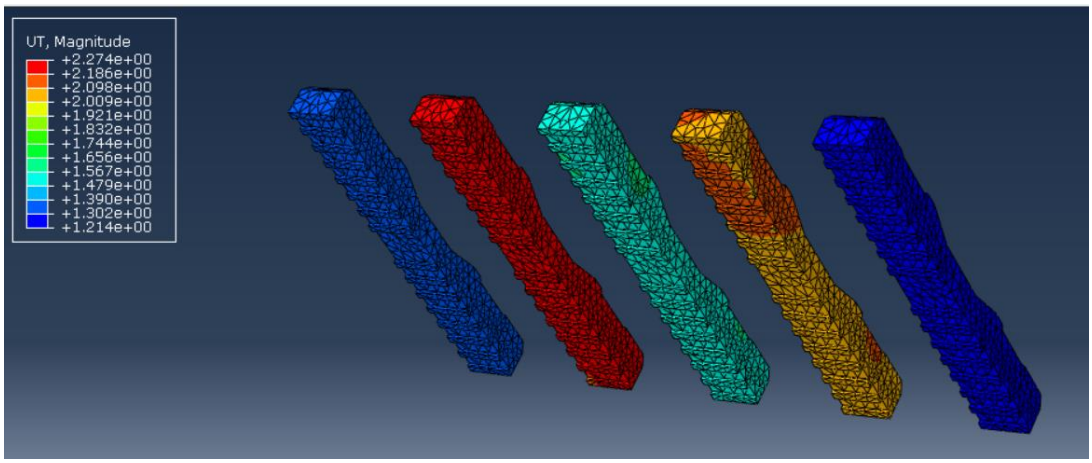

c)

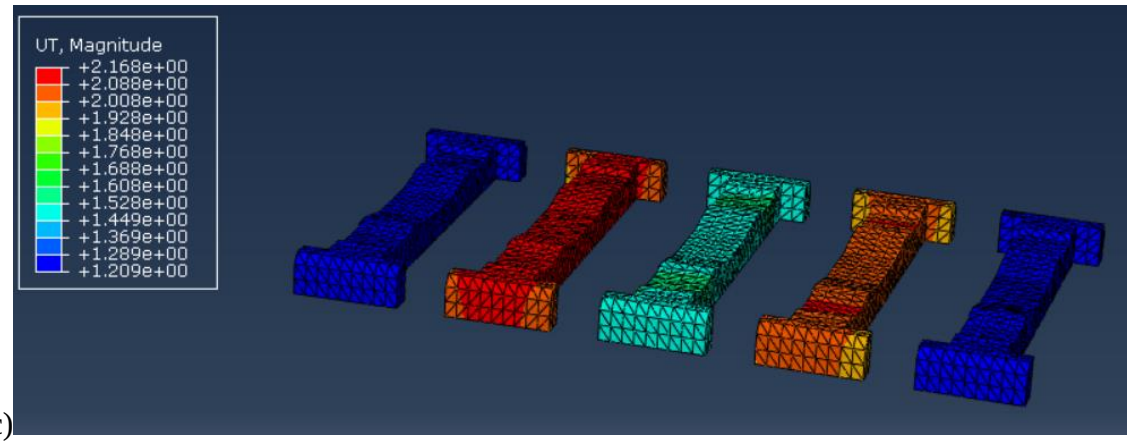

d)

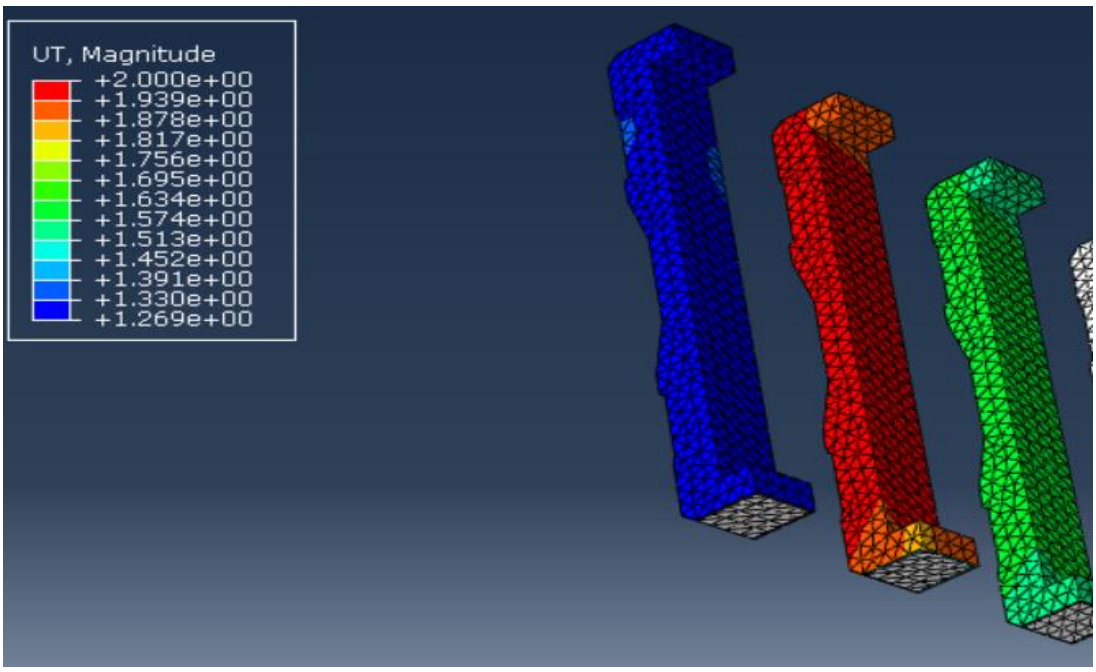

Figure 4-9 lateral displacement at exerted lateral load of 77 KN a) typeII, b) frictional, c) side-winged d) Bottom-winged

Initially, transverse displacement of sleepers results of finite element models for the same loading condition are shown in Figure 4-10. The maximum transverse displacements are registered at the sleeper exactly under the applied load (axel). The maximum of these values at the tracks composed by different sleepers are the following. Side-winged sleeper, bottom-winged sleeper and frictional sleeper has reduced 40%, 41% and 42% in lateral displacement relative to Type II sleeper respectively.

Moreover, the result shows that the sleeper design has high effect on the lateral displacement. For different design of sleepers, the lateral displacement is also different for the same loading condition. Figure 4-10 illustrate a lateral displacement for each sleepers (1- under the load 2-Adjacent to the loaded sleeper 3- second adjacent sleeper from the loaded sleeper) . The figure shows the data from the four different sleeper designs for the same loading scenarios that were investigated in Abaqus simulation.

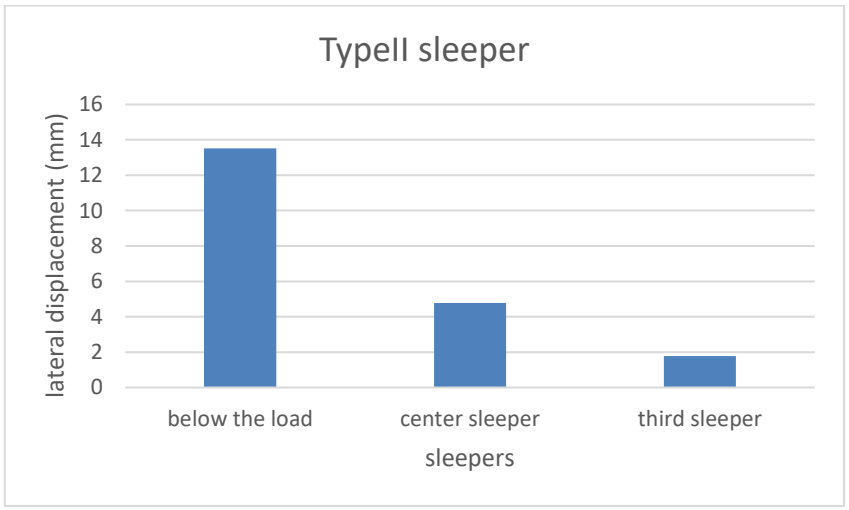

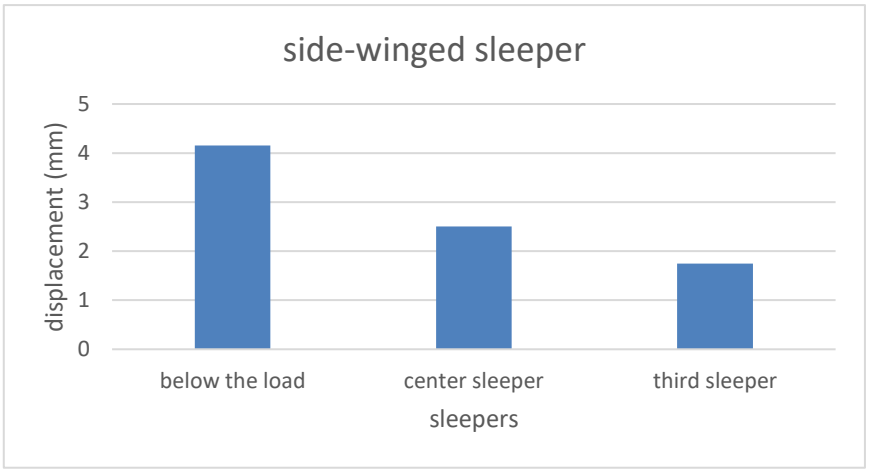

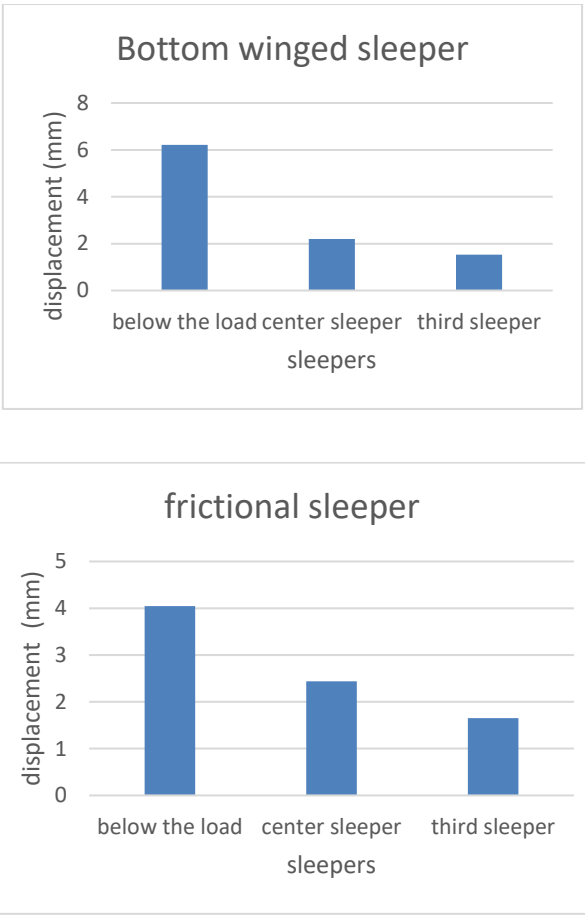

Figure 4-10 Sleepers lateral displacement under the same load (120 Km/h)

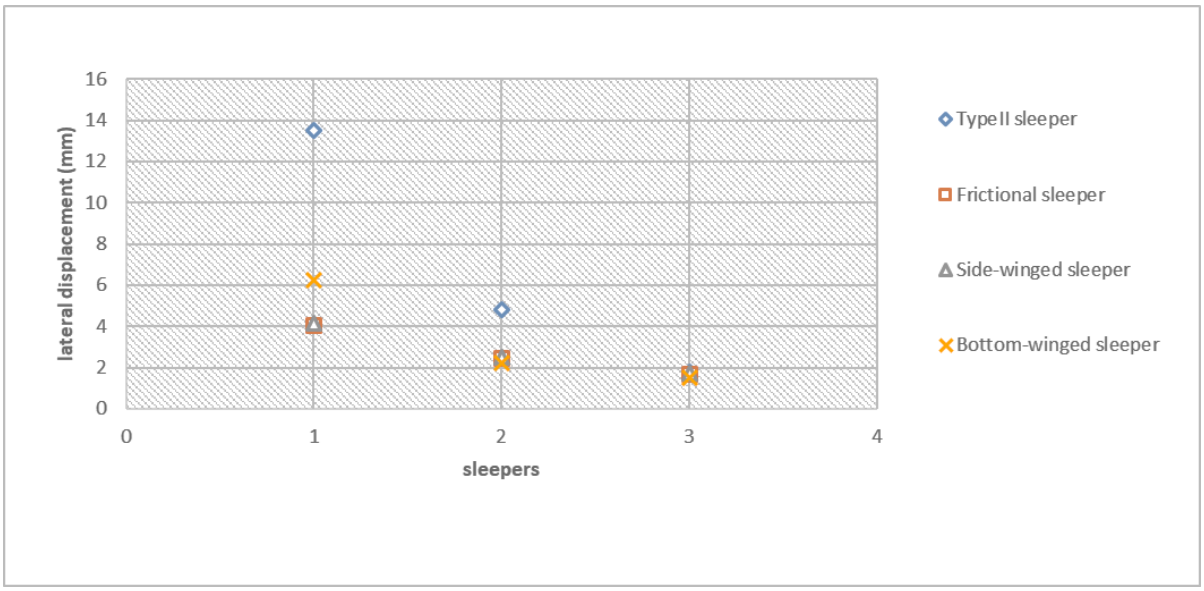

Figure 4-11 Lateral displacement for each types of sleepers (120 Km/h)

From Figure 4-11 it is clear that when the load becomes smaller the lateral resistance of all the four types of concrete sleepers are nearly the same. When the applied lateral force increases the lateral resistance shows large variation for different types of concrete sleepers.

The above analysis on section 4.2and 4.3 indicates the bottom contact is major source for lateral resistance. Improving the bottom contact of sleeper with ballast shows better mechanism to enhance the lateral resistance of the track.

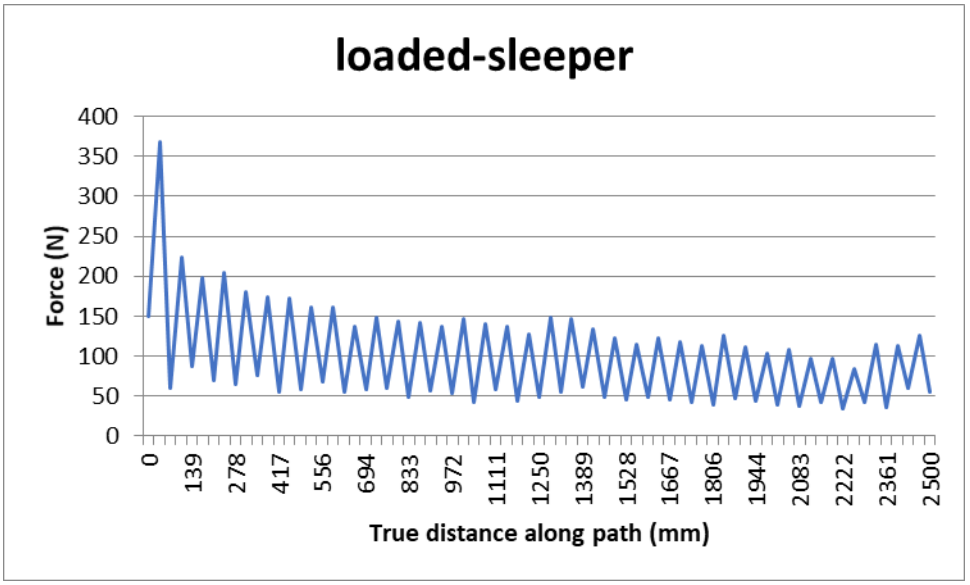

a) TypeII-sleeper

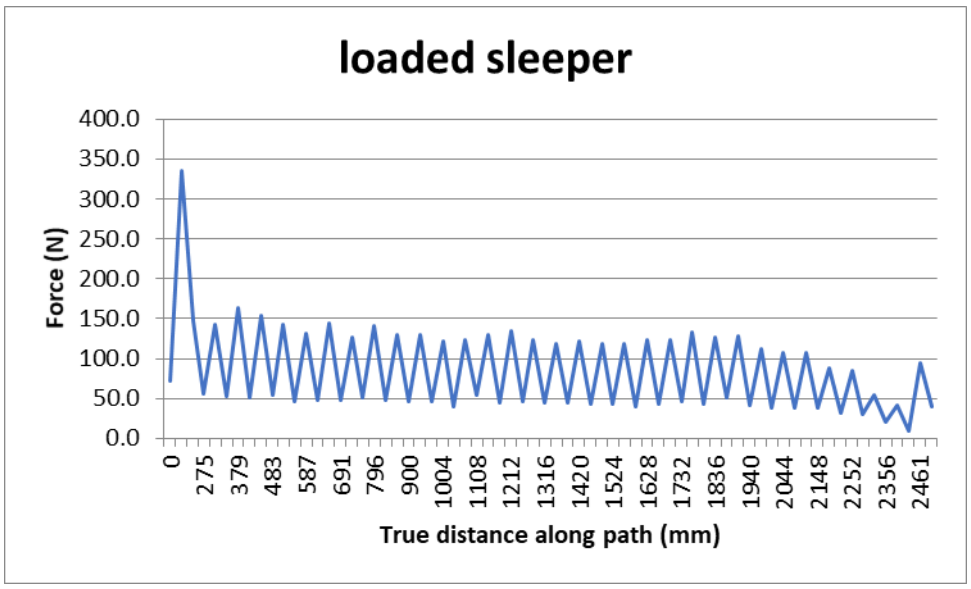

b) Bottom-winged sleeper

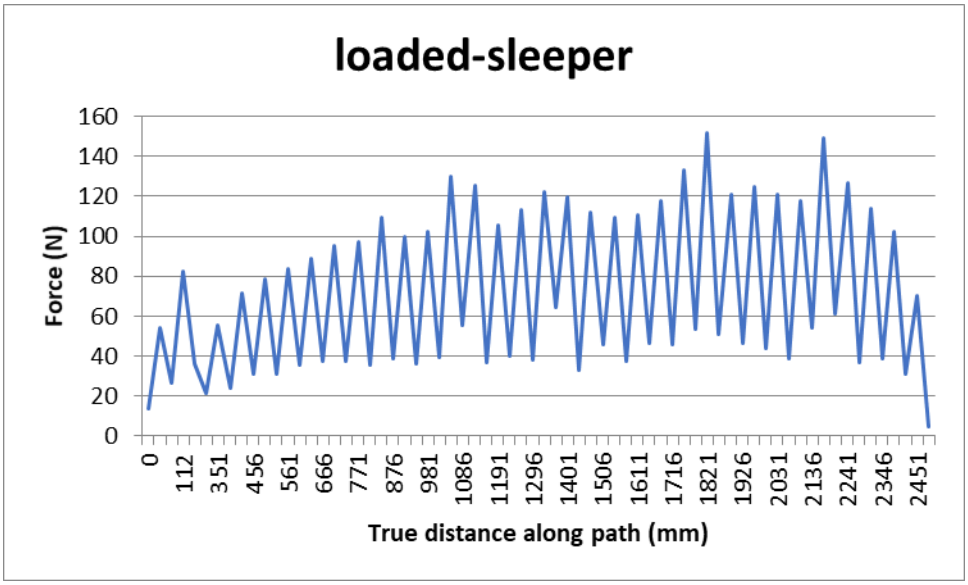

c) Side-winged

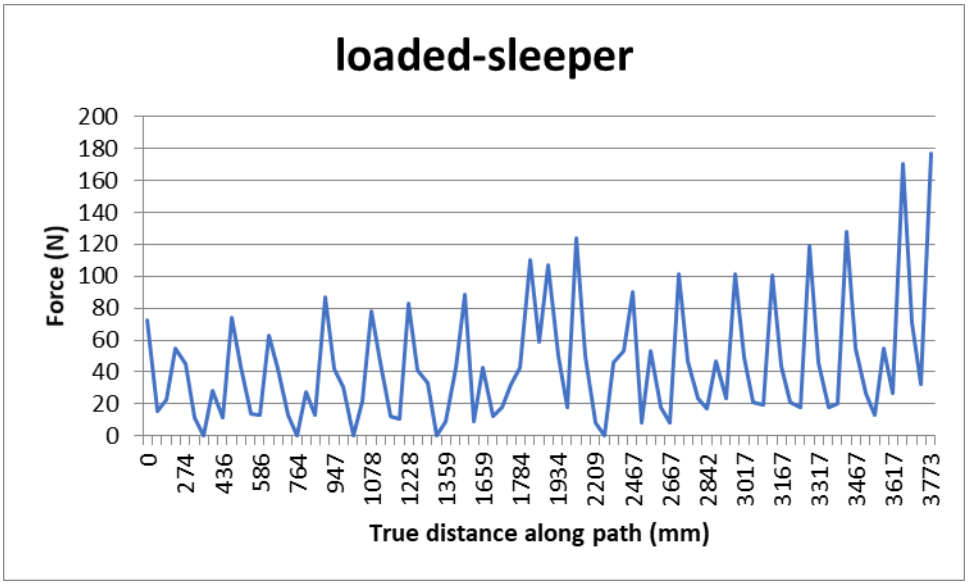

a) Frictional sleeper

Figure 4-12 Sleeper bottom contact shear force along the sleeper length (force in N and distance in mm) Lateral load of 45 KN

From Figure 4-12 we can observe that, contact shear force at the bottom of TypeII sleeper and bottom winged sleeper have the same pattern it begins with higher value and varies from 140 N to 50 N quickly. However, the Type II sleeper shows more rapidity than the bottom-winged one. For the side winged sleeper the bottom contact shear force is higher

at the middle but it varies from 120 N to 40 N. The graph of bottom shear force for frictional sleeper shows that, variation from 0 to 120 N but not rapped as the others.

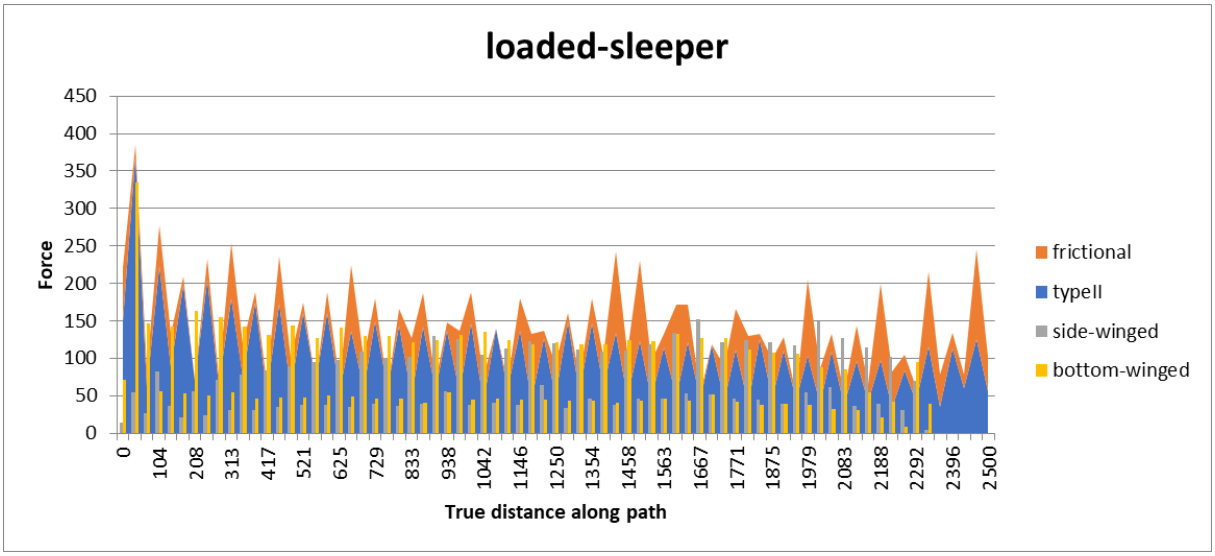

Figure 4-13 Summary of contact force at the bottom of sleepers at lateral load of 45 KN

Figure 4-13 shows that bottom winged sleeper has lower shear force than others and type II and side-winged sleepers have almost the same contact shear force distribution. Frictional sleeper has higher shear force distribution than the others.

Furthermore, an additional case has been studied where the sleepers are subjected to different loads due to the speed of the train. Figure 4-14 illustrates the variation of displacement due to the applied lateral load.

The results from the simulation of 3-D ballast track models show that in the case of increasing train speed and lateral load the amount of sleeper transverse displacement increases.

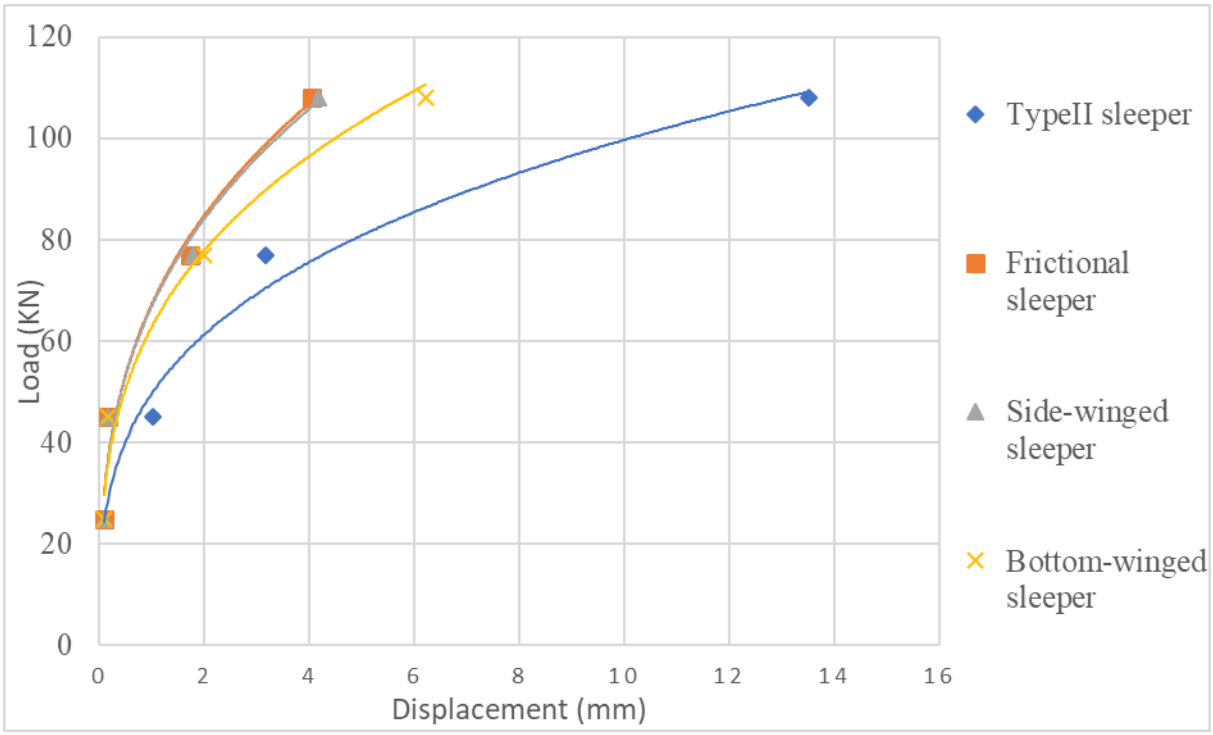

Figure 4-14 Load-displacement graph to different types of sleeper on loaded sleeper

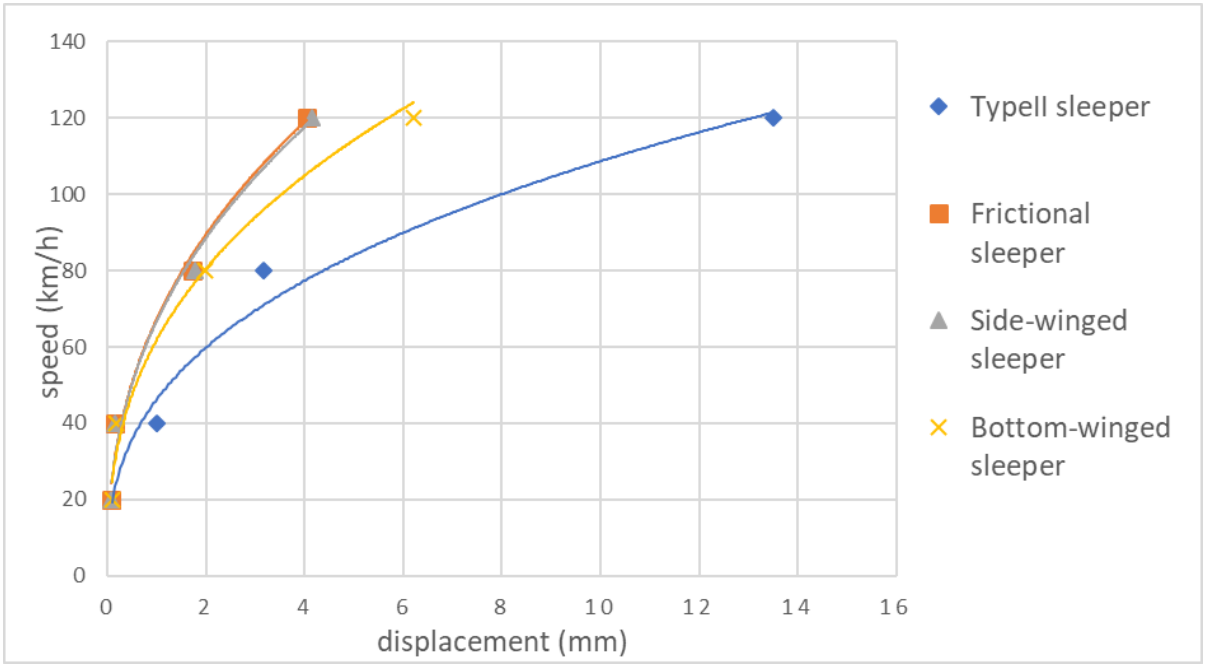

Figure 4-15 Speed versus displacement of sleepers

For small speed the displacement of the sleepers for all type is almost the same but as the speed goes higher the difference of sleeper's displacement gets wider. The difference of lateral displacement between side-winged and frictional sleeper is very small but still the displacement of frictional sleeper is lower than the others. Since the lateral displacement and sleeper resistance are inversely proportional, the frictional sleeper has higher lateral resistance than the other types.

4.4 Effect of Sleeper Spacing

The spacing between sleepers are also another parameter to study on this research. For concrete sleepers, the center to center spacing of sleepers in typical practice ranges between 490 mm and 735 mm. [34] The sleeper spacing of the modeled track in Abaqus was 600 mm which fell in the middle of the code-specified range. On section 4.3 it is clear that the frictional sleeper has improved lateral resistance. On the bases of the result this section study and compare the effect of sleeper spacing for the Type II and frictional sleepers.

The output obtained from FEM and indicated on Figure 4-16, shows lower sleeper spacing has minimum displacement.

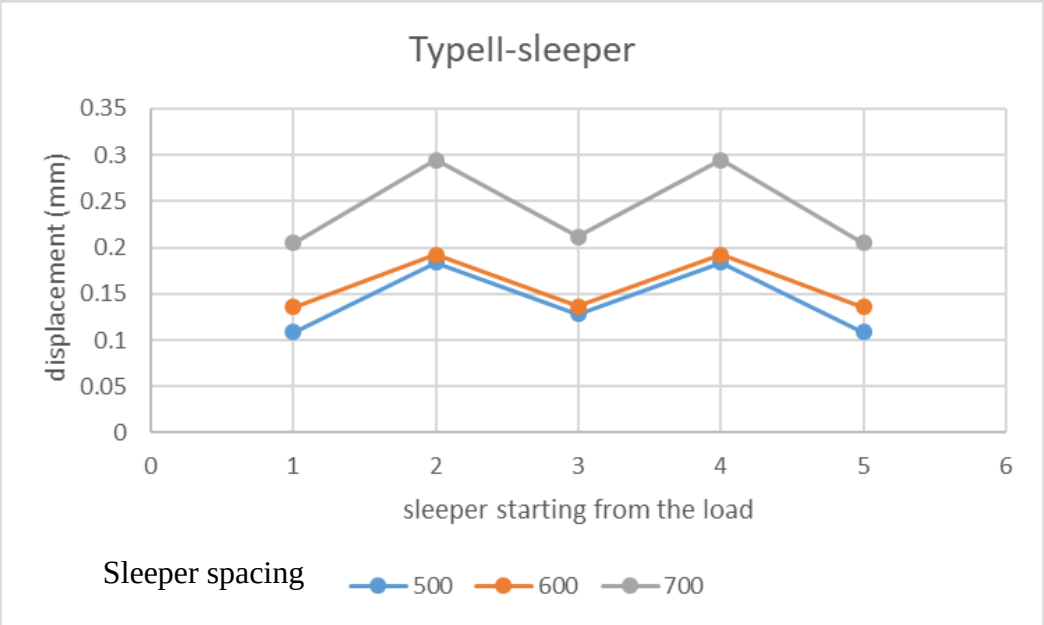

Figure 4-16 Sleeper displacement for different sleeper spacing (Type II sleeper)

As it can be seen in Figure 4-16 wider spacing between sleepers reduce the lateral resistance of the track. In other hand decreasing the spacing between the sleepers indicate lower resistance at the surrounding of the load and increase as it goes far from the load.

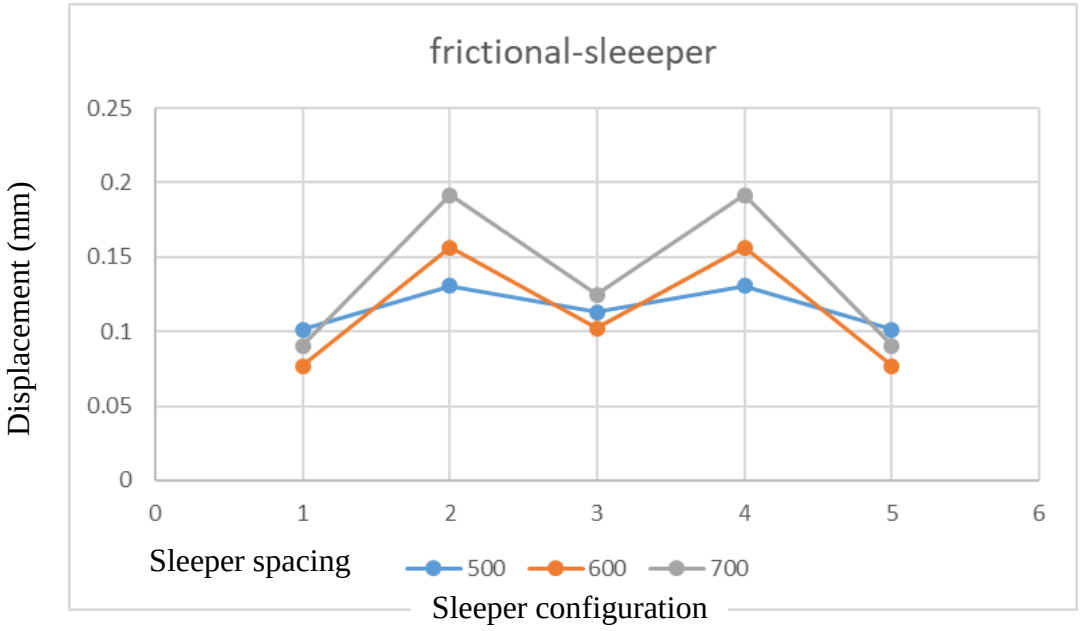

Figure 4-17 Sleeper displacement for different sleeper spacing (frictional sleeper)

For the frictional sleeper the resistance of the sleeper under the wheel has increased when the spacing between the sleeper's decrease. The narrower the spacing the more lateral force distribution to the adjacent sleepers.

As shown on the above figure the load distribution to the for the Type II sleeper displacement under the load for spacing 500 mm is less than that of 600 mm and 700 mm but the difference between spacing 500 mm and 600 mm is not very significant. On the far sleeper the displacement of 600 mm spacing is much larger than that of 500 mm spacing. On the other hand, for the frictional sleeper the reverse is true. Displacement of the sleepers under the load is less for 500 mm spacing. It seems the load is distributed to the adjacent sleepers, it is indicated by the Figure 4-17 that the displacement for the adjacent sleepers are larger from both 600 mm spacing and 700 mm spacing. The stiffer the lateral resistance the more distribution of forces to the adjacent sleeper.

CHAPTER 5 CONCLUSIONS AND RECCOMENDATIONS

5.1 Conclusions

In this work, a brief introduction of the effect of railway sleeper on track lateral resistance at curve section has been presented, mentioning its loading condition depends on speed of the train and radius of curvature. Four different concrete sleeper designs and three spacing between the sleepers were investigated to see the effect on lateral resistance of a track at curved section. A reduction of 40%, 41% and 42% in lateral displacement was observed by applying Side-winged sleeper, bottom-winged sleeper and frictional sleeper respectively. The results indicated sleeper with bottom roughness (frictional sleeper) performed best in attenuating lateral load. TypeII sleeper with 80 km/h displaces equally with frictional sleeper with 120 km/h. The higher the load the larger difference on lateral resistance of the sleeper types. To investigate the relationship between sleeper spacing and load distribution, three different spacing were simulated using FE model. It was realized that the decrease in spacing between sleepers is attributed to more lateral load distributed to the adjacent sleepers.

Some additional conclusions can be made based on the results of the FE analysis:

- Calculations have identified likely lateral magnitudes of load transferred to individual sleepers on low radius curves.
- Sleeper design has observable effect on track lateral resistance
- Improving the bottom friction improves better lateral resistance than providing more mass to resist sleepers.
- Higher spacing between sleepers has lower lateral resistance. However, reducing beyond 600 mm has small effect on the lateral resistance.
- The lateral load distribution on sleepers highly affected by sleeper spacing and type.

5.2 Recommendations

Based on the FE analysis, it was realized that using frictional sleeper can improve the lateral resistance by allowing higher speed. In addition, it is suitable for curved track, especially for high speed trains, in order to minimize the lateral movement and extend the maintenance cycle.

Furthermore, frictional sleeper does not have additional mass than the conventional Type II sleepers and it is easy to fabricate. Based on studies the bottom part of concrete sleeper loss its frictional property with ballast through a time. To minimize this effect, it is recommended to use frictional sleepers.

Having minimum spacing for conventional sleeper reduces the lateral displacement but the effect of minimization beyond 600 mm is insignificant. It was thus likely that using 600 mm spacing is more effective in order to minimize the cost and for maintenance purpose.

5.3 Further research

It has been found numerically lateral resistance of sleepers provided more from the end resistance but, improving the bottom resistance insure better lateral resistance. Therefore, research is recommended to conduct experimental analysis into the contribution of shoulder, crib and bottom resistance.

Consideration of sleeper shape on curved track has shown that in relations to lateral resistance. Providing the more bottom resistance improve better resistance hence investigation in to bottom friction coefficient for each sleeper type using experiments are recommended.

Over the field experiment of this research findings were showed that, each sleeper displaced higher and higher during repetition of wheel load and has residual displacement after the train passed. (Appendex C) Therefore, Studying the sleeper lateral resistance using cyclic loading is recommended for future study.

From field experiment of this study it can be observed that the lateral resistance of the track, for the same type of sleeper, is different from sleeper to sleeper. Thus, further

research to the influence of ballast tamping and compaction level on lateral resistance on track would be benefit to evaluate more parameter that affect lateral resistance.

The obtained result proves the FE model has approximate result to the field output. However, some improvement could be implemented on the model by considering the effect of cant, gauge spacer and additional forces (temperature, wind load etc.).

REFERENCES

[1] A. Kish, "On the Fundamentals of Track Lateral Resistance," American Railway Engineering and Maintenance of Way Association Annual Conference, USA, September 2011.

[2] P. Louis, Le, "Track Behavior: The Importance of The Sleeper to Ballast Interface," PhD Thesis, University of Southampton, 2008.

[3] T. C. Abadi, "Faculty of Engineering and the Environment Effect of Sleeper and Ballast Interventions on Rail Track Performance," *Journal of Rail and Transit,* Vol. 10, No. 5, January 2015, pp.1-12.

[4] E. T. Selig and J. M. Waters, "Track Components and Loading," *Track Geo technology and Substructure Management*, Thomas Telford Publishing, May 2015, pp. 2.1-2.15.

[5] J. A. Zakeri, M. Esmaeili, and A. Kasraei, "A Numerical Investigation on The Lateral Resistance of Frictional Sleepers in Ballasted Railway Tracks," *Journal of Rail and Transit*, Vol. 3, No. 1, June 2014, pp. 1–10.

[6] J. Zakeri, M. Fakhari, and B. Mirfattahi, "Lateral Resistance of Railway Track with Frictional Sleepers,"Institution of Civil Engineers (ice), vol. 165, issue TR2, February 2012, pp. 151–155.

[7] D. Ticali, "High Performance Bi-B Block Sleeper for Improovement the Performances of Ballasted Railway track," S*ciVerse ScienceDirect*, Vol. 3, No. 1, July 2012, pp. 457–462.

[8] Y. Koike, T. Nakamura, K. Hayano, and Y. Momoya, "Numerical Method for Evaluating the Lateral Resistance of Sleepers in Ballasted Tracks," *Soils Foundation.*, Vol. 54, No. 3, January 2014, pp. 502–514.

[9] H. Laura, J. Herraiz, C. Zamorane and T. Real, "Design of a New High Lateral Resistance Sleeper and Performance Comparison with Conventional Sleepers in a Curved Railway Track by Means of Finite Element Models," *Latin America Journal of Solid Structures*, January 2011, Vol. 11, pp. 1238–1250.

[10] L. M. Domingo, C. Z. Martín, C. P. Avilés, and J. I. R. Herráiz, "Analysis of the Influence of Cracked Sleepers Under Static Loading on Ballasted Railway Tracks," The *Scientific World Journal*, Vol. 5, No. 1, October 2014, pp. 1-10.

[11] R. C. Queiroz, *Longitudinal Track Ballast Resistance of Railroad Tracks Considering Four Different Types of Sleepers*, Msc Thesis, Sao Paulo State University, Brazil, 2006.

[12] B. Landuyt, "Modelling of Track Stability in Turnouts with A Finite Element Model," *Soil Dynamics and Earthquake Engineering*, Vol. 82, No. 21, January 2017.

[13] X. Lei and Q. Feng, "Analysis of Stability of Continuously Welded Rail Track with Finite Elements," *Journal of Rail and Rapid Transit*, Vol. 218, No. 1, May 2015, pp. 225–234.

[14] M. Shigeru, "Lateral Track Stability: Theory and Practice in Japan," *Transpation Research*, January 1957, pp. 53–63.

[15] J. A. Zakeri, "Lateral Resistance of Railway Track," *Journal of Rail and Rapid Transit*, Vol. 98, No. 5, May 2014, pp. 1-9.

[16] A. Hosseini and M. Esmaeili, "Effect of Different Contact Surfaces Between Concrete Sleeper and Ballast on Mobilized Lateral Resistance Against Impact Loads," *Journal of Rail and Rapid Transit*, Vol. 12, No. 1, March 2016, pp. 1–12.

[17] A. De Iorio, M. Grasso, F. Penta, G. P. Pucillo, S. Rossi, and M. Testa, "On the Ballast – Sleeper Interaction in the Longitudinal and Lateral Directions," *Journal of Rail and Rapid Transit*, Vol. 114, No. 2, November 2016, pp. 1–12.

[18] G. Saussine, C. Cholet, P. E. Gautier, F. Dubois and C. Bohatier, *Modelling ballast behaviour using a three-dimensional polyhedral Discrete Element method*, 21st International Congress of Theoretical and Applied Mechanics, May 2018.

[19] J. A. Zakeri and M. Barati, "Utilizing The Track Panel Displacement Method for Estimating Vertical Load Effects on The Lateral Resistance of Continuously Welded Railway Track," *Journal of Rail and Rapid Transit*, September 2013, Vol.

6, No. 2, pp. 1–6.

[20] E. Kabo, "A Numerical Study of The Lateral Ballast Resistance in Railway Tracks," *Journal of Rail and Rapid Transit*, Vol. 220, No. 1, February 2015, pp. 425–433.

[21] F. S. González, *Numerical Modelling Of Railway Ballast*, Msc. Thesis, Center Internacional de Metodes Numerics en Enginyeria, June 2015.

[22] M. Esmaeili, S. Majidi-parast, and A. Hosseini, "Comparison of Dynamic Lateral Resistance of Railway Concrete , Wooden and Steel Sleepers Subjected to Impact Loading," *Journal of Road Materials and Pavement Design*, Vol. 629, No. 1, May 2018.

[23] V. Markine and C. Esveld, "Analysis of Longitudinal and Lateral Behavior of a CWR Track Using a Computer System Longin," PhD Thesis, Delft University of Technology, September 2002, pp. 1–10.

[24] N. Lim, S. Han, T. Han, and Y. Kang, "Parametric Study on Stability of Continuous Welded Rail Track -Ballast Resistance and Track Irregularity," *Steel Structures*, Vol. 8, No. 1, August 2008, pp. 171–181.

[25] J. A. Zakeri, S. Mohammadzadeh, and M. Barati, "New Definition of Neutral Temperature in Continuous Welded Railway Track Curves," *Periodica Polytechnica Civil Engineering*, Vol. 62, No. 1, February 2018, pp. 143–147.

[26] M. Esmaeili, S. A. S. Hosseini, and M. Sharavi, "Experimental Assessment of Dynamic Lateral Resistance of Railway Concrete Sleeper," *Soil Dynamics and Earthquake Engineering*, Vol. 82, December 2015, pp. 40–54.

[27] W. Koc, A. Wilk, P. Chrostowski, and S. Grulkowski, "Tests on Lateral Resistance in Railway Tracks," Case Study,Gdansk University, August 2010, pp. 325–340.

[28] A. Bakhtiary, J. A. Zakeri, H. J. Fang, and A. Kasraiee, "An Experimental and Numerical Study on the Effect of Different Types of Sleepers on Track Lateral Resistance," *International Journal of Transportation Engineering*, Vol. 3, No. 1, September 2015, pp. 7–15.

[29] M. Oregui, Z. Li, and R. Dollevoet, "An Investigation into The Vertical Dynamics

of Tracks with Monoblock Sleepers with A 3D Finite-Element Model," *Journal of Rail and Rapid Transit*, Vol. 18, No. 1, December 2015, pp. 1-18.

[30] K. Sakdirat and N. Chayut, "Discrete Element Modeling of Sleeper-Ballast Interaction Under Impact Loading," *second pan American congress on computational mechanics*, New York, July 2018.

[31] W. Jian and X. Youding, "Technical Specifications of Vehicles Addis Ababa E-W & N-S（Phase I） Light Rail Transit Project," Rail way Manual, 2013.

[32] T. Paulos, "Response Evaluation of Concrete Sleeper under Increasing Train Speed and Axle Load," MSc.Thesis, Addis Abbaba University, 2016.

[33] Dassault Systemes, *Abaqus/CAE user's manual*. USA, 2011.

[34] American Railway Engineering and Maintenance of Way Association (AREMA), *Manual for Railway Engineering*, USA, Vol. 1. 2010.

[35] V. Profillidis and P. Poniridis, "The Mechanical Behaviour of The Sleeper-Ballast Interface," *Pergamon Journal*, Vol. 24, No. 3, November 1985, pp. 437-441.

Appendix A: measured versine inspection on NS 6 curve

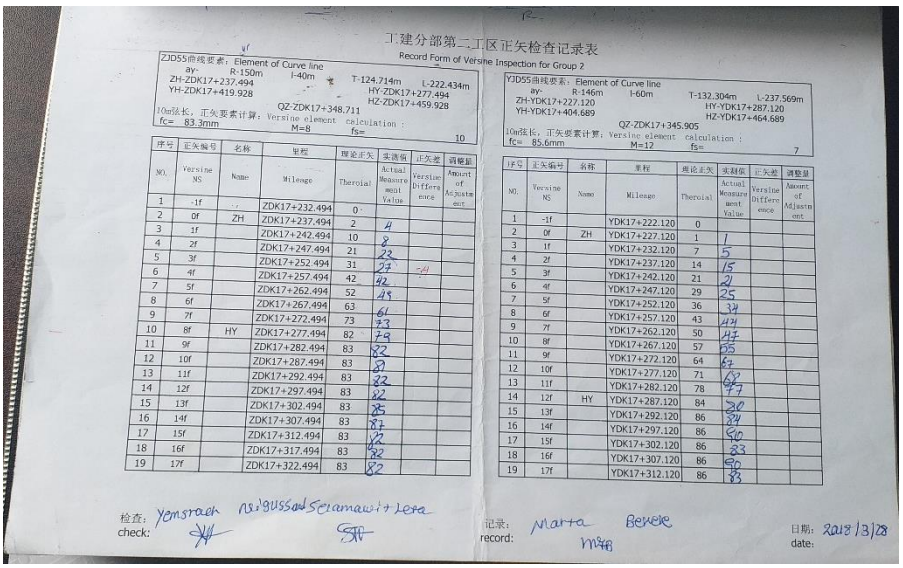

工建分部第二工区正矢检查记录表

Record Form of Versine Inspection for Group 2

ZJD55曲线要素：Element of Curve line
ay- R-150m l-40m T-124.714m L-222.434m
ZH-ZDK17+237.494 HY-ZDK17+277.494
YH-ZDK17+419.928 HZ-ZDK17+459.928
QZ-ZDK17+348.711
10m弦长，正矢要素计算：Versine element calculation：
fc= 83.3mm M=8 fs= 10

序号 NO.	正矢编号 Versine NS	名称 Name	里程 Mileage	理论正矢 Theroial	实测值 Actual Measurement Value	正矢差 Versine Difference	调整量 Amount of Adjustment
1	-1f		ZDK17+232.494	0			
2	0f	ZH	ZDK17+237.494	2	4		
3	1f		ZDK17+242.494	10	8		
4	2f		ZDK17+247.494	21	23		
5	3f		ZDK17+252.494	31	27	-4	
6	4f		ZDK17+257.494	42	42		
7	5f		ZDK17+262.494	52	49		
8	6f		ZDK17+267.494	63	61		
9	7f		ZDK17+272.494	73	73		
10	8f	HY	ZDK17+277.494	82	79		
11	9f		ZDK17+282.494	83	82		
12	10f		ZDK17+287.494	83	81		
13	11f		ZDK17+292.494	83	83		
14	12f		ZDK17+297.494	83	82		
15	13f		ZDK17+302.494	83	85		
16	14f		ZDK17+307.494	83	81		
17	15f		ZDK17+312.494	83	82		
18	16f		ZDK17+317.494	83	82		
19	17f		ZDK17+322.494	83	82		

检查：Yemsrach Nigussa and Selamawit Lera
check:

YJD55曲线要素：Element of Curve line
ay- R-146m l-60m T-132.304m L-237.569m
ZH-YDK17+227.120 HY-YDK17+287.120
YH-YDK17+404.689 HZ-YDK17+464.689
QZ-ZDK17+345.905
10m弦长，正矢要素计算：Versine element calculation：
fc= 85.6mm M=12 fs= 7

序号 NO.	正矢编号 Versine NS	名称 Name	里程 Mileage	理论正矢 Theroial	实测值 Actual Measurement Value	正矢差 Versine Difference	调整量 Amount of Adjustment
1	-1f		YDK17+222.120	0			
2	0f	ZH	YDK17+227.120	1	1		
3	1f		YDK17+232.120	7	5		
4	2f		YDK17+237.120	14	15		
5	3f		YDK17+242.120	21	21		
6	4f		YDK17+247.120	29	25		
7	5f		YDK17+252.120	36	34		
8	6f		YDK17+257.120	43	44		
9	7f		YDK17+262.120	50	47		
10	8f		YDK17+267.120	57	55		
11	9f		YDK17+272.120	64	67		
12	10f		YDK17+277.120	71	68		
13	11f		YDK17+282.120	78	77		
14	12f	HY	YDK17+287.120	84	80		
15	13f		YDK17+292.120	86	84		
16	14f		YDK17+297.120	86	90		
17	15f		YDK17+302.120	86	83		
18	16f		YDK17+307.120	86	90		
19	17f		YDK17+312.120	86	83		

记录：Marta Bekele
record:

日期：2018/3/28
date:

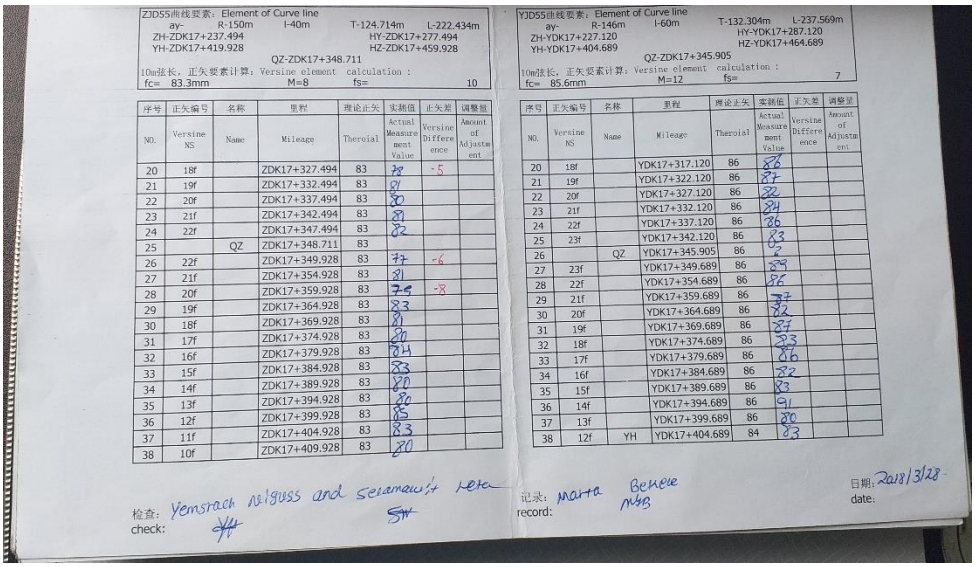

ZJD55曲线要素：Element of Curve line
ay- R-150m l-40m T-124.714m L-222.434m
ZH-ZDK17+237.494 HY-ZDK17+277.494
YH-ZDK17+419.928 HZ-ZDK17+459.928
QZ-ZDK17+348.711
10m弦长，正矢要素计算：Versine element calculation：
fc= 83.3mm M=8 fs= 10

序号 NO.	正矢编号 Versine NS	名称 Name	里程 Mileage	理论正矢 Theroial	实测值 Actual Measurement Value	正矢差 Versine Difference	调整量 Amount of Adjustment
20	18f		ZDK17+327.494	83	78	-5	
21	19f		ZDK17+332.494	83	81		
22	20f		ZDK17+337.494	83	80		
23	21f		ZDK17+342.494	83	81		
24	22f		ZDK17+347.494	83	82		
25		QZ	ZDK17+348.711	83			
26	22f		ZDK17+349.928	83	77	-6	
27	21f		ZDK17+354.928	83	81		
28	20f		ZDK17+359.928	83	75	-8	
29	19f		ZDK17+364.928	83	83		
30	18f		ZDK17+369.928	83	81		
31	17f		ZDK17+374.928	83	80		
32	16f		ZDK17+379.928	83	84		
33	15f		ZDK17+384.928	83	83		
34	14f		ZDK17+389.928	83	80		
35	13f		ZDK17+394.928	83	80		
36	12f		ZDK17+399.928	83	85		
37	11f		ZDK17+404.928	83	83		
38	10f		ZDK17+409.928	83	80		

检查：Yemsrach Nigussa and Selamawit Lera
check:

YJD55曲线要素：Element of Curve line
ay- R-146m l-60m T-132.304m L-237.569m
ZH-YDK17+227.120 HY-YDK17+287.120
YH-YDK17+404.689 HZ-YDK17+464.689
QZ-ZDK17+345.905
10m弦长，正矢要素计算：Versine element calculation：
fc= 85.6mm M=12 fs= 7

序号 NO.	正矢编号 Versine NS	名称 Name	里程 Mileage	理论正矢 Theroial	实测值 Actual Measurement Value	正矢差 Versine Difference	调整量 Amount of Adjustment
20	18f		YDK17+317.120	86	86		
21	19f		YDK17+322.120	86	87		
22	20f		YDK17+327.120	86	82		
23	21f		YDK17+332.120	86	84		
24	22f		YDK17+337.120	86	86		
25	23f		YDK17+342.120	86	83		
26		QZ	YDK17+345.905	86	82		
27	23f		YDK17+349.689	86	89		
28	22f		YDK17+354.689	86	86		
29	21f		YDK17+359.689	86	87		
30	20f		YDK17+364.689	86	82		
31	19f		YDK17+369.689	86	87		
32	18f		YDK17+374.689	86	93		
33	17f		YDK17+379.689	86	86		
34	16f		YDK17+384.689	86	82		
35	15f		YDK17+389.689	86	83		
36	14f		YDK17+394.689	86	91		
37	13f		YDK17+399.689	86	80		
38	12f	YH	YDK17+404.689	84	83		

记录：Marta Bekele
record:

日期：2018/3/28
date:

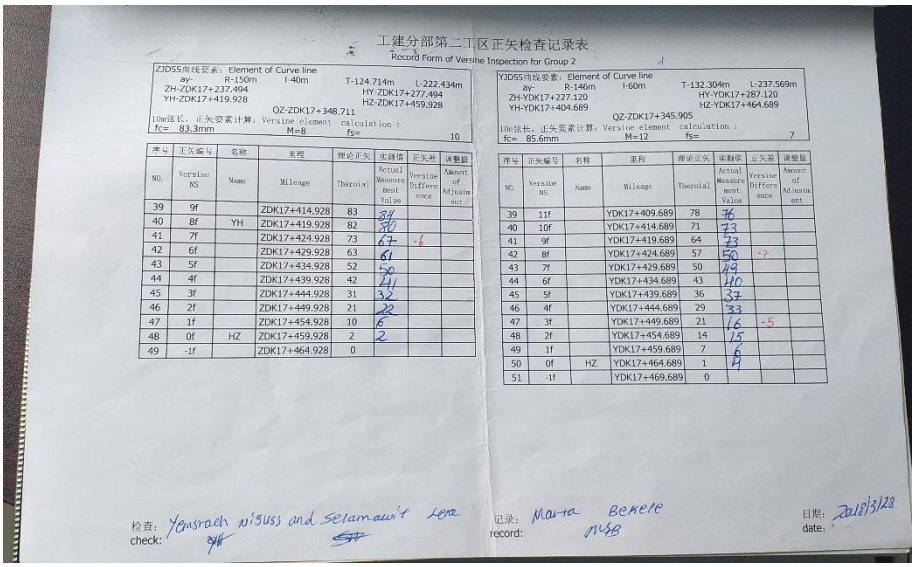

工建分部第二工区正矢检查记录表

Record Form of Versine Inspection for Group 2

ZJD55曲线要素：Element of Curve line
ay- R-150m l-40m T-124.714m L-222.434m
ZH-ZDK17+237.494 HY-ZDK17+277.494
YH-ZDK17+419.928 HZ-ZDK17+459.928
QZ-ZDK17+348.711
10m弦长，正矢要素计算：Versine element calculation：
fc= 83.3mm M=8 fs= 10

序号 NO.	正矢编号 Versine NS	名称 Name	里程 Mileage	理论正矢 Theroial	实测值 Actual Measurement Value	正矢差 Versine Difference	调整量 Amount of Adjustment
39	9f		ZDK17+414.928	83	84		
40	8f	YH	ZDK17+419.928	82	80		
41	7f		ZDK17+424.928	73	67	-6	
42	6f		ZDK17+429.928	63	61		
43	5f		ZDK17+434.928	52	50		
44	4f		ZDK17+439.928	42	41		
45	3f		ZDK17+444.928	31	32		
46	2f		ZDK17+449.928	21	22		
47	1f		ZDK17+454.928	10	6		
48	0f	HZ	ZDK17+459.928	2	2		
49	-1f		ZDK17+464.928	0			

检查：Yemsrach Nigussa and Selamawit Lera
check:

YJD55曲线要素：Element of Curve line
ay- R-146m l-60m T-132.304m L-237.569m
ZH-YDK17+227.120 HY-YDK17+287.120
YH-YDK17+404.689 HZ-YDK17+464.689
QZ-ZDK17+345.905
10m弦长，正矢要素计算：Versine element calculation：
fc= 85.6mm M=12 fs= 7

序号 NO.	正矢编号 Versine NS	名称 Name	里程 Mileage	理论正矢 Theroial	实测值 Actual Measurement Value	正矢差 Versine Difference	调整量 Amount of Adjustment
39	11f		YDK17+409.689	78	76		
40	10f		YDK17+414.689	71	73		
41	9f		YDK17+419.689	64	73		
42	8f		YDK17+424.689	57	50	-7	
43	7f		YDK17+429.689	50	49		
44	6f		YDK17+434.689	43	40		
45	5f		YDK17+439.689	36	37		
46	4f		YDK17+444.689	29	33		
47	3f		YDK17+449.689	21	16	-5	
48	2f		YDK17+454.689	14	15		
49	1f		YDK17+459.689	7	6		
50	0f	HZ	YDK17+464.689	1	1		
51	-1f		YDK17+469.689	0			

记录：Marta Bekele
record:

日期：2018/3/28
date:

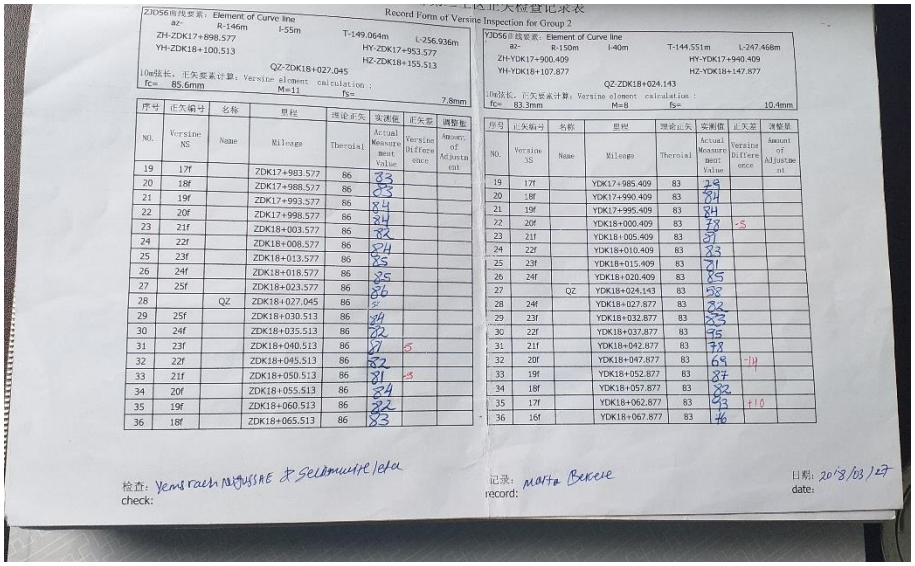

Record Form of Versine Inspection for Group 2

ZJDS6曲线要素：Element of Curve line
az- R-146m l-55m T-149.064m L-256.936m
ZH-ZDK17+898.577 HY-ZDK17+953.577
YH-ZDK18+100.513 HZ-ZDK18+155.513
QZ-ZDK18+027.045
10m弦长，正矢要素计算：Versine element calculation：
fc= 85.6mm M=11 fs= 7.8mm

序号 NO.	正矢编号 Versine NS	名称 Name	里程 Mileage	理论正矢 Theroial	实测值 Actual Measurement Value	正矢差 Versine Difference	调整量 Amount of Adjustment
19	17f		ZDK17+983.577	86	83		
20	18f		ZDK17+988.577	86	83		
21	19f		ZDK17+993.577	86	84		
22	20f		ZDK17+998.577	86	84		
23	21f		ZDK18+003.577	86	82		
24	22f		ZDK18+008.577	86	84		
25	23f		ZDK18+013.577	86	85		
26	24f		ZDK18+018.577	86	85		
27	25f		ZDK18+023.577	86	86		
28		QZ	ZDK18+027.045	86	87		
29	25f		ZDK18+030.513	86	84		
30	24f		ZDK18+035.513	86	82		
31	23f		ZDK18+040.513	86	87	-5	
32	22f		ZDK18+045.513	86	82		
33	21f		ZDK18+050.513	86	81	-5	
34	20f		ZDK18+055.513	86	84		
35	19f		ZDK18+060.513	86	82		
36	18f		ZDK18+065.513	86	83		

检查：Yemsrach Nigussie & Selammite Ieta
check:

YJDS6曲线要素：Element of Curve line
az- R-150m l-40m T-144.551m L-247.468m
ZH-YDK17+900.409 HY-YDK17+940.409
YH-YDK18+107.877 HZ-YDK18+147.877
QZ-ZDK18+024.143
10m弦长，正矢要素计算：Versine element calculation：
fc= 83.3mm M=8 fs= 10.4mm

序号 NO.	正矢编号 Versine NS	名称 Name	里程 Mileage	理论正矢 Theroial	实测值 Actual Measurement Value	正矢差 Versine Difference	调整量 Amount of Adjustment
19	17f		YDK17+985.409	83	79		
20	18f		YDK17+990.409	83	84		
21	19f		YDK17+995.409	83	84		
22	20f		YDK18+000.409	83	78	-5	
23	21f		YDK18+005.409	83	81		
24	22f		YDK18+010.409	83	83		
25	23f		YDK18+015.409	83	81		
26	24f		YDK18+020.409	83	85		
27		QZ	YDK18+024.143	83	88		
28	24f		YDK18+027.877	83	82		
29	23f		YDK18+032.877	83	83		
30	22f		YDK18+037.877	83	95		
31	21f		YDK18+042.877	83	78		
32	20f		YDK18+047.877	83	69	-14	
33	19f		YDK18+052.877	83	87		
34	18f		YDK18+057.877	83	82		
35	17f		YDK18+062.877	83	93	+10	
36	16f		YDK18+067.877	83	76		

记录：Marta Bekele
record:

日期：2018/03/27
date:

检查：Marta Bekele & Yemsrach Nigussie
check:

记录：Selammite Ieta
record:

日期：2018/03/27
date:

Appendex B field test results

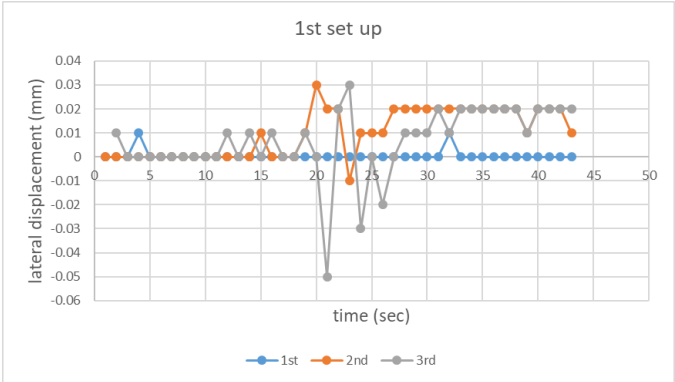

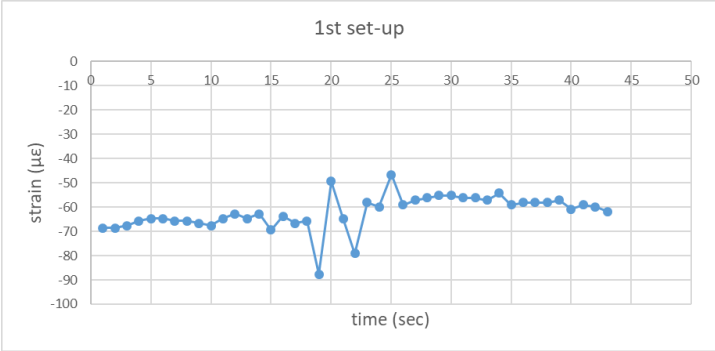

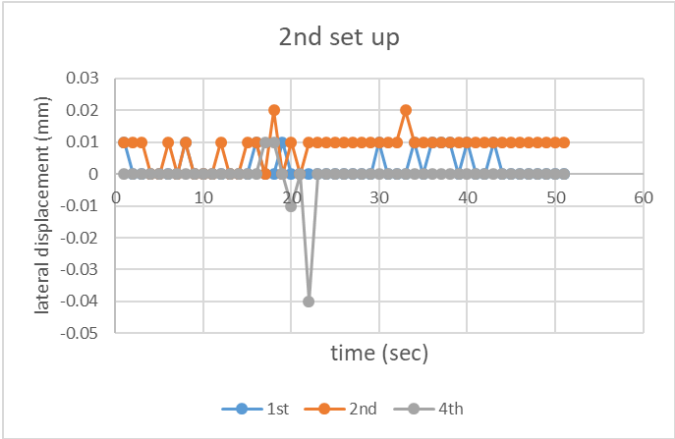

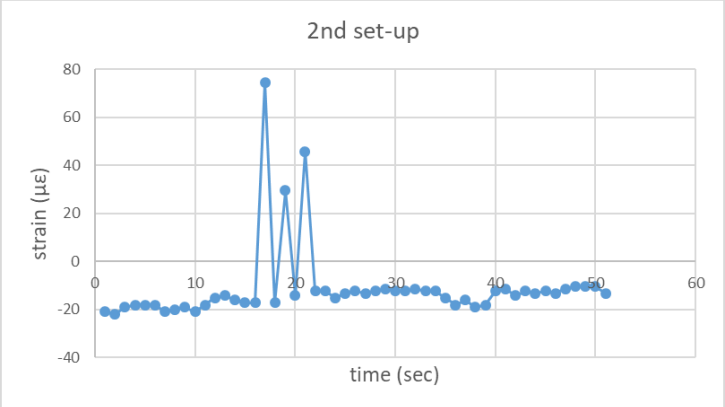

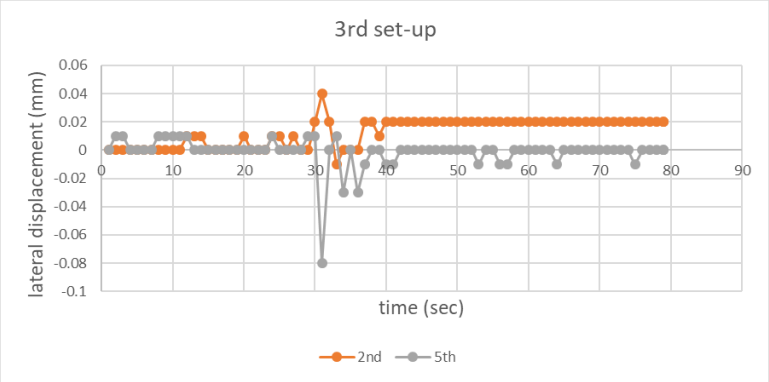
3rd set-up
lateral displacement (mm)
0.06
0.04
0.02
0
-0.02
-0.04
-0.06
-0.08
-0.1
0
10
20
30
40
50
60
70
80
90
time (sec)
2nd
5th

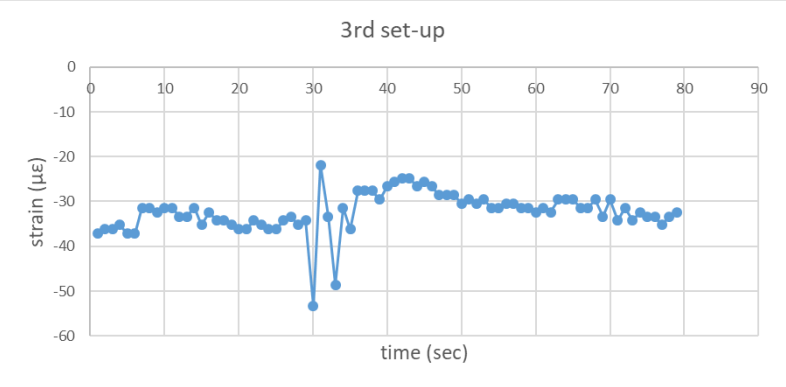
3rd set-up
strain (με)
0
-10
-20
-30
-40
-50
-60
0
10
20
30
40
50
60
70
80
90
time (sec)

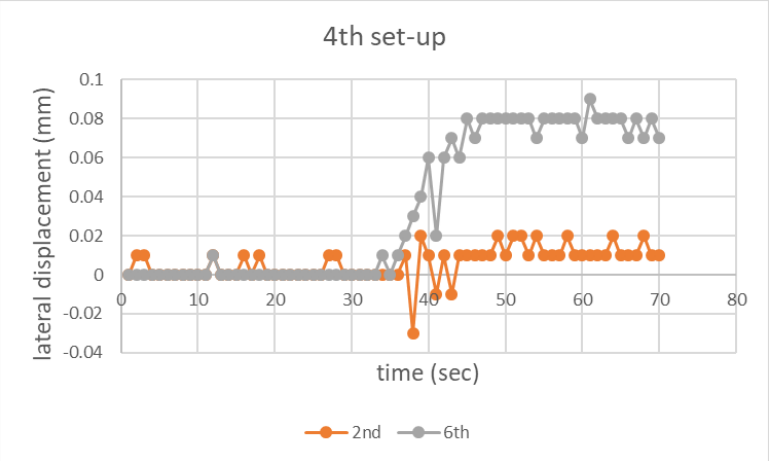
4th set-up
lateral displacement (mm)
0.1
0.08
0.06
0.04
0.02
0
-0.02
-0.04
0
10
20
30
40
50
60
70
80
time (sec)
2nd
6th

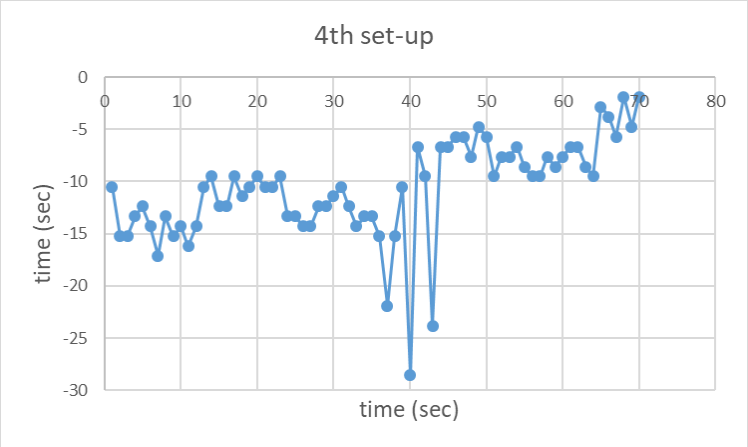
4th set-up
time (sec)
0
-5
-10
-15
-20
-25
-30
0
10
20
30
40
50
60
70
80
time (sec)

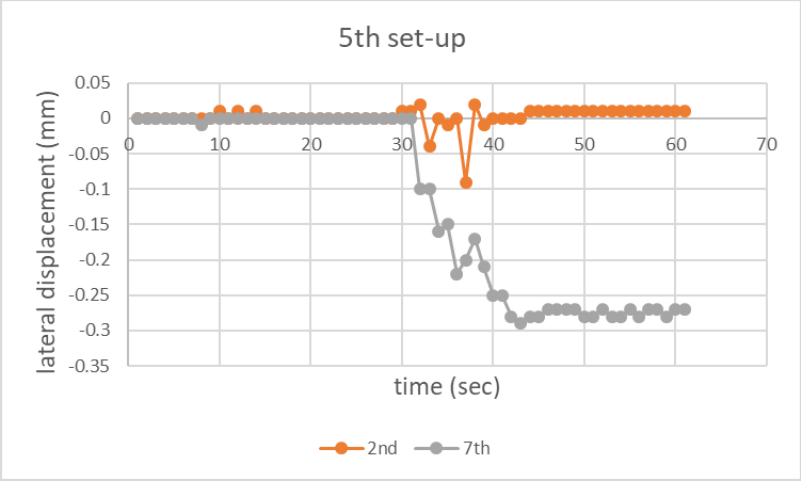
5th set-up
lateral displacement (mm)
0.05
0
-0.05
-0.1
-0.15
-0.2
-0.25
-0.3
-0.35
0
10
20
30
40
50
60
70
time (sec)
2nd
7th

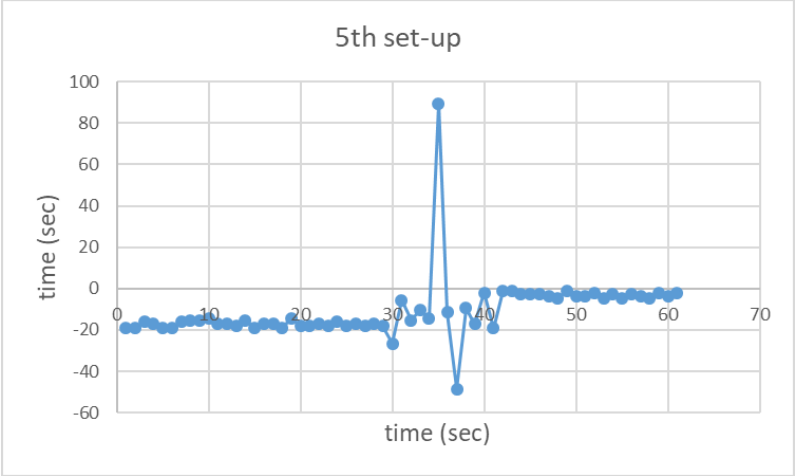
5th set-up
time (sec)
100
80
60
40
20
0
-20
-40
-60
0
10
20
30
40
50
60
70
time (sec)